NXP SEMICONDUCTORS
EINDHOVEN UNIVERSITY OF TECHNOLOGY

# Estimation Methods for IQ Imbalance in Multi-Standard (Near) Zero IF Receivers

**Author:**
A.M.J.M. Schoonen
*Eindhoven University of Technology*
**Supervisors:**
P.G.M. Baltus
*Eindhoven University of Technology*
J. van Sinderen
*NXP Research, Eindhoven*
R. van Veldhoven
*NXP Research, Eindhoven*

**Version:** 1.0.0, May 7, 2009

CIP-DATA STAN ACKERMANS INSTITUUT

Admar Schoonen

Estimation Methods for IQ Imbalance in Multi-Standard (Near) Zero IF Receivers / Admar Schoonen

Eindhoven: Stan Ackermans Instituut, 2008.

A catalogue record is available from the Eindhoven University of Technology Library

ISBN: 978-90-444-0864-5
(Eindverslagen Stan Ackermans Instituut ; 2009/021)

Keywords: blind estimation / down conversion / image rejection ratio / IQ imbalance / multi-standard receivers / rate of convergence / software defined radio / standard independent estimation

# Abstract

IQ imbalance can be a severe limitation in multi-standard wireless receivers. In literature, several standard independent methods are known to estimate and reduce the impact of IQ imbalance. Those methods can be divided in two classes: statistics based methods, which are known for their very slow convergence, and methods based on using a test tone generator, which are known for their risk of (amongst others) LO pulling and test tone radiation.

This document describes the results of a project aimimg at finding standard independent estimators for the IQ imbalance problem that converge faster than the well known statistics based methods, without using a dedicated test tone generator.

In this document several system level models for frequency independent and frequency selective IQ imbalance are described. Furthermore, three novel methods are derived:

- one method which is based on exploiting statistical properties of the received signals, but which uses additional hardware to increase the rate of convergence,
- one method which is based on the statistical method, but can be used to estimate frequency selective IQ imbalance and
- one method which is based on injecting the LO signal into the RF input of the mixer and using LO self-mixing to estimate the IQ imbalance parameters.

All methods are theoretically analyzed and evaluated using simulations. The last method is also evaluated with a prototype system.

It is shown that all methods are unbiased estimators and that the performance of the statistics based estimators is limited by the number of samples that are used for the estimation. Furthermore, it is shown that the LO self-mixing method requires only

16 samples to achieve correct IQ imbalance estimates, however, it is also shown that this method is sensitive to the shape of the injected waveform.

The choice for a particular estimation method therefore depends on the actual implementation of the receiver front-end. For relatively low frequency systems where a very short estimation time is essential, the LO self-mixing method can be used to achieve very fast IQ imbalance estimates, but for very high frequency systems which have more relaxed estimation time requirements, or when frequency selective IQ imbalance compensation is required, the statistical methods can be more preferable.

# Contents

# List of symbols and abbreviations

| | |
|---|---|
| $A$ | amplitude |
| $a$ | complex parameter in IQ imbalance model |
| $a_{\mathrm{r}}$ | real part of $a$ |
| $a_{\mathrm{i}}$ | imaginary part of $a$ |
| $\hat{a}$ | estimate of parameter $a$ |
| $b$ | complex parameter in IQ imbalance model |
| $d$ | duty cycle, normalized on $T$ |
| $\delta$ | gain error (in %) |
| $\mathrm{E}[x]$ | expectation of $x$ |
| $\varepsilon$ | error in estimate |
| $f$ | frequency, in Hz |
| $f_{\mathrm{s}}$ | sample frequency, in Hz |
| $g$ | relative gain error |
| $H(\omega)$ | frequency domain transfer function of a filter |
| $i$ | $\sqrt{-1}$ |
| $K$ | DC gain of low pass filter |
| $\boldsymbol{M}$ | IQ imbalance mixing matrix |
| $N$ | number of samples |
| $P$ | power of signal |
| $r(t)$ | RF received signal, described in time domain |
| $t$ | time |
| $t_{\mathrm{f}}$ | fall time |
| $t_{\mathrm{r}}$ | rise time |
| $X(\omega)$ | frequency domain description of $x(t)$ |
| $x(t)$ | baseband representation of received signal, described in time domain |
| $x_{\mathrm{I}}(t)$ | inphase (real) part of $x(t)$ |
| $x_{\mathrm{Q}}(t)$ | quadrature (imaginary) part of $x(t)$ |
| $y(t)$ | baseband representation of received signal, described in time domain |
| $T$ | reciprocal of frequency, in s |

| | |
|---|---|
| $\tau$ | reciprocal of phase error |
| $\phi$ | phase error |
| $\omega$ | frequency, in rad/s |
| $\omega_{\mathrm{b}}$ | break frequency of low pass filter; also called cutoff frequency |
| $\omega_{\mathrm{c}}$ | center frequency; is identical to frequency of LO |

| | |
|---|---|
| 16QAM | 16-level quadrature amplitude modulation |
| ADC | analog to digital convertor |
| BPF | band pass filter |
| BPSK | binary phase shift keying |
| DC | direct current |
| DFT | discrete Fourier transform |
| DSP | digital signal processor |
| DVB-H | digital video broadcasting for handhelds |
| EDGE | enhanced data rates for gsm evolution |
| FM | frequency modulation |
| FSK | frequency shift keying |
| GPRS | general packet radio service |
| GPS | global positioning system |
| GSM | global system for mobile communications |
| IF | intermediate frequency |
| IQ | inphase / quadrature |
| IRR | image rejection ratio |
| LAN | local area network |
| LNA | low noise amplifier |
| LO | local oscillator |
| LPF | low pass filter |
| MIMO | multiple input, multiple output system |
| OFDM | orthogonal frequency division multiplexing |
| OIP2 | second order output intercept point |
| OIP3 | third order output intercept point |
| RF | radio frequency |
| SDR | software defined radio |
| SIR | signal to interference ratio |
| SNR | signal to noise ratio |
| TIA | transimpedance amplifier |
| UMTS | universal mobile telecommunications system |
| WLAN | wireless local area network |

# Acknowledgments

During evaluation of the results of this project, I realized that the successes of this project could not have been possible without the help of many people. Therefore, I would like to use this page here to thank those people for helping me and enabling me to find new solutions to an, at first sight, impossible problem.

In first place, I would like to thank Leon Kaufmann and Raf Roovers for giving me the space and possibilities to do this project at NXP Research. Without their help, I would not have begun this project in first place.

Furthermore, I would like to thank Jan van Sinderen, Peter Baltus and Robert van Veldhoven for their countless hours of discussions and guidance. The beginning of the project was marked with generating many ideas which where just as quickly thrown away. While this was frustrating at times, I am thankful of the realistic points of view from Jan and Robert. I am certain that it prevented more disappointments down the road.

I would also like to thank Jan ter Maten for reviewing important parts of this document, and Jan Vroomans, Fabio Sebastiano, Frank Leong and Salvatore Drago for the many fruitful discussions we had and for being very pleasant office-mates.

Finally, I would also like to thank Fabio, Frank and Salvatore as well as Piedro, Maristella, Claudio and all the other Italian colleagues for the many nice and fun lunches we had. I am sure that I will miss you at my next occupation.

# Chapter 1

# Introduction

In the last few years we have seen a shift in mobile communications from devices which are specifically made to work with just one standard, to devices which can use more than one standard. Examples of such devices are mobile phones that integrate not only GSM, but also UMTS, bluetooth and wireless LAN and car radio systems that not only integrate FM radio but also GPS, bluetooth and digital radio and television standards such as DVB-H and Sirius and XM radio. While it is possible to include a different RF front-end for every standard, this does occupy precious space and increases manufacturing costs. Besides that, it can cause application problems since some standards are causing interference on other standards; a well known example for this is the interference from bluetooth on wireless LAN as shown for example by Golmie in [1] and by Punnoose in [2].

To overcome these disadvantages, much research has recently been done on flexible radio systems which can adhere to multiple standards. Such so called software defined radio (SDR) systems can dynamically change their RF frequency, IF bandwidth and digital processing and can thus switch on demand between different standards. This results in benefits for application engineers who can have a shorter time to market for their products and for IC designers who can more easily reuse IP blocks in other products. However, the consequence is that such a system must meet or exceed the specifications of all standards of interest.[1] This poses big design challenges on RF, IF and digital designers.

Once specific problem of designing and manufacturing wireless radio systems are the errors that occur in the actual chip due to model imperfections and manufacturing deviations. This is especially true for quadrature down convertors, as explained

[1] Note however, that the system does not need to fulfill all requirements for all standards at the same time.

for example by Razavi in [3]. In such convertors, these limitations impose restrictions on the amount of symmetry between the inphase and quadrature branches of the convertor. In a first order model, those limitations translate in a difference in gain and phase between those two branches. Such a model is called an IQ imbalance model. As will be shown in chapter 2, the IQ imbalance problem results in a reduction in the signal to interference ratio (SIR) of the signal that the receiver wants to decode.

This problem can be solved in many different ways, but for multi-standard receivers, a solution which is standard independent is preferable. In literature, there are two very popular types of standard independent solutions. The first is a statistical method, based on exploiting the differences in variances and covariance of the received signals caused by IQ imbalance, and the second is based on measuring the amount of IQ imbalance by using test tones. Both methods are unbiased and converge to the correct value, but the drawback of statistics based methods is their slow convergence. The drawback of test tone based methods is, amongst others, the problem of generating test tones which are not impaired with any significant IQ imbalance on chip, spectral purity of these test tones and the risk of radiating part of these test tones.

This document describes the result of a project aimed at finding standard independent solutions which converge faster than the well known statistical methods (such as shown for example by Windisch in [4]) without using dedicated hardware to generate test tones. Therefore, this document describes two standard independent solutions; one which is based on the statistical methods and one which is based on injecting part of the LO signal. Both methods will be theoretically analyzed and evaluated using simulations. In addition to that, the method which uses injection of part of the LO signal will be evaluated with an actual prototype system.

The benchmark for both methods is the number of samples that are needed to achieve a certain image rejection ratio and the limitations in estimation accuracy. The assumption here is that the sample frequency $f_{\mathrm{s}}$ is equal to the Nyquist rate.

The outline for this document is as follows. In chapter 2, we will discuss the problem of IQ imbalance. There, we will derive several models for frequency independent and frequency selective IQ imbalance. We will also give an overview of several popular mitigation methods, where we will pay special attention to the class of digital estimators and compensators. In this chapter, we will also derive an equation for the image rejection ratio which can be achieved when the IQ imbalance parameter estimates have limited accuracy. Finally, we will also show a list of requirements which the ideal solutions needs to satisfy.

Chapter 3 will briefly discuss an intuitive way to estimate the IQ imbalance param-

eters and explain why the particular approach discussed in that chapter has a very undesired property.

In chapter 4, we will derive several methods based on exploiting the statistical properties of the received signals, including a method which has a faster convergence than the well known standard statistical method and a method which can estimate frequency selective IQ imbalance parameters. These methods will be theoretically analyzed and evaluated using simulations.

Chapter 5 will derive a method to estimate the IQ imbalance parameters based on injecting a part of the LO signal. This method will be theoretically analyzed and evaluated by simulations. Furthermore, we will discuss the design of a prototype system to test this method and we will evaluate this method with measurement results.

Finally, chapter 6 will summarize our findings from the previous chapters and conclusions and give directions for future work.

# Chapter 2

# Problem description

This chapter will start in section 2.1 with a short overview of the causes of IQ imbalance. After that, system level models will be derived which describe frequency independent IQ imbalance in time domain and in frequency domain and the frequency domain model will be extended to also describe frequency selective IQ imbalance. Section 2.1 will end with a short discussion on typical numbers for the parameters of these models.

Section 2.2 will give an overview of popular methods to mitigate the effect of IQ imbalance where pay special attention will be payed to the class of digital estimation and compensation methods.

Section 2.3 will discuss two very popular all digital methods to compensate for IQ imbalance; one method which operates on the time domain description of the received signal and one method which operates on the frequency domain description. Furthermore, in that section an equation for the image rejection ratio will be derived that can be achieved when the accuracy of the estimate is limited.

This chapter will end with a description of the requirements that the solutions should satisfy in section 2.4.

## 2.1 IQ imbalance modeling

In typical zero-IF or low-IF quadrature receivers, the inphase branch and quadrature branch are ideally symmetrical. However, the symmetry of the two branches is limited by other circuitry on the chip and by design and manufacturing limitations.

A first order approximation of the differences between the two branches results in a model for the gain and phase mismatch and is called an IQ imbalance model.

In literature, two types of system level IQ imbalance models are popular: the symmetrical model where the gain and phase errors are equally distributed over both inphase and quadrature branch as used by Finol in [5] and the asymmetrical model where the inphase branch is used as reference and all errors reside in the quadrature branch as used by Valkama in [6].

While both models take account for the 90 degrees phase mismatch of the local oscillator (LO) and gain errors in the analog processing stages, the main difference is that the second model results in a mathematically more pleasing model, especially for digital estimation of the imbalance parameters. A detailed comparison of both models can be found in [7].

In this section, we will show a derivation for the asymmetric model in time domain for frequency independent IQ imbalance, translate this model to frequency domain and derive a frequency domain model for frequency selective IQ imbalance. We will also show the effect on the received signal caused by IQ imbalance.

### 2.1.1 Modeling frequency independent IQ imbalance in time domain

Figure 2.1 shows a block diagram for a receiver which is impaired with the asymmetric IQ imbalance model. In this figure, $\delta$ indicates the gain error and $\phi$ indicates the phase error in the quadrature branch. The RF stages of the receiver are the antenna, the LNA, the BPF, the LO and (partially), shown on the left hand side of the dashed line in this figure. The IF stages of the receiver are the output of the mixers, the LPFs, the automatic gain controls and the ADCs, shown on the right hand side of the dashed line in this figure.

The low noise amplifier (LNA) and the bandpass filter (BPF) will scale the received signal $r(t)$ and give it a phase delay, but for a system level receiver side IQ imbalance model, this scaling and delaying, as well as the wireless channel transfer function can be modeled in the transmitted complex baseband signal $x(t)$.

Assume for the moment that there is no mismatch between the low pass filters $\mathrm{LPF_I}$ and $\mathrm{LPF_Q}$. The received signal in the inphase branch is then

$$y_{\mathrm{I}}(t) = \mathrm{LPF_I}\{\cos(\omega_{\mathrm{c}} t) r(t)\} \tag{2.1}$$

where $\omega_{\mathrm{c}}$ is the LO frequency, $r(t)$ is the RF signal received by the antenna and $\mathrm{LPF_I}\{\cdot\}$ indicates a low pass filtering operation by filter $\mathrm{LPF_I}$. The received signal

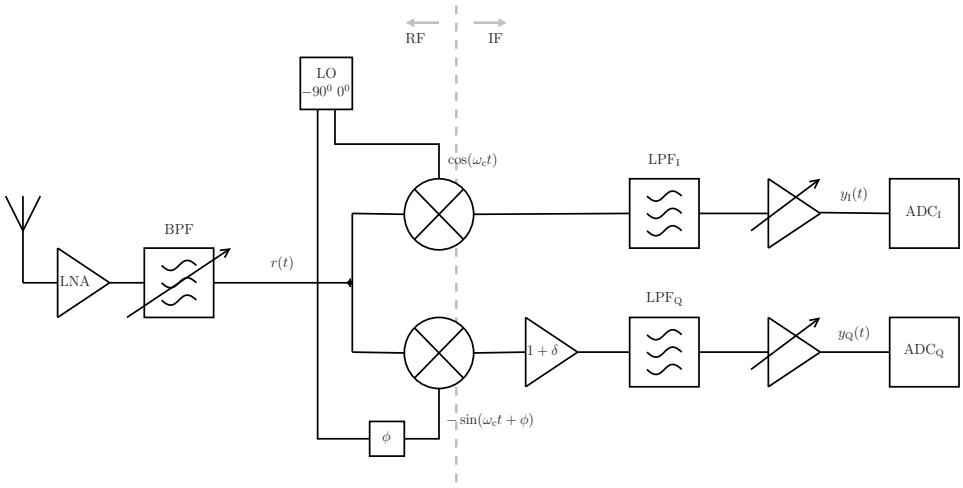


Figure 2.1: System level block diagram of a receiver with IQ imbalance errors $\delta$ and $\phi$.

in the quadrature branch is

$$y_\mathrm{Q}(t) = -\mathrm{LPF}_\mathrm{Q}\{g\sin(\omega_\mathrm{c}t + \phi)r(t)\} \tag{2.2}$$

with $g = 1 + \delta$. Note that for the ideal case, where there is no IQ imbalance and thus $\delta = 0$ and $\phi = 0$, this reduces to

$$y_\mathrm{Q}(t) = -\mathrm{LPF}_\mathrm{Q}\{\sin(\omega_\mathrm{c}t)r(t)\} \tag{2.3}$$

If the received signal $r(t)$ is an up converted band pass signal, i.e.

$$\begin{aligned} r(t) &= \Re\left\{x(t)e^{i\omega_\mathrm{c}t}\right\} \\ &= x_\mathrm{I}(t)\cos(\omega_\mathrm{c}t) - x_\mathrm{Q}(t)\sin(\omega_\mathrm{c}t) \end{aligned} \tag{2.4}$$

where $x(t) = x_\mathrm{I}(t) + ix_\mathrm{Q}(t)$ is the complex band pass signal that the receiver wishes to decode, equations (2.1) and (2.2) can be written as

$$y_\mathrm{I}(t) = \frac{1}{2}x_\mathrm{I}(t) \tag{2.5}$$

and

$$y_\mathrm{Q}(t) = -\frac{g}{2}\left(x_\mathrm{I}(t)\sin(\phi) - x_\mathrm{Q}(t)\cos(\phi)\right) \tag{2.6}$$

respectively.

In digital domain, those signals can be combined as

$$\begin{aligned} y(t) &= 2(y_{\mathrm{I}}(t) + iy_{\mathrm{Q}}(t)) \\ &= x_{\mathrm{I}}(t)\,(1 - ig\sin(\phi)) + ix_{\mathrm{Q}}(t)g\cos(\phi). \end{aligned} \tag{2.7}$$

This can be written as

$$y(t) = ax(t) + bx^*(t) \tag{2.8}$$

where $a$ and $b$ are both complex numbers and $x^*(t)$ denotes the complex conjugate of $x(t)$. In this expression, $a$ scales the wanted complex baseband signal while $b$ scales the interfering complex baseband signal.

With $a = a_{\mathrm{r}} + ia_{\mathrm{i}}$ and $b = b_{\mathrm{r}} + ib_{\mathrm{i}}$, equation (2.8) can be rewritten as

$$y(t) = x_{\mathrm{I}}(a_{\mathrm{r}} + b_{\mathrm{r}} + ia_{\mathrm{i}} + ib_{\mathrm{i}}) + ix_{\mathrm{Q}}(a_{\mathrm{r}} - b_{\mathrm{r}} + ia_{\mathrm{i}} - ib_{\mathrm{i}}). \tag{2.9}$$

When we compare equations (2.7) and (2.9), we observe that

$$1 - ig\sin(\phi) = a_{\mathrm{r}} + b_{\mathrm{r}} + i(a_{\mathrm{i}} + b_{\mathrm{i}}) \tag{2.10}$$

and

$$g\cos(\phi) = a_{\mathrm{r}} - b_{\mathrm{r}} + i(a_{\mathrm{i}} - b_{\mathrm{i}}) \tag{2.11}$$

and thus that

$$a_{\mathrm{r}} + b_{\mathrm{r}} = 1 \tag{2.12}$$

and

$$a_{\mathrm{i}} - b_{\mathrm{i}} = 0. \tag{2.13}$$

From this we can conclude that $b_{\mathrm{i}} = a_{\mathrm{i}}$ and $b_{\mathrm{r}} = 1 - a_{\mathrm{r}}$ and thus we obtain the relationship

$$b = 1 - a^*. \tag{2.14}$$

Furthermore, we find that

$$a_{\mathrm{i}} = -\frac{g\sin(\phi)}{2} \tag{2.15}$$

and

$$a_{\mathrm{r}} = \frac{1 + g\cos(\phi)}{2} \tag{2.16}$$

and thus

$$\begin{aligned} a &= \frac{1 + g\left(\cos(\phi) - i\sin(\phi)\right)}{2} \\ &= \frac{1 + g\left(\cos(-\phi) + i\sin(-\phi)\right)}{2} \\ &= \frac{1 + ge^{-i\phi}}{2}. \end{aligned} \tag{2.17}$$

Using equation (2.14), we find for $b$

$$b = \frac{1 - ge^{i\phi}}{2}. \tag{2.18}$$

Note that when there is no IQ imbalance, we find that $g = 1$ and $\phi = 0$ and therefore $a = 1$ and $b = 0$.

Thus, we can conclude that an gain mismatch $\delta$ and a phase mismatch $\phi$ occurring in the IF and/or RF stages of a receiver can be modeled completely in IF domain as

$$y(t) = ax(t) + bx^*(t) \tag{2.19}$$

where $x(t)$ is the original transmitted complex baseband signal, $y(t)$ is the received complex baseband signal, $a = \frac{1+ge^{-i\phi}}{2}$ and scales the wanted signal and $b = 1 - a^*$ and scales the interfering signal. This is the model as used by Valkama in [6].

The performance of the receiver is usually expressed using the image rejection ratio (IRR), which is the ratio of signal power of the desired signal and the amount of leakage of the image signal. This ratio can be calculated from equation (2.19) with

$$\mathrm{IRR} = 10\log_{10}\left(\frac{|a|^2}{|b|^2}\right). \tag{2.20}$$

The specification of a certain wireless standard mandates a minimum amount of suppression, depending on the distance in frequency domain from the signal of interest. When designing a wireless receiver for such a standard, an IF frequency has to be chosen, and this IF frequency corresponds with the distance in frequency domain from the signal of interest. Therefore, the minimum IRR that a receiver needs to achieve is directly related to the IF frequency and the specification of the wireless standard.

### 2.1.2 Modeling frequency independent IQ imbalance in frequency domain

To analyze the effect of IQ imbalance on a received signal in frequency domain, we need to take the Fourier transform of equation (2.19), which results in

$$Y(\omega) = aX(\omega) + bX^*(-\omega). \tag{2.21}$$

where $X(\omega)$ and $Y(\omega)$ are the Fourier transforms of $x(t)$ and $y(t)$ respectively.

This equation clearly shows that the received signal $Y(\omega)$ contains the desired signal $X(\omega)$, scaled with factor $a$ and an interfering component $X^*(-\omega)$ originating from the mirror frequency $-\omega$, scaled with factor $b$.

Figure 2.2 shows the complex spectrum of the received signal at the antenna of the receiver and the received signal after down conversion. In this figure, signal $R_1$ is the received signal at frequency $\omega_c + \omega_{IF}$ before down conversion, when source 1 transmitted the complex baseband signal $X_1$. Similarly, signal $R_2$ is the received signal at frequency $\omega_c - \omega_{IF}$ before down conversion when source 2 transmitted the complex baseband signal $X_2$.

The receiver wishes to decode signal $R_1$ at frequency $\omega_c + \omega_{IF}$ in presence of a strong interfering signal $R_2$ at frequency $\omega_c - \omega_{IF}$.

This figure visualizes the interference that occurs after down conversion at frequencies $\omega_{IF}$ and $-\omega_{IF}$. If signal $R_2$ is much stronger than $R_1$, decoding the complex baseband signal $X_1$ at frequency $\omega_{IF}$ is very hard, since this signal is impaired by a large amount of interference from signal $X_2$, and it is even possible that the power of this interfering signal is larger than the signal power of $X_1$, as indicated by this figure.

### 2.1.3 Modeling frequency selective IQ imbalance in frequency domain

So far we have only discussed frequency independent IQ imbalance, i.e., the case where gain and phase errors do not depend on the frequency.

In general, this is true for gain and phase errors which originate in the RF stage of the receiver, since the RF stage is designed for a frequency which is typically 100 times (or even more) higher than the signal bandwidth in which we are interested. Thus, at the RF frequency, the parasitics and other sources of IQ imbalance will not change much over the span of this signal bandwidth due to the low Q of the IC process. Therefore, the IQ imbalance can be expected to be fairly constant over

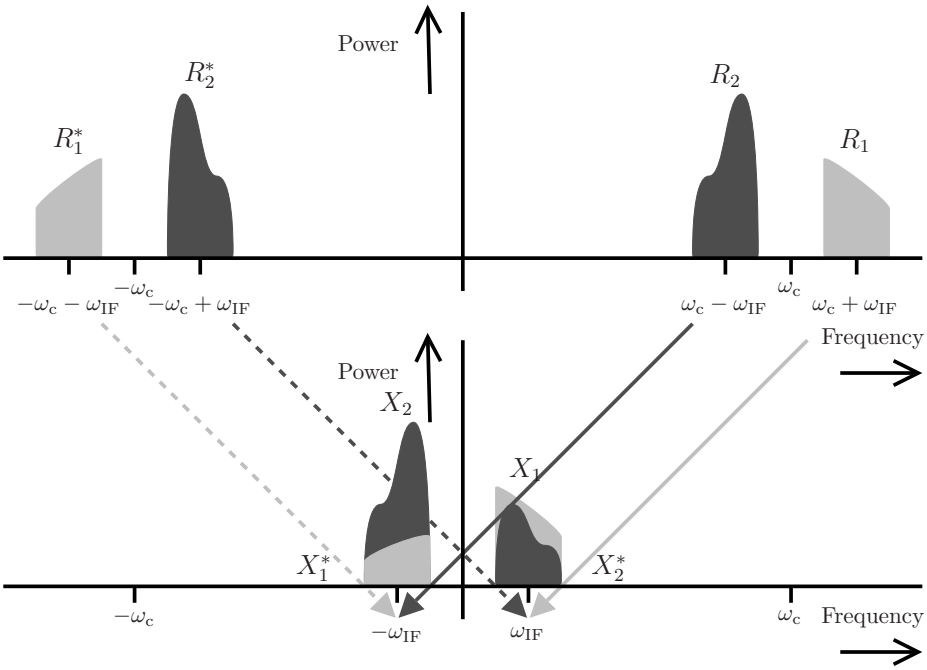


Figure 2.2: Influence of IQ imbalance in the receiver on the received signal spectrum. Top: complex spectrum of received signal at antenna. Bottom: complex spectrum of received signal after down conversion.

that range. Typically, the local oscillator and the mixers contribute the most to IQ imbalance originating in the RF stage.

However, the IF stage is usually designed to have a bandwidth equal to (or slightly larger than) the signal bandwidth for zero-IF receivers, since it has to suppress adjacent signals. This suppression is done using filters $\mathrm{LPF_I}$ and $\mathrm{LPF_Q}$ in the inphase and quadrature branches as shown in figure 2.1, and both filters should ideally have an identical frequency response. In this section the situation where the frequency responses of those filters is not equal will be analyzed, by assuming that the gain and cutoff frequency of filter $\mathrm{LPF_Q}$ is different from $\mathrm{LPF_I}$.

Please note that for low-IF receivers, the IF stage is designed to have a bandwidth equal to (or slightly more than) twice the signal bandwidth IF. However, this will not reduce the expected IQ imbalance, since the signal of interest is in such receivers located on only the positive (or only the negative) side of the complex spectrum, and will thus also be located close to the cutoff frequency of the IF filter.

A simple first order low pass filter in the IF stage has a transfer function

$$H(\omega) = \frac{K}{1 + i\omega/\omega_{\mathrm{b}}} \tag{2.22}$$

where $K$ is the DC gain and $\omega_{\mathrm{b}} = 1/RC$ is the cutoff frequency (or break frequency). If the filters in the inphase branch and the quadrature branch of the receiver of figure 2.1 have the transfer functions

$$H_{\mathrm{I}}(\omega) = \frac{K_{\mathrm{I}}}{1 + i\omega/\omega_{\mathrm{b,I}}} \tag{2.23}$$

and

$$H_{\mathrm{Q}}(\omega) = \frac{K_{\mathrm{Q}}}{1 + i\omega/\omega_{\mathrm{b,Q}}} \tag{2.24}$$

respectively, then the gain error is

$$\begin{aligned} g(\omega) &= \frac{|H_{\mathrm{Q}}(\omega)|}{|H_{\mathrm{I}}(\omega)|} \\ &= \frac{|K_{\mathrm{Q}}|}{|K_{\mathrm{I}}|} \frac{|1 + i\omega/\omega_{\mathrm{b,I}}|}{|1 + i\omega/\omega_{\mathrm{b,Q}}|} \end{aligned} \tag{2.25}$$

and the phase error is the difference of the phase shift of both filters

$$\phi(\omega) = \arctan(-\omega/\omega_{\mathrm{b,Q}}) - \arctan(-\omega/\omega_{\mathrm{b,I}}) \tag{2.26}$$

The gain error as expressed by equation (2.25) is $\frac{|K_{\mathrm{Q}}|}{|K_{\mathrm{I}}|}$ at $\omega = 0$ and will approach its limit $\frac{|K_{\mathrm{Q}}|}{|K_{\mathrm{I}}|}\frac{|\omega_{\mathrm{b,Q}}|}{|\omega_{\mathrm{b,I}}|}$ as the frequency $\omega$ increases. The phase error as expressed by equation (2.26) is 0 at $\omega = 0$, has its maximum at $\omega = (\omega_{\mathrm{b,I}} + \omega_{\mathrm{b,Q}})/2$, and will slowly converge to its limit 0 if $\omega$ increases. This is shown in figure 2.3 for $K_{\mathrm{I}} = 1$, $K_{\mathrm{Q}} = 1$, $\omega_{\mathrm{b,I}} = 1$ and $\omega_{\mathrm{b,Q}} = 1.0201$.

The top figure shows the gain error. As can be seen, the gain error is 1 at $\omega = 0$, which means that there is no difference in gain between the inphase and quadrature branches. However, for $\omega \neq 0$, the gain error increases to approximally $1\%$ at $\omega = \pm\omega_{\mathrm{I}}$ and approaches the limit of $1.0201$ for $\omega \to \pm\infty$.

The middle figure shows the phase error. As can be seen, the phase erorr is 0 at $\omega = 0$, has a maximum of $\pm 0.5701^0$ at $\omega = \pm(\omega_{\mathrm{I}} + \omega_{\mathrm{Q}})/2$ and approaches its limit 0 for $\omega \to \pm\infty$.

The bottom figure shows the resulting image rejection ratio. As can be seen in this figure, the IRR approaches $\infty$ for $\omega \to 0$, decreases to 39 dB at $\omega = \pm\omega_{\mathrm{b,I}}$ and approaches the limit of $40dB$ for $\omega \to \pm\infty$.

From equations (2.25) and (2.26), we can observe the following properties:

$$g(-\omega) = g(\omega) \tag{2.27}$$

and

$$\phi(-\omega) = -\phi(\omega). \tag{2.28}$$

With $a(\omega) = \frac{1+g(\omega)e^{-i\phi(\omega)}}{2}$ we obtain thus

$$a(-\omega) = a^*(\omega) \tag{2.29}$$

and with $b(\omega) = 1 - a^*(\omega)$ we also obtain

$$b(-\omega) = 1 - a(\omega). \tag{2.30}$$

Therefore, the received signal at frequency $\omega$ can be expressed as

$$Y(\omega) = a(\omega)X(\omega) + b(\omega)X^*(-\omega). \tag{2.31}$$

Note that the properties from equations (2.27) and (2.28) only hold for IQ imbalance in the IF stage. If the receiver is also affected by frequency independent IQ imbalance in the RF stage, these equations are not valid to express the total IQ

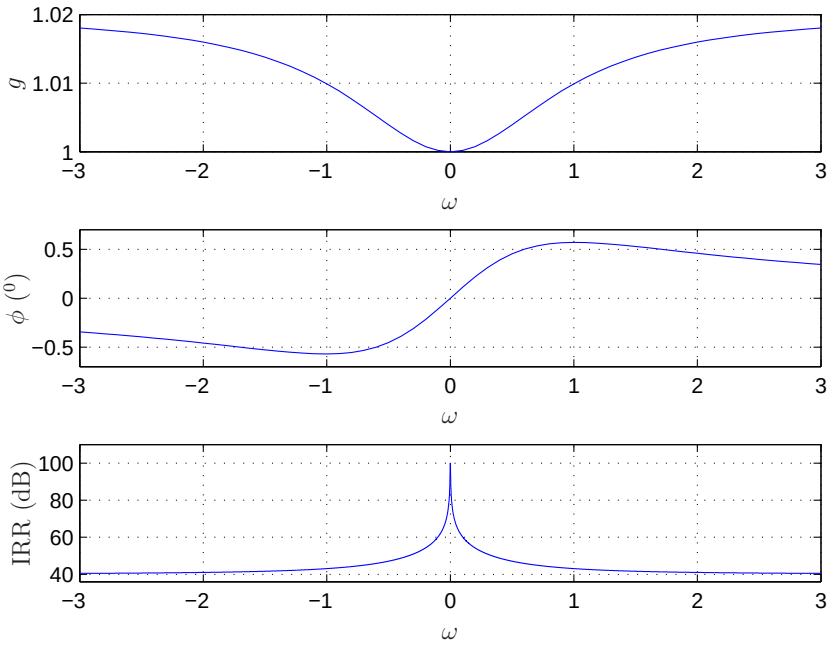


Figure 2.3: Frequency selective IQ imbalance in the receiver caused by a mismatch of the cut off frequencies in the IF low pass filters. Top: gain error, middle: phase error, bottom: image rejection ratio.

imbalance of the receiver. In that case, the total IQ imbalance of the system can be expressed as

$$\begin{aligned} a(\omega) &= \frac{1 + g_{\text{IF}}(\omega) g_{\text{RF}} e^{-i(\phi(\omega_{\text{IF}}) + \phi_{\text{RF}})}}{2} \\ &= \frac{1 + g_{\text{IF}}(\omega) g_{\text{RF}} e^{-i\phi(\omega_{\text{IF}})} e^{-i\phi_{\text{RF}}}}{2} \end{aligned} \tag{2.32}$$

and for negative frequencies we find

$$\begin{aligned} a(-\omega) &= \frac{1 + g_{\text{IF}}(-\omega) g_{\text{RF}} e^{-i\phi(-\omega_{\text{IF}})} e^{-i\phi_{\text{RF}}}}{2} \\ &= \frac{1 + g_{\text{IF}}(\omega) g_{\text{RF}} e^{i\phi(\omega_{\text{IF}})} e^{-i\phi_{\text{RF}}}}{2}. \end{aligned} \tag{2.33}$$

where $g_{\text{IF}}(\omega)$ and $\phi_{\text{IF}}(\omega)$ express the IQ imbalance occurring in the IF stage and $g_{\text{RF}}$ and $\phi_{\text{RF}}$ express the IQ imbalance occurring in the RF stage. In this case, a straightforward relationship between $a(\omega)$ and $a(-w)$ does not exist.

### 2.1.4 Time varying IQ imbalance

In the previous section we have discussed frequency selective IQ imbalance, which is the effect that the gain and phase errors have different values when measured at a different frequency. The assumption there was that those values were constant over time. Time varying IQ imbalance on the other hand, is the effect that the values for the gain and phase errors at a certain frequency can change over time, for example due to ageing or due to a change in temperature. This change in temperature can be caused for instance by moving the chip to a different environment or switching on or off some parts of the chip.

When mitigating IQ imbalance using digital estimation, a higher image rejection ratio will also mean that the system is more sensitive to changes in IQ imbalance parameters. Such a system will therefore need to update or re-estimate the IQ imbalance parameters more often.

For this project however, we will limit ourselves by assuming that the IQ imbalance does not change over time.

### 2.1.5 Typical numbers

In the previous sections, we have theoretically derived several models for IQ imbalance. In this section, we will briefly discuss the typical values that one can expect for those parameters in an actual receiver.

In a state of the art quadrature receiver without advanced analog IQ filtering, the phase error ($\phi$) in the RF stage is in the order of a few degrees, worst case about $3^0$. The gain error ($\delta$) in such a system is in the order of a few percent, worst case about 3%. These errors are caused by component mismatches, temperature gradients and/or LO timing errors. Figure 2.4 shows the real and imaginary parts of $b$ and the image rejection ratio as colormaps for $g = 0.95 - 1.05$ and $\phi = -5 - 5^0$.

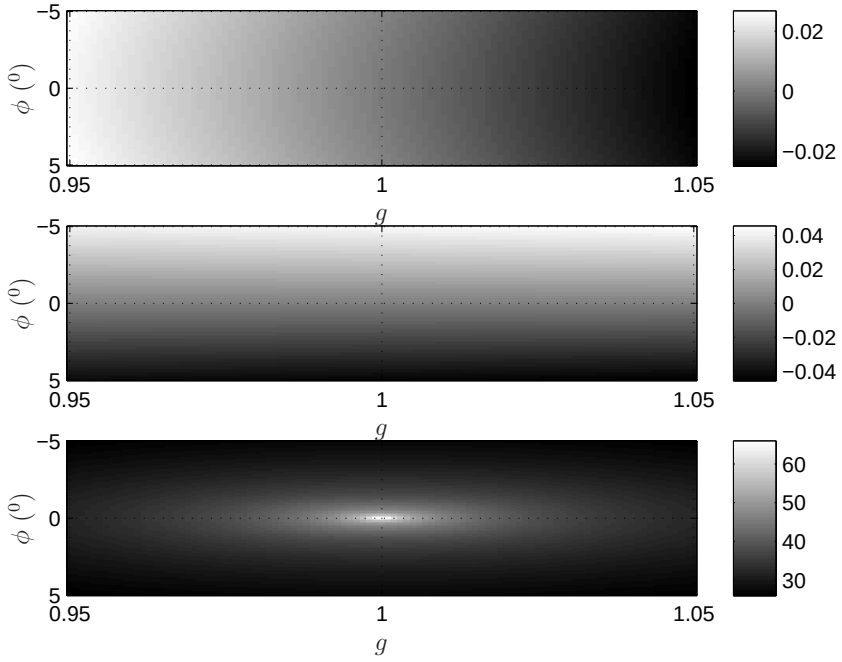


Figure 2.4: Image rejection ratio parameters for different values of $g$ and $\phi$. Top: real part of $b$, middle: imaginary part of $b$, bottom: image rejection ratio (dB).

Using equations (2.17) and (2.18) to calculate parameters $a$ and $b$, we find that for $\phi = 3^0$ and $\delta = 3\%$, $a = 1.0143 - 0.0270i$ and thus $b = -0.0143 - 0.0270i$. This results in an IRR for the RF stage in the order of 30 dB.

For the IF stage, the cutoff frequency is often limited by the mismatch in resistors and capacitors, which is can be up to 1%. With 1% mismatch for both resistors and capacitors, the gain mismatch of two simple first order low pass filters is 1% and the mismatch in cutoff frequency is 2.01%. This results in an IRR for the IF stage varying between 46 dB at DC and 39 dB at the cutoff frequency, as shown in figure

2.3.

Therefore, in a typical quadrature receiver, the frequency independent IQ imbalance in the RF stage will be dominant, but if one wants to achieve very high image rejection ratios, the frequency dependent IQ imbalance in the IF stage should be accounted for.

## 2.2 Mitigation methods

As the previous section showed, IQ imbalance can limit the performance of a wireless receiver. There are several methods to reduce the impact of IQ imbalance in receivers:

- better matching between inphase and quadrature branches and better orthogonality between the LO signals,
- tunable RF band pass filter to reduce the image before down conversion,
- polyphase filter between mixer outputs and ADC inputs,
- digital estimation and correction using test tones ,
- digital estimation and correction using pilot tones ,
- digital estimation and correction using data structure ,
- digital estimation and correction using signal structure ,
- digital estimation and correction using statistical signal properties ,
- digital estimation and correction using deliberate LO self mixing.

Better matching between inphase and quadrature branches and better orthogonality between the LO signals is often not possible, since the inphase and quadrature branches often already have a careful layout on chip, and orthogonality of the LO signals is one of the design parameters. This gives an IRR of 30 to 40 dB, which is not enough for some systems, and additional methods such as listed above are needed to increase the IRR. We will discuss these methods briefly.

### 2.2.1 Tunable band pass filter

A traditional method to improve the image rejection ratio is to include a tunable band pass filter (BPF) before the mixer, as indicated in figure 2.1. The main purpose of this filter filter is to reduce the image component. However, such a filter can have very strong requirements. For example, if the receiver operates at an IF frequency of 200 kHz and the RF frequency of the signal of interest is 1900.2 MHz, the image will be located at 1899.8 MHz. If the receiver has an IRR of 30 dB without this filter, and the intended IRR is 50 dB, the band pass filter should reduce the signal at 1899.8 MHz with 20 dB, while leaving the signal at 1900.2 MHz unaffected. Unfortunately, a tunable filter with such requirements is very difficult to integrate on chip and therefore this method was discarded for this project.

### 2.2.2 Polyphase filter in IF stage

Another method to reduce the impact of IQ imbalance is to apply a polyphase filter between mixer outputs and ADC inputs. A polyphase filter will reduce the image signal, since it suppresses negative frequency components while leaving positive frequency components unaffected. However, since this filter can only be applied after the mixer, it cannot improve the IRR of the mixer and the LO. Any IQ imbalance in the mixer and the LO, which typically are the most dominant contributors to the total IQ imbalance in the system, therefore has already caused image leakage in the received signal and this cannot be undone by this filter. The total impact of a polyphase filter on the total system performance with respect to IQ leakage is thus very limited.[1]

### 2.2.3 Digital estimation methods

With the increase of digital computation power and better integration of analog and digital circuits, a recent trend is to use digital methods to estimate the IQ imbalance parameters.

A simple but important observation for digital estimation is that the DSP which performs the computations needs either some information about the structure or statistics of the signal or it needs test tones. We will classify the digital estimation methods based on the type of information that it exploits.

[1] Note however that the use of a polyphase filter can be very beneficial if it is necessary to reduce a very strong image signal in order to prevent clipping of the ADC. This is therefore usually the prime reason of integrating a polyphase filter.

One of the properties of a digital estimator is whether the receiver needs to be switched off during estimation. If it needs to be switched of, the method is called an offline method and the receiver cannot receive data while performing the estimation. If the receiver does not need to be switched off, the method is an online method and the receiver can receive data while performing the estimation.

**Digital estimation using test tones**

The most intuitive way to digitally estimate IQ imbalance parameters is to use a test tone. This test tone should be a frequency close to the LO frequency and should be injected just before the RF input of the mixer (or earlier). This method is used for example by Maeda in [8] to compensate for IQ imbalance in the receiver and by Liu in [9] to compensate for IQ imbalance in a MIMO OFDM transmitter. The advantages of using test tones are:

- simple and straight forward estimation of IQ imbalance parameters,
- completely standard independent,
- very fast,
- possibility to estimate frequency dependent IQ imbalance,

The disadvantages are:

- offline,
- risk of LO pulling to test tone frequency,
- risk of radiation of test tone due to leakage of test tone to antenna,
- spectral purity of the test tone requires a big silicon area, which increases costs,
- additional hardware needed to generate test tone.

**Digital estimation using pilot tones**

Instead of generating a test tone on chip, it is also possible to use pilot tones present in the received signal. Such tones are present for example in IEEE 802.11g wireless LAN signals. The advantages of using these pilot tones are:

- very fast,
- possibility to estimate frequency dependent IQ imbalance,
- online.

The disadvantages are:

- very standard dependent,
- may require a large buffer (depending on the location of the pilot tones).

Methods based on this principle used for example by Schenk in [10] to compensate for frequency selective IQ imbalance in both transmitter and receiver, by Schoonen in [7] to compensate for IQ imbalance in both transmitter and receiver, by Tubbax in [11] to compensate for IQ imbalance in the receiver and by Tarighat in [12] to compensate for frequency selective IQ imbalance in the receiver.

**Digital estimation using data structure**

Since most systems today use digital modulation, the signal is in principle limited to a finite number of levels (2 for an FSK modulated signals for example, and 16 for 16QAM). Deviations from these levels are caused amongst others by noise, nonlinear distortions and IQ imbalance. When IQ imbalance is the main source of these deviations, decision feedback can be used to estimate the IQ imbalance parameters. This is used for example by Schoonen in [7]. The advantages are:

- very fast,
- possibility to estimate frequency dependent IQ imbalance,
- online.

The disadvantages are:

- very standard dependent.

### Digital estimation using signal structure

If all signals from the standards that the multi-standard receiver should work with, have constant modulus, a possible solution can be to use a method based on the constant modulus algorithm. This algorithm, as described for example by Van der Veen in [13], is typically used to spatially separate two sources which transmit at the same frequency, but it might be possible to modify this method to separate the wanted and the interfering signal in an IQ imbalance impaired receiver. The main assumption for this system would be that both the wanted and the interfering signal have a constant modulus. The advantages are:

- works with multiple systems (as long as the individual baseband signals are constant modulus),
- online.

The disadvantages are:

- slow convergence,
- not completely standard independent[2].

Since the requirements for our method are that it is very fast and completely standard independent, this method was not further investigated.

### Digital estimation using statistical signal properties

The most common technique for a truly standard independent method is to exploit the differences in the variances and covariance caused by IQ imbalance in the received signals. This method is used for example by Wetzker in [14], by Windisch in [4] and in an actual 90 nm GSM implementation by Elahi in [15]. A low complexity implementation of this method is used by Moseley in [16]. A similar method, but with a different approach is used by Yu in [17]. In [5], Finol uses a very low complexity statistical method to compensate the gain and phase errors in analog domain. All previously mentioned references use such methods to estimate frequency independent IQ imbalance, but it is also possible to use this principle to estimate frequency selective IQ imbalance, as proposed by Valkama in [18].

The advantages of this method are are:

[2]This method is not completely standard independent, since more modern standards use non-constant modulus signals to increase bandwidth efficiency

- completely standard independent,
- online,
- works also when there is no signal present (only noise originating from the antenna and LNA),
- can be used to track time varying IQ imbalance.

The disadvantages are:

- very slow convergence.

Since the requirements for our method included a very fast convergence, this solution was initially rejected. However, because it is such a popular method, this method is included as a reference in this report in chapter 4. In that chapter we will also show a way to increase the rate of convergence and we will show a derivation of this method to estimate frequency selective IQ imbalance.

**Digital estimation using deliberate LO self mixing**

From reviewing the digital estimation methods above, one could conclude that the stronger the requirement for standard independency, the slower the convergence of the estimate will be, with the exception of the method which uses test tones. If both standard independency and very fast convergence are very strong requirements, a method which works by only considering the received signal will not be sufficient.

In this report we will present a method which uses the signals from the LO as test tones to estimate the IQ imbalance parameters. The advantages of this method are

- completely standard independent,
- very fast.

The disadvantages are

- offline,
- not possible to estimate frequency selective IQ imbalance,
- rather complicated method,

- performance depends on the shape of the LO signals.

Compared to the method which uses test tones, this method has no risk of LO pulling. Although there is a risk of radiating the LO signal, in most standards some LO leakage radiation is allowed. Furthermore, no additional test tone generator hardware is needed. This method will be discussed in more detail in chapter 5.

### 2.2.4 Method selection

From the class of digital mitigation methods, only the methods which use test tones, statistical properties or which use deliberate LO self mixing are truly standard independent. Since the disadvantages of using test tones were considerable, we decided to discard this method and to focus only on methods which use the statistical properties of the received signal or which use deliberate LO self mixing. These methods will be explained in the following chapters. In the next section, compensation methods which can be used in combination with digital estimation methods will be discussed.

## 2.3 Digital compensation methods

The class of digital estimation methods discussed in the previous section require a compensation method. In this section, we will discuss two methods to compensate for IQ imbalance which can be used in a digital feed-forward estimator-compensator combination: the first method operates on the time domain description of a received signal, while the second method operates on the frequency domain description. Since the latter method operates in frequency domain, it can easily be used to compensate for frequency selective IQ imbalance. Furthermore, at the end of this section, a formula will be derived for the image rejection ratio that can be achieved when the accuracy of the estimated parameters is limited.

### 2.3.1 Time domain compensation

If the receiver has perfect knowledge of the parameters $a$ and $b$, a trivial compensation method is to simply invert the imbalance equations.

For the received signal, we can write the time domain equations as expressed in equation (2.19) as

$$\begin{pmatrix} y^*(t) \\ y(t) \end{pmatrix} = \boldsymbol{M} \begin{pmatrix} x^*(t) \\ x(t) \end{pmatrix} \tag{2.34}$$

where

$$\boldsymbol{M} = \begin{pmatrix} a^* & b^* \\ b & a \end{pmatrix}. \tag{2.35}$$

Thus, we can obtain the least squares estimates of $x(t)^*$ and $x(t)$ by inverting the matrix $\boldsymbol{M}$ in this equation:

$$\begin{pmatrix} \hat{x}^*(t) \\ \hat{x}(t) \end{pmatrix} = \boldsymbol{M}^{-1} \begin{pmatrix} y^*(t) \\ y(t) \end{pmatrix}, \tag{2.36}$$

where $\hat{x}(t)$ is the estimate of $x(t)$.

If the receiver is only interested in signal $x(t)$, it is sufficient to compute

$$\hat{x}(t) = \frac{1}{d}\left(a^* y(t) - b y^*(t)\right) \tag{2.37}$$

where $d$ is the determinant of $\boldsymbol{M}$, defined as

$$\begin{aligned} d &= \det \begin{pmatrix} a^* & b^* \\ b & a \end{pmatrix} \\ &= |a|^2 - |b|^2 \\ &= 2a_{\mathrm{r}} - 1. \end{aligned} \tag{2.38}$$

Note that here we used the identity $a = 1 - b^*$ and that $a_{\mathrm{r}}$ indicates the real part of $a$. For typical values of $a$, the determinant $d$ is close to 1. Hence, for typical values of IQ imbalance, the inverse does exist.

### Implementation costs

Implementing the compensation algorithm shown in equation 2.37 requires two complex multipliers and one adder. These multipliers cannot be shared, unless the clock frequency of the DSP is doubled. Furthermore, the DSP needs to calculate once the inverse of the determinant. If the calculation of this division is allowed to take a relatively long time, this can be implemented using only additions by using a restoring division algorithm, as shown by Goldschmidt in [19].

If faster division is needed, one could use for example the Newton-Raphson method, which requires an additional multiplier.

### 2.3.2 Frequency domain compensation

When it is more convenient to apply the IQ imbalance compensation in frequency domain, for example, for certain OFDM systems or when the receiver is limited by frequency selective IQ imbalance, one can write the equations for frequency selective IQ imbalance in frequency domain, as expressed in equation (2.31), as

$$\begin{pmatrix} Y^*(-\omega) \\ Y(\omega) \end{pmatrix} = \boldsymbol{M}(\omega) \begin{pmatrix} X^*(-\omega) \\ X(\omega) \end{pmatrix} \tag{2.39}$$

where

$$\boldsymbol{M}(\omega) = \begin{pmatrix} a^*(-\omega) & b^*(-\omega) \\ b(\omega) & a(\omega) \end{pmatrix}. \tag{2.40}$$

Therefore, we can obtain $X^*(-\omega)$ and $X(\omega)$ by inverting the matrix $\boldsymbol{M}(\omega)$ in this equation. If the receiver is only interested in signal $X(\omega)$, it is sufficient to compute

$$\hat{X}(\omega) = \frac{1}{d(\omega)} \left( a^*(-\omega)Y(\omega) - b(\omega)Y^*(-\omega) \right) \tag{2.41}$$

where $\hat{X}(\omega)$ is the estimate of $X(\omega)$ and $d(\omega)$ is the determinant of $\boldsymbol{M}(\omega)$:

$$\begin{aligned} d(\omega) &= \det\left(\boldsymbol{M}(\omega)\right) \\ &= a^*(-\omega)a(\omega) - b^*(-\omega)b(\omega). \end{aligned} \tag{2.42}$$

The implementation costs of this algorithm are similar to the implementation costs of the time domain compensation algorithm.

Both this method and the time domain method can be done purely in digital domain. There may be other compensation techniques in digital, analog or mixed digital/analog domain than the ones shown above. However, since the main focus of this work is on estimating the imbalance parameter $a$, we will not investigate the compensation aspect any further in this document.

### 2.3.3 Image rejection ratio gain

If the receiver has imperfect estimates of the imbalance parameters, a residual image will be present after compensation. In this section we will calculate what the image rejection ratio will be after compensating with these imperfect estimates. In this section, we will assume the system is impaired with frequency independent IQ

imbalance. However, a similar analysis can be made for imperfect estimates for the frequency selective IQ imbalance parameters.

Suppose the receiver makes an error $\varepsilon$ in estimating $a$, i.e.

$$\hat{a} = a + \varepsilon \tag{2.43}$$

and thus

$$\hat{b} = b - \varepsilon^* \tag{2.44}$$

where $\varepsilon$ is complex valued.

In that case, the receiver only has an estimate of the imbalance matrix $\boldsymbol{M}$:

$$\hat{\boldsymbol{M}} = \begin{pmatrix} \hat{a}^* & \hat{b}^* \\ \hat{b} & \hat{a} \end{pmatrix}. \tag{2.45}$$

The determinant of this matrix is

$$\begin{aligned} \hat{d} &= |\hat{a}|^2 - |\hat{b}|^2 \\ &= 2\Re\{a + \varepsilon\} - 1 \\ &= 2a_{\mathrm{r}} + 2\varepsilon_{\mathrm{r}} - 1 \end{aligned} \tag{2.46}$$

with $a = a_{\mathrm{r}} + ia_{\mathrm{i}}$ and $\varepsilon = \varepsilon_{\mathrm{r}} + i\varepsilon_{\mathrm{i}}$.

The estimate of signal $x(t)$ after compensation is then

$$\begin{aligned} \hat{x}(t) &= \frac{d - \varepsilon}{d} x(t) + \frac{\varepsilon^*}{d} x^*(t) \\ &= \alpha x(t) + \beta x^*(t) \end{aligned} \tag{2.47}$$

with $\beta = 1 - \alpha^*$.

The image rejection ratio (IRR) after compensation is thus

$$\begin{aligned} \mathrm{IRR}_{\mathrm{post}} &= 10 \log_{10} \left( \frac{|\alpha|^2}{|\beta|^2} \right) \\ &= 10 \log_{10} \left( \frac{(2a_{\mathrm{r}} - 1)^2 + 2\varepsilon_{\mathrm{r}}(2a_{\mathrm{r}} - 1) + |\varepsilon|^2}{|\varepsilon|^2} \right). \end{aligned} \tag{2.48}$$

This equation predicts the IRR of a receiver after compensation with an estimate of $a$ when this estimate has an error $\varepsilon$. The gain in image rejection ratio is

$$\mathrm{IRR}_{\mathrm{gain}} = \mathrm{IRR}_{\mathrm{post}} - \mathrm{IRR}_{\mathrm{pre}} \tag{2.49}$$

with

$$\mathrm{IRR}_{\mathrm{pre}} = 10 \log_{10} \left( \frac{|a|^2}{|b|^2} \right). \tag{2.50}$$

## 2.4 Estimator and compensator requirements

In the previous sections, we have discussed several mitigation methods. In this section we will discuss in more detail the requirements that those methods should meet for a multi-standard radio receiver.

For a system that can handle GSM, GPRS, EDGE, UMTS and LTE and which should be as standard independent as possible, as discussed in chapter A.1, it is clear that it should have at least an IRR which satisfies all these standards. When the LO frequency in the receiver is chosen such that the adjacent channel coincides with the frequency of the image signal, the GSM standard mandates the largest IRR of 50 dB, as shown by Maeda in [8].

While the gain and phase mismatch can change slightly over frequency and time, we can for simplicity assume that the dominant errors are frequency and time independent.

The requirements for the estimator and compensator were given as:

- the method should achieve at least 50 dB IRR for frequency independent IQ imbalance and under the assumption that the IQ imbalance parameters do not change over time,
- the method should have at least 100 times faster convergence speed than the well known statistical methods,
- it should be possible to integrate the method on chip,
- the method should not use test tones, generated with additional test tone generation hardware,
- the method should be completely standard independent.

## 2.5 Summary

In this chapter, we derived a time domain model for IQ imbalance in the analog front-end of a wireless receiver. The model showed the effect of gain and phase errors in the analog front-end on the received signal, under assumption that these errors were time and frequency independent. We have also shown a similar model for a frequency domain description of the received signal, such as is often used in ODFM systems, and we derived a frequency domain description for frequency

selective gain and phase errors in the IF front-end, which typically occur when the IF filters have a cutoff frequency mismatch.

We have also given an overview of mitigation methods where we paid special attention to methods which used digital estimation and compensation. Furthermore, we derived an equation for the image rejection ratio when the estimation accuracy is limited and we concluded this chapter with a list of requirements for the mitigation method for this project.

# Chapter 3

# Source neglecting method

A very intuitive approach to estimating IQ imbalance parameters could be to assume that the interfering signal ($X(-\omega)$) is much stronger than the wanted signal ($X(\omega)$). Since $X(-\omega)$ is very strong, the received signal $Y(\omega)$ will have a strong leakage component originating from $X(-\omega)$; the power of the leaked signal is possibly even larger than the signal power of $X(\omega)$. However, the received signal $Y(-\omega)$ will hardly have any leakage from $X(\omega)$ and it will be very easy to decode $Y(-\omega)$. The method of source neglecting assumes that there is no leakage at all on signal $X(-\omega)$, and this signal could be used as a pure reference to estimate the IQ imbalance parameters.

This chapter show why this approach is not a very good approach and why more effort is needed to find an appropriate standard independent estimator.

## 3.1 Derivation

In frequency domain, the problem can be described as

$$\begin{pmatrix} Y^*(-\omega) \\ Y(\omega) \end{pmatrix} = \begin{pmatrix} a^* & b^* \\ b & a \end{pmatrix} \begin{pmatrix} X^*(-\omega) \\ X(\omega) \end{pmatrix} \tag{3.1}$$

for two narrowband signals $X(-\omega)$ and $X(\omega)$ at frequencies $-\omega$ and $\omega$.

The method now assumes that the leakage of $X(\omega)$ onto $X(-\omega)$ can be neglected, and that $Y(-\omega)$ is clean, in other words: it assumes that the previous equation can be approximated by

$$\begin{pmatrix} Y^*(-\omega) \\ Y(\omega) \end{pmatrix} \approx \begin{pmatrix} a^* & 0 \\ b & a \end{pmatrix} \begin{pmatrix} X^*(-\omega) \\ X(\omega) \end{pmatrix}. \tag{3.2}$$

Furthermore, this method assumes that

$$Y(-\omega) + Y^*(\omega) = X(-\omega) + X^*(\omega) \tag{3.3}$$

can be approximated by

$$Y(-\omega) + Y^*(\omega) \approx X(-\omega). \tag{3.4}$$

Now $a$ can be estimated (approximately) by calculating

$$\hat{a} = \frac{Y(-\omega)}{Y(-\omega) + Y^*(\omega)}. \tag{3.5}$$

## 3.2 Residual error

In the previous section, we derived an estimator for the IQ imbalance parameter $a$, assuming that the leakage signal from the weakest signal can be neglected. However, if we use this estimate to compensate for IQ imbalance using the compensator as described in section 2.3.2, it will not completely cancel the interference from signal $X(-\omega)$ onto $X(\omega)$. The amount of interference that is left depends on the type of signals and the exact realization of the signals. Hence, we can conclude now that this method is not very accurate neither very standard independent and a different approach is needed to find a standard independent estimator.

# Chapter 4

# Statistical methods

This chapter will discuss estimation algorithms based on the statistical properties of the received signals. Section 4.1 will discuss some basic statistical signal properties. In section 4.2 an algorithm which operates on signals in time domain to estimate frequency independent IQ imbalance will be discussed, followed by a very similar algorithm based on signals in frequency domain representation in section 4.3. Furthermore, the frequency domain algorithm will be extended to estimate frequency selective IQ imbalance in section 4.4.

Additionally, algorithms from the models presented in chapter 2 will be derived, it will be prove that they converge to the correct values, their rate of convergence will be analyzed and the results will be compared using simulations. Furthermore, a method to increase the rate of convergence for this class of estimators will be proposed in section 4.3.1.

This chapter will end with a short summary of the results and findings.

## 4.1 Statistical properties

The expectation of a stochastic signal $x(t)$ is defined as

$$\begin{aligned} \mathrm{E}[x(t)] &= \int_{-\infty}^{\infty} x(t)dt \\ &= \mu_x. \end{aligned} \tag{4.1}$$

The variance of signal $x(t)$ is defined as

$$\begin{aligned} \mathrm{var}[x(t)] &= \mathrm{E}[(x(t)-\mu_x)(x(t)-\mu_x)^*] \\ &= \mathrm{E}[x(t)x^*(t)] - \mu_x\mu_x^* \\ &= \sigma_x^2, \end{aligned} \tag{4.2}$$

where $(x(t)-\mu_x)^*$ is the complex conjugate of $(x(t)-\mu_x)$.

The covariance of these two signals is defined as

$$\begin{aligned} \mathrm{cov}\left[x(t)y^*(t)\right] &= \mathrm{E}\left[(x(t)-\mu_{\mathrm{x}})(y(t)-\mu_{\mathrm{y}})^*\right] \\ &= \mathrm{E}[x(t)y^*(t)] - \mu_x\mu_y^*. \end{aligned} \tag{4.3}$$

Note that for most wireless standards, the expectation of the transmitted complex baseband signal is 0, and therefore, the expectation, variance and covariance reduce to

$$\mathrm{E}[x(t)] = 0, \tag{4.4}$$

$$\mathrm{var}[x(t)] = \mathrm{E}[x(t)x^*(t)] \tag{4.5}$$

and

$$\mathrm{cov}[x(t)y^*(t)] = \mathrm{E}[x(t)y^*(t)]. \tag{4.6}$$

When $x(t)$ and $y(t)$ are also real valued signals, the variance and covariance reduce to

$$\mathrm{var}[x(t)] = \mathrm{E}[x^2(t)] \tag{4.7}$$

and

$$\mathrm{cov}[x(t)y(t)] = \mathrm{E}[x(t)y(t)]. \tag{4.8}$$

These properties will be used extensively in the next sections.

## 4.2 Frequency independent IQ imbalance estimation using time domain signal descriptions

The time domain system model for frequency independent IQ imbalance as derived in section 2.1.1 can be written as a combination of a real and an imaginary part:

$$\begin{aligned} y(t) &= ax(t) + bx^*(t) \\ &= x_{\mathrm{I}}(t) + i(2a_{\mathrm{i}}x_{\mathrm{I}}(t) + (2a_{\mathrm{r}} - 1)x_{\mathrm{Q}}(t)). \end{aligned} \tag{4.9}$$

Thus we find for the real part of the received signal

$$y_{\mathrm{I}}(t) = x_{\mathrm{I}}(t) \tag{4.10}$$

and for the imaginary part

$$y_{\mathrm{Q}}(t) = 2a_{\mathrm{i}}x_{\mathrm{I}}(t) + (2a_{\mathrm{r}} - 1)x_{\mathrm{Q}}(t). \tag{4.11}$$

The variance of the real part is

$$\mathrm{E}\left[y_{\mathrm{I}}^2(t)\right] = P_{x_{\mathrm{I}}}, \tag{4.12}$$

and of the imaginary part, it is

$$\mathrm{E}\left[y_{\mathrm{Q}}^2(t)\right] = 4a_{\mathrm{i}}^2 P_{x_{\mathrm{I}}} + (2a_{\mathrm{r}} - 1)^2 P_{x_{\mathrm{Q}}}, \tag{4.13}$$

where $\mathrm{E}\left[z(t)\right]$ is the expectation of signal $z(t)$ and $P_{x_{\mathrm{I}}}$ is the power of the received signal in the inphase branch and $P_{x_{\mathrm{Q}}}$ is the power of the received signal in the quadrature branch. Furthermore, the covariance of signals $y_{\mathrm{I}}(t)$ and $y_{\mathrm{Q}}(t)$ is

$$\mathrm{E}\left[y_{\mathrm{I}}(t)y_{\mathrm{Q}}(t)\right] = 2a_{\mathrm{i}}P_{x_{\mathrm{I}}}. \tag{4.14}$$

Assume now that $P_{x_{\mathrm{Q}}} = P_{x_{\mathrm{I}}}$, which holds when the transmitted data $x_{\mathrm{I}}(t)$ is independent of $x_{\mathrm{Q}}(t)$. This is true for most wireless receiver systems which do not synchronize the LO signal with the received signal. We can then estimate the imaginary part of $a$ with

$$\hat{a}_{\mathrm{i}} = \frac{\mathrm{E}\left[y_{\mathrm{I}}(t)y_{\mathrm{Q}}(t)\right]}{2\,\mathrm{E}\left[y_{\mathrm{I}}^2(t)\right]} \tag{4.15}$$

and the real part with

$$\hat{a}_{\mathrm{r}} = \frac{\sqrt{R} + 1}{2} \tag{4.16}$$

where

$$R = \frac{\mathrm{E}\left[y_{\mathrm{Q}}^2(t)\right] - 2\hat{a}_{\mathrm{i}}\,\mathrm{E}\left[y_{\mathrm{I}}(t)y_{\mathrm{Q}}(t)\right]}{\mathrm{E}\left[y_{\mathrm{I}}^2(t)\right]}. \tag{4.17}$$

The assumption here is that $\mathrm{E}\left[y_{\mathrm{Q}}^2(t)\right] - 2\hat{a}_{\mathrm{i}}\,\mathrm{E}\left[y_{\mathrm{I}}(t)y_{\mathrm{Q}}(t)\right] \geq 0$. This assumption is valid since $\mathrm{E}\left[y_{\mathrm{Q}}^2(t)\right] - 2\hat{a}_{\mathrm{i}}\,\mathrm{E}\left[y_{\mathrm{I}}(t)y_{\mathrm{Q}}(t)\right] = (2a_{\mathrm{r}} - 1)^2 P_{x_{\mathrm{I}}}$ and $a_{\mathrm{r}} \in \mathbb{R}$.

The method described above is used for example by Wetzker in [14], and a computationally more efficient method is used by Moseley in [16].

In an actual implementation, the expectations for $y_{\mathrm{I}}^2(t)$, $y_{\mathrm{Q}}^2(t)$ and $y_{\mathrm{I}}(t)y_{\mathrm{Q}}(t)$ can be estimated by calculating the sample mean for these signals, i.e. $E = \frac{1}{N}\sum_{n=1}^{N} z[n]$ is the sample mean for $z[n]$, the sampled version of $z(t)$ with $z[n] = z(n/f_{\mathrm{s}})$. $z(t)$ here, can be $y_{\mathrm{I}}^2(t)$, $y_{\mathrm{Q}}^2(t)$ or $y_{\mathrm{I}}(t)y_{\mathrm{Q}}(t)$. It can be proven that the sample mean estimator is optimum from a maximum likelihood point of view, and because $\mathrm{E}[y(t)] = 0$, this estimator is also unbiased.

Since this method is sensitive to DC offsets, it is recommended to perform a static DC offset calibration on the received signal $y(t)$ before calculating the variances and covariance, or to perform an online blind DC offset calibration for example by using

$$\tilde{y}(t) = y(t) - \mathrm{E}\left[y(t)\right] \tag{4.18}$$

and to calculate the statistical properties from equations (4.12) - (4.14) based on signal $\tilde{y}(t)$ instead of $y(t)$.

### Implementation costs

An implementation of this algorithm requires three multipliers to calculate the sample means. These multipliers cannot be shared without increasing the clock speed of the DSP. Once the sample means are calculated, the DSP needs to calculate one division, for which one of the multipliers can be reused. Furthermore, a square root needs to be calculated, which can be implemented for example by using the Newton-Raphson method as shown by Kaw in [20]. This method requires one multiplier, for which also one of the multipliers can be reused. Therefore, this algorithm requires only three multipliers to implement.

### 4.2.1 Rate of convergence

The statistical method for frequency independent IQ imbalance, as derived in the previous section is rather simple and convergence of the means to the correct estimate is guaranteed when the receiver can take an infinite number of samples. In reality however, this is not possible and thus the receiver will never have a perfect estimate of $a$ and thus the image rejection ratio will always be finite.

In order to predict how large the IRR will be when the receiver has $N$ samples, with $N < \infty$, we need an expression for the rate of convergence of the estimate of $a$. This is an expression for the number of samples that are needed to achieve a certain accuracy of $\hat{a}$, assuming that the input signals are sampled at the Nyquist rate. This expression can be used to derive an expression for the expected IRR. Unfortunately, deriving a equation for the rate of convergence for the time domain estimator is not trivial and in fact it is easier to do in the frequency domain.

In section 4.3.1 we will analyze the rate of convergence for the algorithm based on calculating statistical properties of the received signals in frequency domain, and there we will also show a derivation for the expected IRR as function of the number of samples $N$ and the power of the received signals. For now, it is sufficient to revert to simulations and to present the equation for an approximation of the expectation of the IRR:

$$\mathrm{E}\left[\mathrm{IRR}_{\mathrm{post}}\right] \approx 10 \log_{10}\left(\frac{4N(P_{\mathrm{n}} + P_{\mathrm{p}})^2}{P_{\mathrm{n}} P_{\mathrm{p}}}\right). \tag{4.19}$$

In this equation $P_{\mathrm{n}}$ is the power of the received signal on the negative side of the spectrum, $P_{\mathrm{p}}$ is the power of the received signal on the positive side of the spectrum and $N$ is the number of samples. The assumption here is that the sample frequency is twice the cutoff frequency $f_{\mathrm{b}}$ of the IF filters and that the spectral densities of the received signals from $-f_{\mathrm{b}}$ to 0 and from 0 to $f_{\mathrm{b}}$ are both uniform.

Figure 4.1 shows the result of simulations which compute the image rejection ratios after compensation for different power levels of the input when the input signal $x(t)$ is noise with a complex Gaussian distribution $x(t) \sim \mathrm{N}(0, \mathrm{P_n} + \mathrm{P_p})$, where 0 is the expectation of $x(t)$ and $P_{\mathrm{n}} + P_{\mathrm{p}}$ is its variance. The horizontal axis shows the number of samples and the vertical axis shows the image rejection ratio. The horizontal line indicates the image rejection ratio before compensation, the noisy line indicates the IRR after compensation and the slanted line without marks shows the expected IRR according to equation (4.19).

As we can see from these figures, the IRR scales logarithmically with the number of samples and with the difference in power of $P_{\mathrm{n}}$ and $P_{\mathrm{p}}$ (in dB). Furthermore,

we observe that the expected IRR from equation (4.19) coincides very well with the results of the simulations.

We conclude now that, depending on the power levels of the received signals, the receiver needs to collect $10^1$ to $10^5$ samples to achieve an IRR of 50 dB, and $10^2$ to $10^6$ samples to achieve 60 dB.

## 4.3 Frequency independent IQ imbalance estimation using frequency domain signal descriptions

The frequency independent IQ imbalance model as derived in section 2.1.2 can be rewritten in discrete frequency domain as

$$Y_k = aX_k + bX^*_{-k} \tag{4.20}$$

where $k$ is the frequency index and $X_k = X\left(\frac{2k}{NT}\right)$ (with $-N/2 \leq k < N/2$) is the discrete time Fourier transform of $x(t)$, $T$ is the sampling period and $N$ is the number of samples.

The complex conjugate of the received signal at frequency index $-k$ is

$$Y^*_{-k} = a^* X^*_{-k} + b^* X_k. \tag{4.21}$$

Combining these two equations we find the property

$$Y_k + Y^*_{-k} = X^*_{-k} + X_k. \tag{4.22}$$

Assume now that $X_k$ and $X_{-k}$ are statistically independent and have unknown signal powers $P_k$ and $P_{-k}$. Furthermore, assume that the input signals contain signal components occurring only on frequencies $\frac{2k}{NT}$, such that no spectral leakage occurs when applying a discrete Fourier transform. This is valid for example in typical OFDM systems.

We then find for the covariance of $Y_k + Y^*_{-k}$

$$\mathrm{E}\left[|Y_k + Y^*_{-k}|^2\right] = P_k + P_{-k} \tag{4.23}$$

and for the covariance of $Y_k$ and $Y^*_{-k}$

$$\mathrm{E}\left[Y_k Y_{-k}\right] = ab(P_k + P_{-k}). \tag{4.24}$$

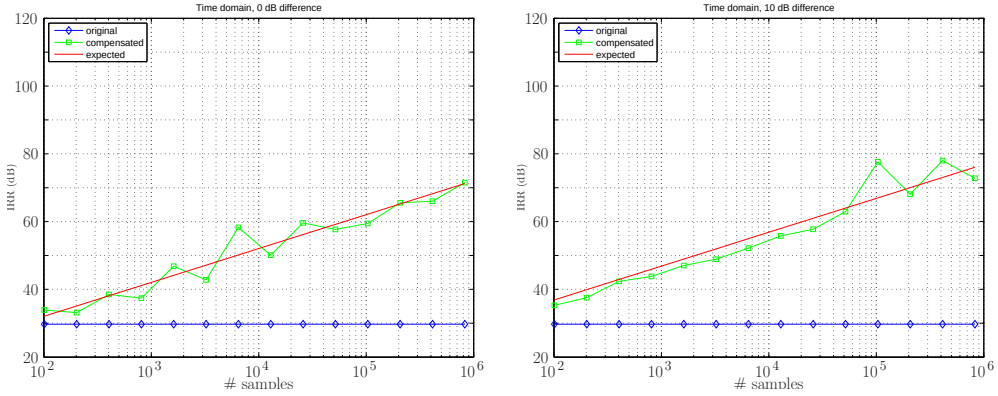


a: $P_{\mathrm{p}} = 0$ dB, $P_{\mathrm{n}} = 0$ dB




b: $P_{\mathrm{p}} = 0$ dB, $P_{\mathrm{n}} = 10$ dB

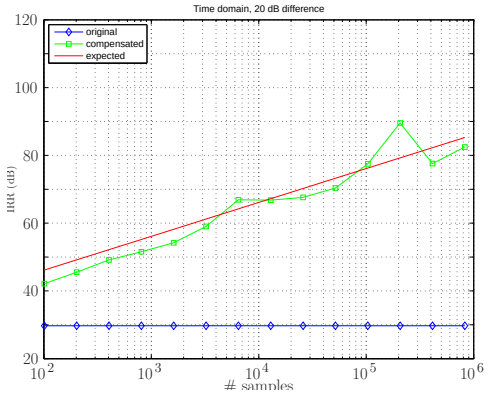


c: $P_{\mathrm{p}} = 0$ dB, $P_{\mathrm{n}} = 20$ dB

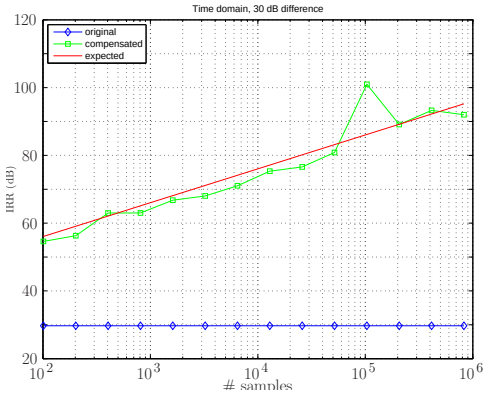


d: $P_{\mathrm{p}} = 0$ dB, $P_{\mathrm{n}} = 30$ dB

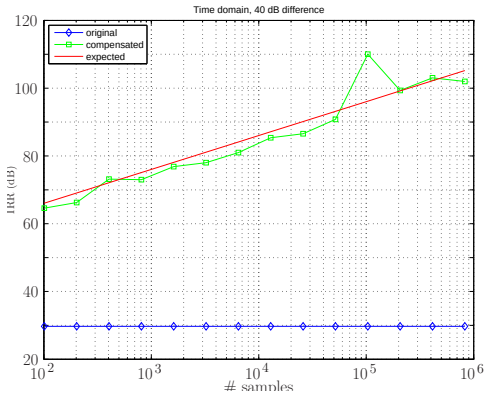


e: $P_{\mathrm{p}} = 0$ dB, $P_{\mathrm{n}} = 40$ dB

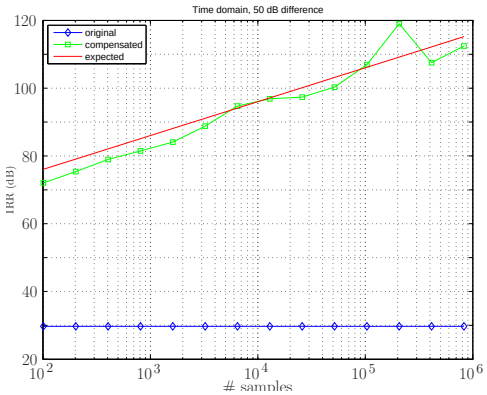


f: $P_{\mathrm{p}} = 0$ dB, $P_{\mathrm{n}} = 50$ dB

Figure 4.1: IRR achieved by the frequency independent IQ imbalance estimator using statistical properties of time domain signals versus the number of samples for different power levels of the received signals.

From the ratio $R = \frac{\mathrm{E}[Y_k Y_{-k}]}{\mathrm{E}\left[|Y_k + Y_{-k}^*|^2\right]}$, we now find

$$\begin{aligned} R &= \frac{\mathrm{E}\left[Y_k Y_{-k}\right]}{\mathrm{E}\left[|Y_k + Y_{-k}^*|^2\right]} \\ &= ab \\ &= a - |a|^2 \end{aligned} \tag{4.25}$$

where we again used the property $b = 1 - a^*$. Note that this ratio is independent of frequency index $k$.

Writing $a = a_\mathrm{r} + i a_\mathrm{i}$, we find

$$R = a_\mathrm{r} - a_\mathrm{r}^2 - a_\mathrm{i}^2 + i a_\mathrm{i}. \tag{4.26}$$

Thus, if we also split $R$ in real and imaginary parts with $R = R_\mathrm{r} + i R_\mathrm{i}$, we can estimate the I/Q imbalance parameters $a_\mathrm{r}$ and $a_\mathrm{i}$ with

$$\hat{a}_\mathrm{i} = R_\mathrm{i} \tag{4.27}$$

and

$$\hat{a}_\mathrm{r} = \frac{1}{2} \pm \frac{1}{2}\sqrt{1 - 4(\hat{a}_\mathrm{i}^2 + R_\mathrm{r})}. \tag{4.28}$$

For this method, it is easy to see that when either $X_k = 0$ or $X_{-k} = 0$ (in other words: when there is no interfering signal), the estimate of $a$ is converged to the correct value already after two samples.

In an actual implementation, the expectation of signal $Z_k$ can be estimated using the sample mean of $Z_k$: $E = \frac{1}{N}\sum_{n=1}^{N} Z_{k,n}$ where $Z_{k,n} = Y_k Y_{-k}$ or $Z_{k,n} = |Y_k + Y_{-k}^*|^2$. It can be proven that this estimator is optimum in maximum likelihood sense, and since $\mathrm{E}[Y_k] = \mathrm{E}[Y_{-k}] = 0$, the sample mean estimator is also unbiased.

Note that this method, in contrast to the time domain based method of the previous section, is independent of DC offsets.

### Implementation costs

Implementation of this method requires two complex multipliers to calculate the sample means. Once the sample means are calculated, one division, multiplier and one square root are needed to estimate $a_\mathrm{r}$ and $a_\mathrm{i}$. The division method can be implemented using Newton-Raphson, which requires one multiplier. This multiplier can be reused from the previous multipliers. Once this division is calculated, the same multiplier can be used to calculate $\hat{a}_\mathrm{i}$, and after that, again the same multiplier can be used to calculate the square root function by using for example Newton-Raphson.

### 4.3.1 Rate of convergence

#### Theoretical analysis

As we have observed in simulations in section 4.2.1, the rate of convergence of the time domain statistical method depends on the number of samples $N$ and on the power levels $P_{\mathrm{n}}$ and $P_{\mathrm{p}}$ of the received signals. In this section, we will analyze the rate of convergence of the method presented in the previous section depending on $N$ and $P_{\mathrm{n}}$ and $P_{\mathrm{p}}$. Note that we assume in this analysis that the signals are sampled at the Nyquist rate, that we have received $N$ samples and that we take an $N$-point DFT to have a frequency domain description of this signal.

The method shown in the previous section calculates

$$\begin{aligned} R &= \frac{E_{\mathrm{p}}}{E_{\mathrm{s}}} \\ &= \frac{\mathrm{E}\left[Y_k Y_{-k}\right]}{\mathrm{E}\left[|Y_k + Y_{-k}^*|^2\right]}. \end{aligned} \tag{4.29}$$

The numerator is calculated by taking the mean for $N$ samples by

$$\begin{aligned} E_{\mathrm{p}} &= \frac{1}{N}\sum_{k=1}^{N} Y_k Y_{-k} \\ &= ab\frac{1}{N}\sum_{k=1}^{N}\left(|X_k|^2 + |X_{-k}|^2\right) + a^2\frac{1}{N}\sum_{k=1}^{N} X_{-k}X_k + b^2\frac{1}{N}\sum_{k=1}^{N} X_{-k}^* X_k^*. \end{aligned} \tag{4.30}$$

When $X_{-k}$ and $X_k$ have a complex Gaussian distribution with zero mean and variances $P_{-k}$ and $P_k$ respectively, then $|X_{-k}|^2$ and $|X_k|^2$ have a Chi square distribution with 2 degrees of freedom, as shown by Proakis in [21], noted as

$$\begin{aligned} |X_k|^2 &\sim \chi_2^2(P_k, P_k^2) \\ |X_{-k}|^2 &\sim \chi_2^2(P_{-k}, P_{-k}^2) \end{aligned} \tag{4.31}$$

where $P_k$ and $P_k^2$ are the mean and variance of $|X_k|^2$, and $P_{-k}$ and $P_{-k}^2$ are the mean and variance of $|X_{-k}|^2$, respectively. Furthermore, both $X_{-k}X_k$ and $X_{-k}^* X_k^*$ have a normal product distribution with zero mean and variance $P_{-k}P_k$.

The denominator is calculated by

$$\begin{aligned} E_{\mathrm{s}} &= \frac{1}{N}\sum_{k=1}^{N}|Y_{-k}^{*}+Y_k|^2 \\ &= \frac{1}{N}\sum_{k=1}^{N}\left(|X_k|^2+|X_{-k}|^2\right)+\frac{1}{N}\sum_{k=1}^{N}X_{-k}X_k+\frac{1}{N}\sum_{k=1}^{N}X_{-k}^{*}X_k^{*}. \end{aligned} \tag{4.32}$$

The ratio $R$ is then

$$\begin{aligned} R = ab\frac{\frac{1}{N}\sum_{k=1}^{N}\left(|X_{-k}|^2+|X_k|^2\right)}{\frac{1}{N}\sum_{k=1}^{N}\left(|X_{-k}|^2+|X_k|^2\right)+\frac{1}{N}\sum_{k=1}^{N}X_{-k}X_k+\frac{1}{N}\sum_{k=1}^{N}X_{-k}^{*}X_k^{*}}+ \\ a^2\frac{\frac{1}{N}\sum_{k=1}^{N}X_{-k}X_k}{\frac{1}{N}\sum_{k=1}^{N}\left(|X_{-k}|^2+|X_k|^2\right)+\frac{1}{N}\sum_{k=1}^{N}X_{-k}X_k+\frac{1}{N}\sum_{k=1}^{N}X_{-k}^{*}X_k^{*}}+ \\ b^2\frac{\frac{1}{N}\sum_{k=1}^{N}X_{-k}^{*}X_k^{*}}{\frac{1}{N}\sum_{k=1}^{N}\left(|X_{-k}|^2+|X_k|^2\right)+\frac{1}{N}\sum_{k=1}^{N}X_{-k}X_k+\frac{1}{N}\sum_{k=1}^{N}X_{-k}^{*}X_k^{*}} \end{aligned} \tag{4.33}$$

which can also be written as

$$\begin{aligned} R = ab-ab\frac{2\Re\left\{\frac{1}{N}\sum_{k=1}^{N}X_{-k}X_k\right\}}{\frac{1}{N}\sum_{k=1}^{N}\left(|X_{-k}|^2+|X_k|^2\right)+2\Re\left\{\frac{1}{N}\sum_{k=1}^{N}X_{-k}X_k\right\}}+ \\ a^2\frac{\frac{1}{N}\sum_{k=1}^{N}X_{-k}X_k}{\frac{1}{N}\sum_{k=1}^{N}\left(|X_{-k}|^2+|X_k|^2\right)+2\Re\left\{\frac{1}{N}\sum_{k=1}^{N}X_{-k}X_k\right\}}+ \\ b^2\frac{\frac{1}{N}\sum_{k=1}^{N}X_{-k}^{*}X_k^{*}}{\frac{1}{N}\sum_{k=1}^{N}\left(|X_{-k}|^2+|X_k|^2\right)+2\Re\left\{\frac{1}{N}\sum_{k=1}^{N}X_{-k}X_k\right\}}. \end{aligned} \tag{4.34}$$

This equation shows the limit value of $R$, which is $ab$, and the error in $R$ when $N$, the number of samples, is limited.

Using the property

$$|p|^2+|q|^2+2\Re\{pq\}\le 2\left(|p|^2+|q|^2\right) \tag{4.35}$$

we find $R\le R_{\mathrm{UB}}$ with

$$\begin{aligned} R_{\mathrm{UB}} = ab+ \\ \frac{a^2\frac{1}{N}\sum_{k=1}^{N}X_{-k}X_k-2ab\Re\left\{\frac{1}{N}\sum_{k=1}^{N}X_{-k}X_k\right\}+b^2\frac{1}{N}\sum_{k=1}^{N}X_{-k}^{*}X_k^{*}}{2\frac{1}{N}\sum_{k=1}^{N}\left(|X_{-k}|^2+|X_k|^2\right)}. \end{aligned} \tag{4.36}$$

We have seen before that $|X_{-k}|^2$ and $|X_k|^2$ are Chi square distributed. Using the central limit theorem according to Montgomery in [22] and Weisstein in [23], we then find that $2\frac{1}{N}\sum_{k=1}^{N}\left(|X_{-k}|^2+|X_k|^2\right)$ is Gaussian distributed with mean $2\left(P_{-k}+P_k\right)$ and variance $\frac{4\left(P_{-k}^2+P_k^2\right)}{N}$. When $N$ is large, this variance will be small and $\frac{1}{\frac{1}{N}\sum_{k=1}^{N}(|X_{-k}|^2+|X_k|^2)}$ can be approximated with

$$\frac{1}{2\frac{1}{N}\sum_{k=1}^{N}\left(|X_{-k}|^2+|X_k|^2\right)} \approx \frac{1}{2\left(P_{-k}+P_k\right)}. \tag{4.37}$$

For typical values of IQ imbalance, $a$ is close to 1 and thus $b$ and $ab$ are close to 0, and therefore, the term $a^2\frac{1}{N}\sum_{k=1}^{N}X_{-k}X_k$ will have the largest influence on the error term in $R_{\mathrm{UB}}$. Thus, we approximate $R_{\mathrm{UB}}$ with

$$R_{\mathrm{UB}} \approx ab + a^2\frac{1}{2\left(P_{-k}+P_k\right)}\frac{1}{N}\sum_{k=1}^{N}X_{-k}X_k. \tag{4.38}$$

We have also seen that $X_{-k}X_k$ is distributed according to the zero mean normal product distribution, with variance $P_{-k}P_k$. Using the central limit theorem, we find that $a^2\frac{1}{2(P_{-k}+P_k)}\frac{1}{N}\sum_{k=1}^{N}X_{-k}X_k$ has variance $\frac{a^4P_{-k}P_k}{4N(P_{-k}+P_k)^2}$, which, for practical values of $a$, is close to $\frac{P_{-k}P_k}{4N(P_{-k}+P_k)^2}$. Therefore, the error term $\varepsilon$ in the estimate of $a$ has a complex Gaussian distribution with zero mean and variance

$$\sigma_\varepsilon^2 \approx \frac{P_{\mathrm{n}}P_{\mathrm{p}}}{4N(P_{\mathrm{n}}+P_{\mathrm{p}})^2}. \tag{4.39}$$

Recall from equation (2.48) in section 2.3.3 that the image rejection ratio after compensation is

$$\mathrm{IRR}_{\mathrm{post}} = 10\log_{10}\left(\frac{(2a_{\mathrm{r}}-1)^2+2\varepsilon_r(2a_{\mathrm{r}}-1)+|\varepsilon|^2}{|\varepsilon|^2}\right). \tag{4.40}$$

Since $\varepsilon$ is complex Gaussian distributed, $|\varepsilon|^2$ is Chi square distributed with two degrees of freedom. The mean of $|\varepsilon|^2$ is $\sigma_\varepsilon^2$, and its variance is $\sigma_\varepsilon^4$.

For practical values of $a$ we have $a \approx 1$, hence $(2a_{\mathrm{r}}-1)$ is close to 1, and we can approximate the expected image rejection ratio after compensation with

$$\begin{aligned}\mathrm{IRR}_{\mathrm{post}} &\approx 10\log_{10}\left(\frac{(2a_{\mathrm{r}}-1)^2}{|\varepsilon|^2}\right)\\ &\approx 10\log_{10}\left(\frac{1}{|\varepsilon|^2}\right).\end{aligned} \tag{4.41}$$

For the expected IRR, we now deduce

$$\mathrm{E}\left[\mathrm{IRR}_{\mathrm{post}}\right] \approx 10\log_{10}\left(\frac{4N(P_{\mathrm{n}}+P_{\mathrm{p}})^2}{P_{\mathrm{n}}P_{\mathrm{p}}}\right). \tag{4.42}$$

This equation confirms our result from the previous section that when either $P_{\mathrm{n}}$ or $P_{\mathrm{p}}$ is 0 (thus, when there is no interfering signal), the estimate of $a$ is converged to the correct value already after two samples, and the IRR after compensation is infinite. Furthermore, this equation corresponds well with the equation derived by Windisch in [24].

A plot of the order of the number of samples $N$ that one needs in order to achieve a certain expected IRR given a certain interference level ($P_{\mathrm{p}}$) is shown in figure 4.2. As we can see from this image, if the power of the interfering signal is more than 10 dB larger than the power of the wanted signal, the IRR scales approximately linear with the power of this interfering signal (for a given number of samples).

This leads us to the following conclusion: if the number of samples used for the estimation is fixed, the IRR after compensation scales almost linear with the strength of the interfering signal: if the interfering is 10 dB stronger, the IRR after compensation will also be 10 dB stronger.

Thus, by fixing $N$ to, for example, 1000, the expectation of the IRR after compensation will be approximately 60 dB in case the interfering signal is 30 dB stronger than the wanted signal, but it will only be 40 dB in case the interfering signal is just 10 dB stronger. The IRR is therefore dynamic: high when the interfering signal is high, but low when the interfering signal is also low, and the signal to interference ratio after compensation will be approximately constant.

Therefore, an implementation can be based on a fixed number of samples without having to detect and adapt to the interference level. Note however, that a straightforward implementation of this estimator with a fixed number of samples can have a significant drawback. If a fixed number of samples is used, the target signal to interference ratio (SIR) is reached immediately after the estimation period. However, if after this estimation period, the power level of the interfering signal is increased (or similarly, the power level of the wanted signal is decreased), the SIR after compensation will decrease and can become lower than the target SIR if no additional measures are taken.

### Simulations

Figure 4.3 shows the image rejection ratios for different power levels of the input signals. As we can see from this figure, the IRR for this algorithm also scales

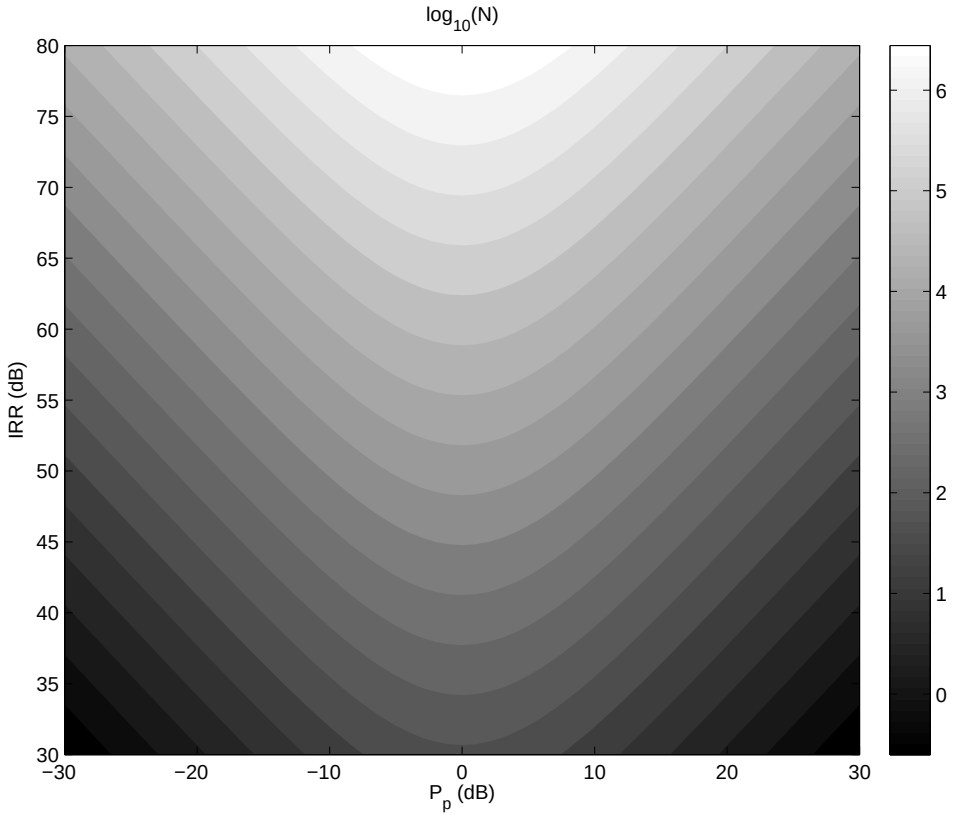


Figure 4.2: Number of samples (indicated by gray values) that are needed to achieve a certain image rejection ratio (on vertical axis) against the power difference between wanted signal and interfering signal (on horizontal axis) (using the time domain statistical method)

logarithmically with the number of samples.

Furthermore, the performance of this algorithm when $P_{\mathrm{p}}$ is 0, 10 or 20 dB, is identical to the performance of the time domain algorithm shown in figure 4.1 and the rate of convergence increases 10 dB for every 10 dB increase of $P_{\mathrm{p}}$. However, if $P_{\mathrm{n}}$ is more than 20 dB larger than $P_{\mathrm{p}}$, the rate of convergence becomes limited: if $P_{\mathrm{n}}$ is 30 dB, we see approximately 5 dB improvement, and when $P_{\mathrm{n}}$ is more than 30 dB, we don't see any improvement at all in the rate of convergence.

The explanation for this saturation of the rate of convergence is that the frequency domain method uses a DFT to transform the time domain samples into a frequency domain signal, and then calculates the covariance of $Y_k$ and $Y_{-k}$. This method assumes that for an $N$ point time domain signal, a corresponding $N$ point DFT is calculated. However, when $N$ is large, this becomes very computationally inefficient. In order to increase the speed of the simulations, we used a block based approach, where the block size of the DFT was significantly smaller than $N$. Simulations confirmed that by increasing the block size, the level at which saturation of the IRR convergence rate occurred was increased and the algorithm came closer to the performance of the time domain statistical method.

We can conclude now that, depending on the power levels of the signals, the receiver needs to collect $10^3$ to $10^5$ samples to achieve an expected IRR of 50 dB, and $10^4$ to $10^6$ samples to achieve 60 dB. This however, does depend on the block size of the DFT.

### Improving the rate of convergence

Equation (4.42) shows the rate of convergence for the estimators derived in sections 4.2 and 4.3. Since these estimators are optimal from a maximum likelihood point of view, the rate of convergence cannot be increased by more advanced filtering of the digital signals. However, we have seen that the expected IRR depends not only on the number of samples, but also on the difference in power in the negative and the positive side of the frequency spectrum. Therefore, by influencing this power spectrum, we can influence the rate of convergence.

One way to influence this power spectrum is to add an adjustable notch filter between the LNA and the mixer. This filter should be adjustable so that during estimation it is always placed on the weakest of both wanted and interfering signal.

Suppose that a receiver needs an IRR of 50 dB. Assuming an input spectrum according to figure 4.4, the receiver would need at least N samples. In this figure, $P_{\mathrm{d}}$ is the difference between the power of the interfering signal and the wanted signal

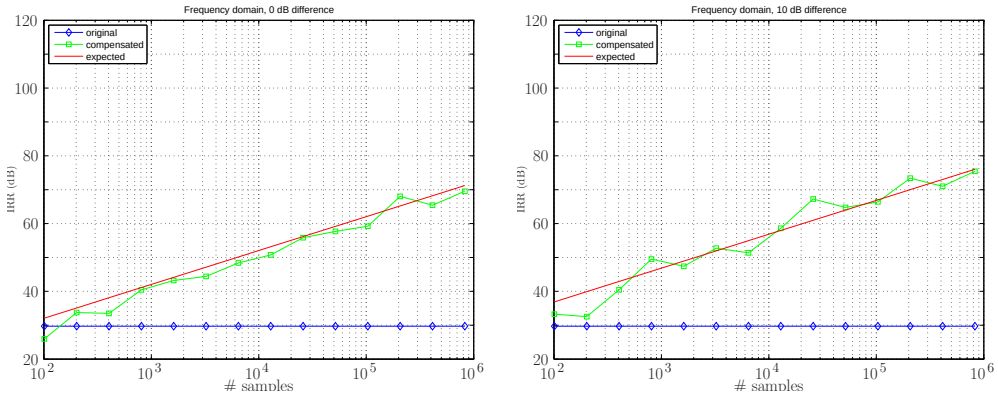


a: $P_{\mathrm{p}} = 0$ dB, $P_{\mathrm{n}} = 0$ dB




b: $P_{\mathrm{p}} = 0$ dB, $P_{\mathrm{n}} = 10$ dB

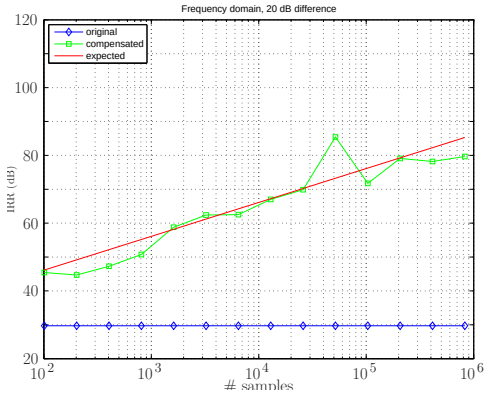


c: $P_{\mathrm{p}} = 0$ dB, $P_{\mathrm{n}} = 20$ dB

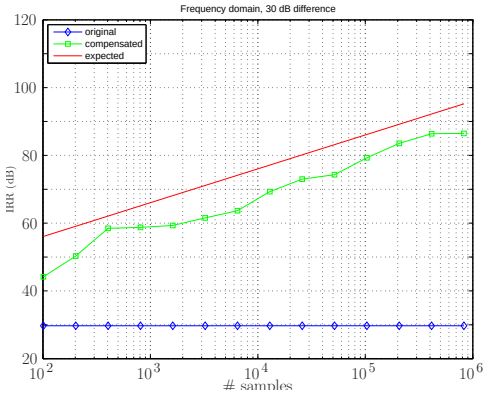


d: $P_{\mathrm{p}} = 0$ dB, $P_{\mathrm{n}} = 30$ dB

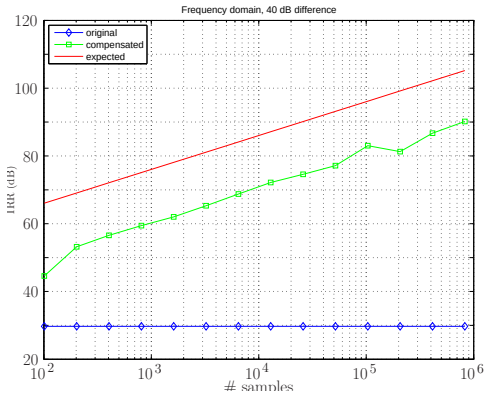


e: $P_{\mathrm{p}} = 0$ dB, $P_{\mathrm{n}} = 40$ dB

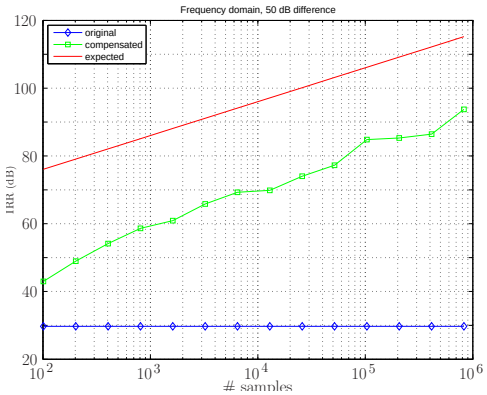


f: $P_{\mathrm{p}} = 0$ dB, $P_{\mathrm{n}} = 50$ dB

Figure 4.3: IRR achieved by the frequency independent IQ imbalance estimator using statistical properties of frequency domain signals versus the number of samples for different power levels of the received signals.

(in dB). For the following section, assume that the power of the interfering signal is much larger than the power of the wanted signal.

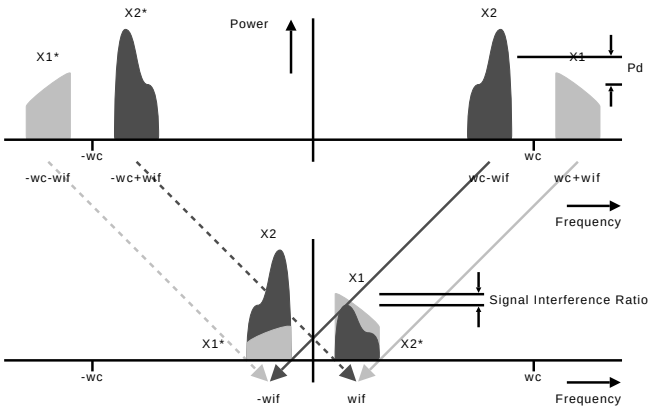


Figure 4.4: Spectrum before and after down conversion.

Assume now that the receiver contains a tunable RF notch filter that attenuates the interfering signal by 3 dB, as indicated by figure 4.5.

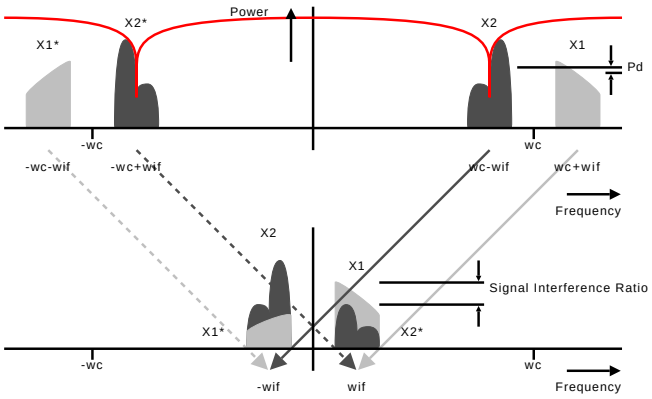


Figure 4.5: Spectrum before and after down conversion when the notch is placed on the interfering signal.

In that case, the IRR that has to be achieved by the rest of the system is reduced by 3 dB. However, since $P_{\mathrm{d}}$ is also reduced by 3 dB, the receiver still needs N samples to achieve a total IRR of 50 dB.

However, if the receiver tunes the notch filter to suppress the wanted signal during estimation, $P_{\mathrm{d}}$ is increased by 3 dB, as is indicated by figure 4.6.

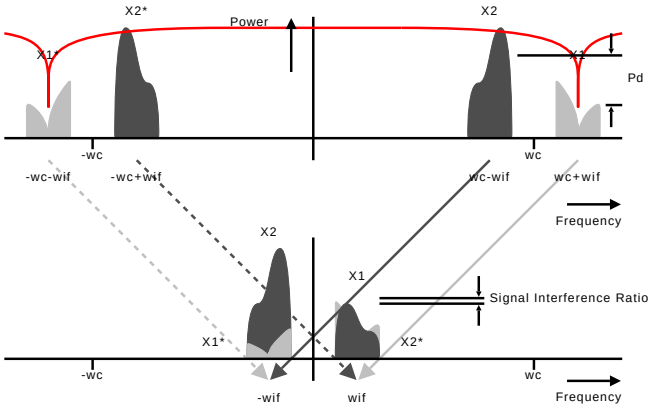


Figure 4.6: Spectrum before and after down conversion when the notch is placed on the interfering signal.

$P_{\mathrm{d}}$ is now 6 dB larger compared to when the notch was placed on the interfering signal. Since the IRR that has to be achieved by the rest of the system (without the notch filter) is 3 dB lower, the number of samples that the receiver needs is reduced by a factor 4.

We can conclude now that by adding a notch filter which suppresses the power of the weakest signal of interfering and wanted signal during estimation time and then moving the notch over to the interfering signal after estimation, the number of samples that are needed to achieve a certain SIR is reduced by approximately a factor of 4 for every 3 dB suppression that this filter will give in case there is a large difference in signal strength between the interfering and the wanted signal. Therefore, in case the interfering signal is the strongest of both, the number of samples that would have to be considered lost is reduced by a factor of 4. Additionally, the estimation time is reduced and thus the system has a shorter start-up delay and needs to perform less calculations.

Note however, that in a practical implementation, a notch filter which suppresses the image with more than 3 dB is very difficult to realize. Suppressions of 1.5 to 3 dB are more realistic, which correspond with a reduction by a factor of 2 to 4. However, this number depends on the IF frequency and the bandwidths of the wanted and interfering signals.

## 4.4 Frequency selective IQ imbalance estimation using frequency domain signal descriptions

In the previous section we have derived a method to estimate the IQ imbalance errors using statistical properties of the received signal in frequency domain. This method results in an estimate of $a$ for every pair of frequency indices $k$ and $-k$ where obviously $\hat{a}_{-k} = \hat{a}_k$, since the IQ imbalance was assumed to be frequency independent. In this section we will derive a method to estimate IQ imbalance errors in case the IQ imbalance is frequency dependent.

In section 2.1.3 we have derived a model for frequency selective IQ imbalance occurring in the IF stages of a receiver. When the received signal is sampled and transformed using a DFT, we obtain the following signal model for the received signal on frequency index $k$

$$Y_k = a_k X_k + b_k X_{-k}^*. \tag{4.43}$$

For completeness, the conjugated received signal on frequency index $-k$ is

$$Y_{-k}^* = a_{-k}^* X_{-k}^* + b_{-k}^* X_k. \tag{4.44}$$

Note that $b_k = 1 - a_k^*$ and thus that $a_k + b_k = 1 + 2\ i\ a_{k,\mathrm{i}}$ and $a_k - b_k = 2a_{k,\mathrm{r}} - 1$. Note also that $|a_k|^2 - |b_k|^2 = 2a_{k,\mathrm{r}} - 1$. These properties will be used in the following derivation.

Please note furthermore that $g_{-k} = g_k$ and $\phi_{-k} = -\phi_k$. This results in $a_{-k} = a_k^*$ and $b_{-k} = b_k^*$ and thus $|a_{-k}|^2 = a_{-k}\ a_{-k}^* = a_k^* a_k = |a_k|^2$.

Assume further that the transmitted signals on frequencies $k$ and $-k$, i.e. $X_k$ and $X_{-k}$, are statistically independent and have unknown signal powers $P_k$ and $P_{-k}$.

Let us now define $E_1$ as the variance of $Y_k + Y_{-k}^*$

$$\begin{aligned} E_1 &= \mathrm{E}\left[|Y_k + Y_{-k}^*|^2\right] \\ &= \mathrm{E}\left[|(a_k + b_k)(X_k + X_{-k}^*)|^2\right] \\ &= (1 + 4a_{k,\mathrm{i}}^2)(P_k + P_{-k}) \end{aligned} \tag{4.45}$$

and $E_2$ as the variance of $Y_k - Y_{-k}^*$

$$\begin{aligned} E_2 &= \mathrm{E}\left[|Y_k - Y_{-k}^*|^2\right] \\ &= \mathrm{E}\left[|(a_k - b_k)(X_k - X_{-k}^*)|^2\right] \\ &= (2a_{k,\mathrm{r}} - 1)^2 (P_k + P_{-k}). \end{aligned} \tag{4.46}$$

The variance of $Y_k$ is $\mathrm{E}\left[|Y_k|^2\right] = |a_k|^2 P_k + |b_k|^2 P_{-k}$. Let us furthermore define $E_3$ as the difference in variance of signals $Y_k$ and $Y_{-k}$:

$$\begin{aligned} E_3 &= \mathrm{E}\left[|Y_k|^2\right] - \mathrm{E}\left[|Y_{-k}|^2\right] \\ &= (|a_k|^2 - |b_k|^2)(P_k - P_{-k}) \\ &= (2a_{k,\mathrm{r}} - 1)(P_k - P_{-k}). \end{aligned} \tag{4.47}$$

Finally, using the covariance of signals $Y_k$ and $Y_{-k}$

$$\mathrm{E}\left[Y_k Y_{-k}\right] = a_k b_k^* P_k + a_k^* b_k P_{-k} \tag{4.48}$$

we define

$$\begin{aligned} E_4 &= \mathrm{E}\left[Y_k^* Y_{-k}^*\right] - \mathrm{E}\left[Y_k Y_{-k}\right] \\ &= (a_k^* b_k - a_k b_k^*)(P_k - P_{-k}) \\ &= 2i\, \Im\left\{a_k^* b_k\right\}(P_k - P_{-k}) \\ &= 2i\, a_{k,\mathrm{i}}(2a_{k,\mathrm{r}} - 1)(P_k - P_{-k}) \end{aligned} \tag{4.49}$$

where $\Im\{x\}$ indicates the imaginary part of $x$.

We can now estimate the imaginary part of $a_k$ using

$$\hat{a}_{k,\mathrm{i}} = -i\frac{E_4}{2E_3}. \tag{4.50}$$

Moreover, using

$$\frac{E_2}{E_1} = \frac{(2a_{k,\mathrm{r}} - 1)^2}{1 + 4a_{k,\mathrm{i}}^2} \tag{4.51}$$

we can estimate the real part of $a_k$ with

$$\hat{a}_{k,\mathrm{r}} = \frac{1}{2} \pm \frac{1}{2}\sqrt{\frac{E_2}{E_1}}\sqrt{1 + 4\hat{a}_{k,\mathrm{i}}^2}. \tag{4.52}$$

Thus, $\hat{a}_k$ is found using $\hat{a}_k = \hat{a}_{k,\mathrm{r}} + i\hat{a}_{k,\mathrm{i}}$, and we obtain $\hat{a}_{-k}$ with $\hat{a}_{-k} = \hat{a}_k^*$.

### Implementation costs

An actual implementation of this algorithm using $K$ frequency bins requires $5K$ complex multipliers to calculate the sample means for every pair of frequencies $k$ and $-k$.

Once the sample means are known, the DSP needs to calculate $\hat{a}_{k,\mathrm{i}}$, for which $K$ multipliers can be reused. At the same time, $K$ other multipliers can be used to calculate $E_2/E_1$ for every frequency pair $k$ and $-k$. Finally, $K$ multipliers can be used to calculate the square root in equation 4.52 to estimate $\hat{a}_{k,\mathrm{r}}$.

The implementation costs for this method are quite modest for one frequency pair and comparable to the implementation costs of the frequency independent estimators. However, the costs can be high if the system needs to calculate the estimates for many frequency pairs, since the costs scale linearly with the number of frequency pairs.

### Nonlinear fitting

The estimator as derived in the previous section results in independent estimates for every frequency pair $k$ and $-k$, in other words: in general, $a_k \neq a_l$ for all $l \neq k$ and $a_k \neq a_l^*$ for all $l \neq -k$. When the number of frequency indices is large and the number of samples relatively small, there are few samples which can be used to estimate $a_k$. This results in quite noisy estimates of $a_k$.

If the frequency selective IQ imbalance is caused by a mismatch in the IF filters the actual cause of this frequency selective behaviour is a mismatch in cutoff frequencies of those filters. Thus, by estimating the cutoff frequencies, we might be able to smooth the IQ imbalance estimates. To do this, we will fit the estimated IQ imbalance errors with the expected filter error transfer function, assuming that the IF filters are first order low pass filters.

Recall first that $a_k = \frac{1+g_k e^{-i\phi_k}}{2}$, and thus the gain error $g$ at frequency index $k$ results from the estimate $a_k$ by calculating

$$\begin{aligned} g_k &= |2a_k - 1| \\ &= \sqrt{4a_{k,\mathrm{r}}^2 - 4a_{k,\mathrm{r}} + 1 + 4a_{k,\mathrm{i}}^2}. \end{aligned} \tag{4.53}$$

The phase error $\phi$ at frequency index $k$ follows from calculating

$$\phi_k = -\arctan\left(\frac{2a_{k,\mathrm{i}}}{2a_{k,\mathrm{r}} - 1}\right). \tag{4.54}$$

The transfer functions of the first order filters in the inphase branch and quadrature

branch are

$$H_{\mathrm{I}} = \frac{K_{\mathrm{I}}}{1 + i\omega/\omega_{\mathrm{I}}} \tag{4.55}$$

$$H_{\mathrm{Q}} = \frac{K_{\mathrm{Q}}}{1 + i\omega/\omega_{\mathrm{Q}}} \tag{4.56}$$

where $K_{\mathrm{I}}$ and $K_{\mathrm{Q}}$ are the gains of the filters and $\omega_{\mathrm{I}}$ and $\omega_{\mathrm{Q}}$ are the cutoff frequencies.

The gain error is then

$$\begin{aligned} g(\omega) &= \frac{|H_{\mathrm{Q}}|}{|H_{\mathrm{I}}|} \\ &= \frac{|K_{\mathrm{Q}}|}{|K_{\mathrm{I}}|} \frac{|1 + i\omega/\omega_{\mathrm{I}}|}{|1 + i\omega/\omega_{\mathrm{Q}}|}. \end{aligned} \tag{4.57}$$

The frequency independent gain error is $g_0 = g(0) = \frac{|K_{\mathrm{Q}}|}{|K_{\mathrm{I}}|}$.

The phases of the signals at the output of the filters are:

$$\phi_{\mathrm{I}}(\omega) = \arctan(-\omega/\omega_{\mathrm{I}}) \tag{4.58}$$

$$\phi_{\mathrm{Q}}(\omega) = \arctan(-\omega/\omega_{\mathrm{Q}}). \tag{4.59}$$

Therefore, the phase error is:

$$\phi(\omega) = \arctan(-\omega/\omega_{\mathrm{Q}}) - \arctan(-\omega/\omega_{\mathrm{I}}). \tag{4.60}$$

Using $\arctan(x) = \frac{i}{2}\left(\ln(1 - ix) - \ln(1 + ix)\right)$, we find:

$$\phi(\omega) = \frac{1}{2} i \left\{\ln(1 + i\omega/\omega_{\mathrm{Q}}) - \ln(1 - i\omega/\omega_{\mathrm{Q}}) - \ln(1 + i\omega/\omega_{\mathrm{I}}) + \ln(1 - i\omega/\omega_{\mathrm{I}})\right\} \tag{4.61}$$

If we now define

$$f(\omega) = e^{-i2\phi(\omega)}, \tag{4.62}$$

we obtain

$$\begin{aligned} f(\omega) &= \frac{(1 + i\omega/\omega_{\mathrm{Q}})(1 - i\omega/\omega_{\mathrm{I}})}{(1 - i\omega/w_Q)(1 + i\omega/\omega_{\mathrm{I}})} \\ &= \frac{1 - i\omega(1/\omega_{\mathrm{I}} - 1/\omega_{\mathrm{Q}}) + \omega^2/(\omega_{\mathrm{I}}\omega_{\mathrm{Q}})}{1 + i\omega(1/\omega_{\mathrm{I}} - 1/\omega_{\mathrm{Q}}) + \omega^2/(\omega_{\mathrm{I}}\omega_{\mathrm{Q}})} \end{aligned} \tag{4.63}$$

or written differently:

$$f(\omega)(1 + i\omega(1/\omega_{\mathrm{I}} - 1/\omega_{\mathrm{Q}}) + \omega^2/(\omega_{\mathrm{I}}\omega_{\mathrm{Q}})) = \\ 1 - i\omega(1/\omega_{\mathrm{I}} - 1/\omega_{\mathrm{Q}}) + \omega^2/(\omega_{\mathrm{I}}\omega_{\mathrm{Q}}) \tag{4.64}$$

We can rewrite this as

$$(f(\omega) + 1)i\omega(1/\omega_{\mathrm{I}} - 1/\omega_{\mathrm{Q}}) + (f(\omega) - 1)\omega^2/(\omega_{\mathrm{I}}\omega_{\mathrm{Q}}) + f(\omega) - 1 = 0. \tag{4.65}$$

If we now use vector notation, where $\underline{f}$ is a vector where the element $f_k$ indicates the value of $f(\omega)$ for frequency $\omega_k$, and $\underline{\omega}$ is a vector with the corresponding frequencies, we find

$$(1 - \underline{f}) = \begin{pmatrix} (\underline{f} + 1)i\underline{\omega} & (\underline{f} - 1)\underline{\omega}^2 \end{pmatrix} \begin{pmatrix} \alpha \\ \beta \end{pmatrix} \tag{4.66}$$

where

$$\alpha = 1/\omega_{\mathrm{I}} - 1/\omega_{\mathrm{Q}} \tag{4.67}$$

and

$$\beta = 1/(\omega_{\mathrm{I}}\omega_{\mathrm{Q}}). \tag{4.68}$$

Let us now define

$$\underline{v} = (1 - \underline{f}) \tag{4.69}$$

$$\boldsymbol{F} = \begin{pmatrix} (\underline{f} + 1)i\underline{\omega} & (\underline{f} - 1)\underline{\omega}^2 \end{pmatrix} \tag{4.70}$$

and

$$\underline{u} = \begin{pmatrix} \alpha \\ \beta \end{pmatrix}. \tag{4.71}$$

We can now write equation (4.66) as a product of matrix $\boldsymbol{F}$ and vector $\underline{u}$:

$$\underline{v} = \boldsymbol{F}\underline{u}. \tag{4.72}$$

In this equation, vector $\underline{v}$ is a $K \times 1$ vector with our observations (where $K$ is the total number of frequency indices), since, after using equations (4.62) and (4.69), $\underline{v}$ contains the phase errors $\phi(\omega_k)$ of all frequency pairs $k$ and $-k$. Furthermore,

$\boldsymbol{F}$ is a $K \times 2$ matrix which contains a combination of phase error observations and frequency indices according to equation (4.70) and $\underline{u}$ is a $2 \times 1$ vector which contains a combination of the cutoff frequency errors which we wish to estimate, according to equations (4.67), (4.68) and (4.71).

Therefore, if we have noisy estimates $\hat{\phi}_k$ for phase error $\phi_k$ for all frequencies $k$, for example, as provided by the algorithm in the previous section, we can smooth the estimates by defining

$$\begin{aligned} \underline{\hat{f}} &= e^{-i2\underline{\hat{\phi}}} \\ \underline{\hat{v}} &= (1 - \underline{\hat{f}}) \\ \hat{\boldsymbol{F}} &= \begin{pmatrix} (\underline{\hat{f}} + 1)i\underline{\omega} & (\underline{\hat{f}} - 1)\underline{\omega}^2 \end{pmatrix} \end{aligned} \tag{4.73}$$

where $\underline{\hat{\phi}}$ is a $K \times 1$ vector with the unsmoothed phase error estimates.

We can now estimate $\alpha$ and $\beta$ with

$$\underline{\hat{u}} = \hat{\boldsymbol{F}}^{\dagger} \underline{\hat{v}} \tag{4.74}$$

where

$$\underline{\hat{u}} = \begin{pmatrix} \hat{\alpha} \\ \hat{\beta} \end{pmatrix} \tag{4.75}$$

and where $\hat{\boldsymbol{F}}^{\dagger}$ is the Moore-Penrose pseudo inverse of $\hat{\boldsymbol{F}}$.

Once $\hat{\alpha}$ and $\hat{\beta}$ known, we can estimate the cutoff frequencies as follows. Using

$$1/\omega_{\mathrm{I}} = \alpha + 1/\omega_{\mathrm{Q}} \tag{4.76}$$

we find

$$\beta - \alpha/\omega_{\mathrm{Q}} - 1/\omega_{\mathrm{Q}}^2 = 0. \tag{4.77}$$

Therefore, the cutoff frequency of the IF filter in the quadrature branch can be estimated with

$$\hat{\omega}_Q = \frac{-2}{\hat{\alpha} \pm \sqrt{\hat{\alpha}^2 + 4\hat{\beta}}} \tag{4.78}$$

and the cutoff frequency of the IF filter in the inphase branch can be estimated with

$$\hat{\omega}_I = \frac{1}{\hat{\alpha} + 1/\hat{\omega}_Q} \tag{4.79}$$

These frequencies can be used to create new estimates for the frequency dependent phase and gain errors, using

$$\hat{\phi}_k = \arctan(-\omega_k/\hat{\omega}_{\mathrm{Q}}) - \arctan(-\omega_k/\hat{w}_{\mathrm{I}}) \tag{4.80}$$

and

$$\hat{g}_k = \hat{g}_0 \frac{|1 + i\omega_k/\hat{\omega}_{\mathrm{I}}|}{|1 + i\omega_k/\hat{\omega}_{\mathrm{Q}}|} \tag{4.81}$$

assuming $\hat{g}_0$ is known.

#### Implementation costs

This algorithm in its current form requires several nonlinear operations, such as $\arctan$ and square roots. Furthermore, the algorithm requires the calculation of the pseudo inverse of a rectangular matrix.

While it is possible to implement this algorithm in dedicated hardware, the costs are significant. Therefore, it is probably more efficient to implement this algorithm on the processor, which can then use idle cycles to use this algorithm to improve the frequency selective estimates. For mobile devices which have a limited battery lifetime, this is most likely not feasible, but for base stations this could be an option.

## 4.5 Combining frequency independent and frequency selective IQ imbalance

In an actual system, a combination of frequency independent IQ imbalance and frequency selective IQ imbalance will occur: the frequency independent IQ imbalance originates from the RF and IF stages and the frequency selective IQ imbalance originates from the IF stages, most notably the IF filters.

Neither the frequency independent nor the frequency selective algorithms presented in the previous sections can estimate the exact gain and phase errors on their own. However, it is possible to combine both methods.

Therefore, we should first estimate the frequency independent errors by using the statistical method described in section 4.3. However, we should only use this method for IF frequencies around 0, since for those frequencies, the gain and phase errors will be relatively frequency independent. This will provide estimates for $g_0$ and $\phi_0$, which are the gain and phase error estimates around $\omega = 0$.

After estimating the frequency independent errors, we should compensate for these estimated gain and phase errors and after compensation the assumptions for the frequency dependent estimator should hold, so the algorithms as described in sections 4.4 and (optionally) 4.4 can be used to estimate the frequency dependent errors.

Figure 4.5 shows the simulation results for this concatenation.

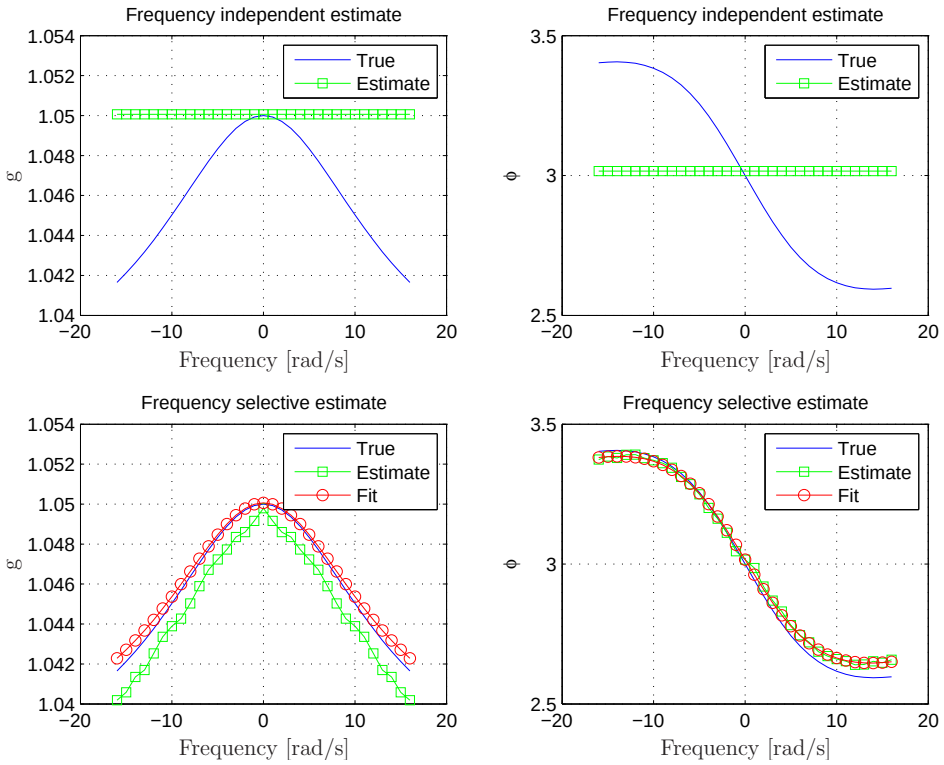


Figure 4.7: Simulation results with 33 subcarriers, $\omega_{\mathrm{I}} = 14.2$ rad/s, $\omega_{\mathrm{Q}} = 14$ rad/s, $K_{\mathrm{I}} = 1.00$, $K_{\mathrm{Q}} = 1.05$, $\phi_0 = 3^0$. Resolution bandwidth is 1 rad/s

The two top figures show the output of the frequency independent estimator. As we can see, the results are close to the actual values for frequency index 0. The two bottom figures show the output of the frequency selective estimator, both with and without the nonlinear fitting. The nonlinear fitting improved the estimation of the phase error a little. However, impact of the nonlinear fitting is more visible on the estimation of the gain error, since the scale of that plot is smaller and small deviations are easier to observe there. The original IRR was 30 dB, and after compensation the IRR over the whole frequency domain was between 63 and 83

dB.

There is one notable disadvantage of this concatenation of estimators. The frequency independent estimator has to be the first estimator, since typically the frequency independent error is the most dominant. However, this estimator can only operate on frequency indices close to 0, to avoid influence of frequency selective IQ imbalance behaviour. Therefore, this estimator will converge very slowly, and the output will be relatively noisy.

Since the frequency selective estimator operates on data which is compensated for frequency independent errors based on this noisy estimate, the performance of the frequency selective estimator will be influenced by this as well.

## 4.6 Summary

In the previous sections we have seen that frequency independent IQ imbalance can be estimated by using statistical properties of the received signals. The estimation can be done both for time domain signals and for frequency domain signals and the estimators can operate on actual signals as well as on noise occurring in the RF stages. The methods are unbiased, and thus in principle, the IRR that can be achieved is unlimited, provided that enough samples can be taken and that the IQ imbalance does not change over time.

The implementation costs of the frequency flat estimators are modest, requiring three real multipliers for the time domain method and two complex multipliers for the frequency domain method.

The rate of convergence was theoretically analyzed and shown in simulations to depend on the difference in power of the desired signal and the interfering signal. It was shown both theoretically and in simulations that if the input signals are sampled at the Nyquist rate and the number of samples is fixed, the expected IRR changes dynamically: the expected IRR will be high when it needs to be high (when there is a strong interfering signal), and will be low when it is allowed to be low (when there is a weak interfering signal).

This dynamic behaviour occurs both for the time domain and for the frequency domain methods. However, in a practical implementation of the frequency domain method, one will most likely use a block based DFT operation with a limited block size (a block size significantly smaller than the total number of samples of the received signal). This limited block size can cause a saturation of the rate of convergence for the frequency domain method, and thus, if very high levels of image

rejection ratio are required, care must be taken that either enough samples are used or that the DFT block size is large enough.

We have also seen that adding a tunable notch filter can increase the rate of convergence. If this notch is placed over the weakest signal of both interfering and wanted signals during estimation and after estimation the notch is moved to the location of the interfering signal, the number of samples that are needed to achieve a certain SIR can be reduced by a factor of 4 for every 3 dB of suppression that this filter gives. This results in a dramatically shorter estimation time, less samples that need to be discarded and less computations in the DSP.

Furthermore, we have derived an estimator for frequency selective IQ imbalance caused by the IF stages and a nonlinear fitting function that can be used to estimate the cutoff frequencies of the IF filters and thereby used to smooth the IQ imbalance estimates.

The implementation costs for these estimators are significantly higher than the implementation costs for the frequency independent estimators. The implementation cost for the basic frequency selective estimator scales linearly with the number of frequency bins for which these estimates have to be computed, while for the nonlinear fitting function, the required operations are so complex that it is more convenient to implement this algorithm in the digital processor of the system. A mobile system which is has a limited battery lifetime might therefore only implement the basic frequency selective estimator to estimate for frequency selective IQ imbalance, while a system which is not limited in power consumption and costs can additionally implement the nonlinear fitting function to improve these estimates. These improvements can be calculated for example in the idle time of the processor of a base station.

Finally, we have shown that the concatenation of the frequency independent and frequency selective methods can be used to estimate the IQ imbalance parameters in a system which is impaired with both frequency independent and frequency selective IQ imbalance. Simulations showed that the image rejection ratio after compensation was between 63 and 83 dB for the whole IF band.

# Chapter 5

# Deliberate LO self mixing method

In this chapter, the principle behind deliberate LO self mixing to estimate IQ imbalance parameters will be discussed. The system model and necessary hardware blocks will be explained in section 5.1 and in section 5.2 signal models for these blocks will be discussed. In section 5.3, estimators for a system based on these models will be derived.

In section 5.4, simulation results for those estimators will be discussed and in section 5.5, the design and implementation of such a system will be shown. Section 5.6 will describe the measurement results from this prototype and this chapter will end with a short summary in section 5.7.

## 5.1 System model

The principal of deliberate LO self mixing for gain and phase error estimation is to use the local oscillator (LO) in the receiver chain to not only drive the LO side of the mixer, but also the LNA input of the mixer. By mixing the LO signal with itself, the result is a signal that contains a DC offset and some components at twice the LO frequency. The signal components at twice the LO frequency will be removed by the IF filters and the amount of DC offset that remains depends on the gain and phase mismatch, as will be explained later.

For this method to work, the receiver needs to be equipped with switches that can select between different RF signals. In figure 5.1, a block diagram is shown for a receiver that has switches at several places and several sources for IQ imbalance. In this system, it is possible to inject an RF signal at the output of the LNA.

Switch S_LNA controls which kind of signal is injected: in position "n", no signal is injected (signal is floating or connected to ground), in position "C" the signal which drives the LO side of the inphase mixer is selected, in position "S" the signal which drives the LO side of the quadrature mixer is selected.

Switch S_OSC selects the signal which drives the LO side of the mixer: in position "C", the inphase mixer is driven with the $0^0$ signal from the LO and the quadrature mixer is driven with the $90^0$ signal; in position "S", those two signals are swapped.

Finally switch S_filter can swap the inputs of the inphase and quadrature low pass filters.

Since the IQ imbalance parameters $g$ and $\phi$ can occur at any part of the system, they are split in different parts and distributed in the block diagram, shown as gray boxes. These boxes labeled with $g_x$ and $\phi_x$ show which signals will be amplified by factor $g_x$ and phase delayed by $\phi_x$. $g_\mathrm{o}$ and $\phi_\mathrm{o}$ represent the gain and phase error in the LO, $g_\tau$, $\phi_\tau$ represent the difference of these errors when switch S_OSC is in the "S" position, $g_\mathrm{i}$, $\phi_\mathrm{i}$ represents the change in gain and phase caused by the injection into the LNA, $g_\mathrm{m}$, $\phi_\mathrm{m}$ represents the gain and phase mismatch between the mixers and finally $g_\mathrm{f}$ represents the gain mismatch in the filter.

Note that in normal operating mode, S_OSC and S_filter are in position C and S_LNA is in position n, and thus only $g_\mathrm{o}$, $\phi_\mathrm{o}$, $g_\mathrm{m}$, $\phi_\mathrm{m}$ and $g_\mathrm{f}$ are influencing the received signal, and therefore only those parameters determine the image rejection ratio (IRR). The IRR can be calculated using equation (2.20), repeated here as reference:

$$\mathrm{IRR}\ [\mathrm{dB}] = 10 \log_{10} \left( \frac{|a|^2}{|b|^2} \right). \tag{5.1}$$

In this equation $b = 1 - a^*$ and

$$a = \frac{1 + g_\mathrm{f} g_\mathrm{o} g_\mathrm{m} e^{-i(\phi_\mathrm{o} - \phi_\mathrm{m})}}{2}. \tag{5.2}$$

Since the exact output of the mixer depends on the behaviour of the switches, the LO and the mixer, we will discuss models for these components in the next section.

## 5.2 Device modeling

### 5.2.1 Switch modeling

The switches used in this circuit are modeled as ideal switches, with infinite isolation in case the switch is open and no loss and no phase delay when closed.

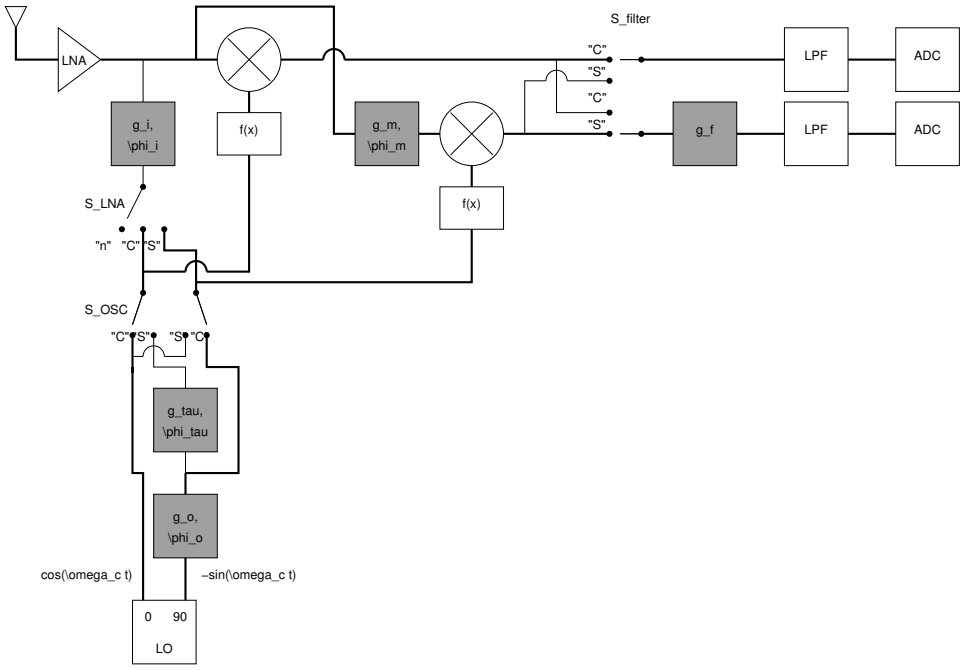


Figure 5.1: Block diagram of a receiver with LO-LNA injection switches and several sources of IQ imbalance

Furthermore, we assume that the switches will not show any frequency selective behaviour in the band of interest, nor that they will introduce any nonlinear distortions.

### 5.2.2 LO modeling

#### Waveform tradeoffs

From a mathematical point of view, a sine wave is ideal to perform a down conversion from RF to IF, since no other frequency components are down converted to the same IF bandwidth. However, in practical implementations often a waveform which more closely resembles a square wave is used, since a square wave has much steeper zero crossings compared to a sine wave. This has three benefits:

- The transistors in the mixer are switched between "on" and "off", and only a very short time is spent in the linear region. Therefore, the amount of signal lost in the switching process is significantly smaller.
- If the driving signal is close to the zero crossing, the output signal is very sensitive to noise. Since for a square wave, the time spent around the zero crossing is very small, the output signal is not very sensitive to additive noise on the LO input.
- Linearity of the mixer is improved. For a mixer driven with a sine wave, the transistors in the mixer are operated in their linear region, but since the transfer curve of a transistor is essentially nonlinear, this region must be very small to reduce nonlinear effects. However, this reduces the conversion gain of the mixer. A mixer driven with a square waveform is not affected by this since the transistors are in either conducting or non-conducting state.

The two major disadvantages of down converting with a square waveform are:

- A square wave contains many odd harmonics and thus signal components at harmonic frequencies received at the antenna input will be down converted as well and fold to the same IF bandwidth as the wanted signal. However, in most cases, these components can be easily filtered out at the RF side before entering the mixer.
- The many harmonics of a square wave require a very large bandwidth. For state of the art systems at 2.4 GHz, there is typically not enough bandwidth

to accurately create a square waveform, and the resulting signal will rather have a more trapezoid like shape. At 60 GHz, the harmonics are at such high frequencies, that virtually no odd harmonics may be present, and the resulting signal looks more like an ideal sine wave.

Considering these advantages and disadvantages, designers typically aim for square wave outputs from the local oscillator, if enough bandwidth in the process is available.

#### Duty cycle

While an ideal square wave has a duty cycle of exactly 50%, this is often very difficult to realize and sometimes even undesired: with a duty cycle of 50%, a small threshold voltage offset in one of the transistors of the mixer can cause that both transistors will be conducting simultaneously, which is very undesired. To avoid this, sometimes a duty cycle less than 50% is chosen. However, in order to achieve a high conversion gain in the mixer, the duty cycle must not be too low. Typically, the duty cycle is between 40 and 50%.

### 5.2.3 Mixer modeling

For the derivation of this method, we distinguish two models for the behaviour of the mixer. In the first case, we model the mixer as a device which multiplies the signal at the RF input with the sign of the differential signal at the LO input. In the second case, we model the mixer as a device which performs an ordinary mathematical multiplication of both signals. We will derive estimation methods for both models.

## 5.3 Estimating IQ imbalance using LO self-mixing

In this section we will derive several estimators to estimate the IQ imbalance parameters for the different device models shown in the previous section. In the derivations we will assume that the received signal after the AD convertor is free of any DC offsets. In an actual implementation, accurate DC offset calibration of the IF stages for all possible positions of the switches is necessary. This can be done for example by not injecting a signal (setting switch S_LNA in position "n") and measuring the received signal for all possible combinations of the other switches.

### 5.3.1 Mixer modeled as sign()-multiplier

In this section, we will evaluate the output signal of the mixer for two types of LO signals: the first is a square wave form with a duty cycle $d$ smaller than 50% and the second is a trapezium wave form with duty cycle of 50%, but with rise and fall times which are larger than 0.

#### Square wave form

Figure 5.2 shows the differential signal of a square wave form with a duty cycle $d$, normalized on one period. In this section, we will first investigate the output signal when the mixer is driven with an LNA signal of this type that is (almost) orthogonal the LO signal, and later on when the LNA signal is (almost) inphase with the LO signal.

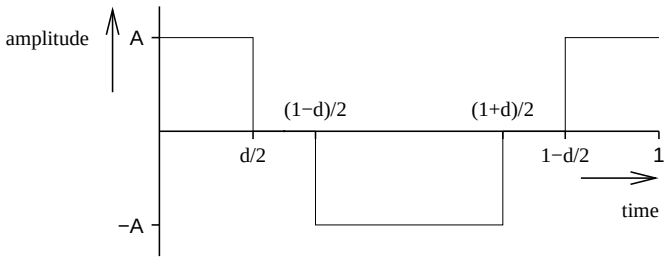


Figure 5.2: Differential LO output signal for square waveform with duty cycle $d < 50\%$.

**Multiplication of two almost orthogonal square wave forms** In this situation, the input signal at the LO port of the mixer is a square wave form as shown in figure 5.2, and the input signal at the LNA port of the mixer is a scaled and almost $90^0$ shifted version of this signal. These signals, as well as the output signal of the mixer, are shown in figure 5.3.

The DC content of the output signal of the mixer is in this case $4\phi gA$, as can be seen by integrating the output signal by one period. Note that it is not necessary to integrate an integer number of periods in case the mixers are followed by low pass filters, as proposed by the system in figure 5.1.

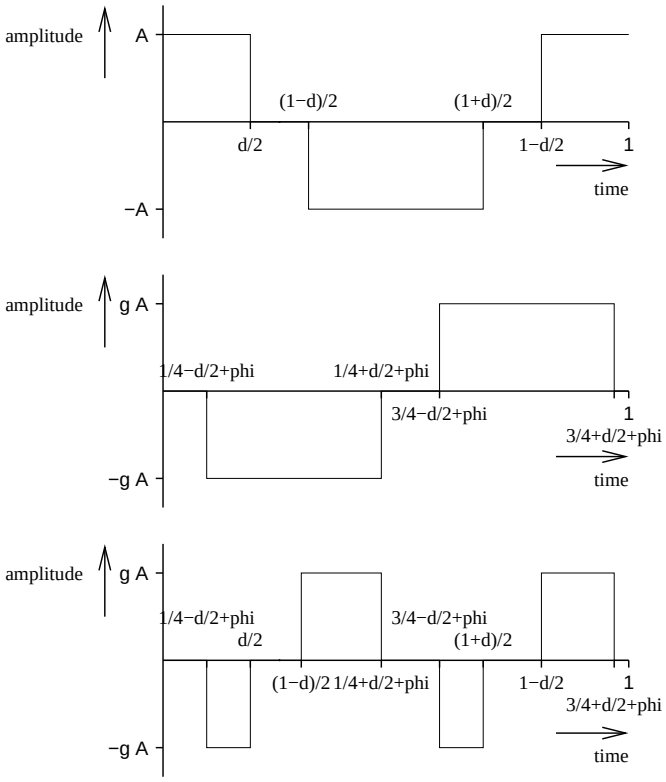


Figure 5.3: Input and output signals for mixer with almost orthogonal signals. Top: input signal at LO port. Middle: input signal at LNA port. Bottom: output signal.

**Multiplication of two almost identical square wave forms** If the input signal at the LO side of the mixer is a square wave form as shown in figure 5.2 and the input at the LNA side is a slightly delayed and scaled version of the same signal, the output of the mixer depends on the amount of phase delay (or phase shift) of the LNA signal. If the phase shift $\phi$ is positive, we can distinguish two cases:

- $0 \leq \phi < \frac{1}{2} - d$: In this case, the zero crossings of the input signals are partially overlapping. The DC content of the output signal is then $2(d - \phi)gA$. This situation is shown in figure 5.4.
- $\frac{1}{2} - d \leq \phi \leq d$: In this case, the zero crossings do not overlap. The DC content of the output signal is then $(1 - 4\phi)gA$. This situation is shown in figure 5.5.

If we also consider negative phase errors, we can distinguish four possible values for the DC content of the output signal of the mixer, as summarized in table 5.1.

Table 5.1: DC content of the output signal of the mixer, depending on phase shift $\phi$ and duty cycle $d$.

| DC content | Conditions |
|---|---|
| $(1 + 4\phi)gA$ | $-d \leq \phi \leq -\left(\frac{1}{2} - d\right)$ |
| $2(d + \phi)gA$ | $-\left(\frac{1}{2} - d\right) < \phi < 0$ |
| $2(d - \phi)gA$ | $0 \leq \phi < \frac{1}{2} - d$ |
| $(1 - 4\phi)gA$ | $\frac{1}{2} - d \leq \phi \leq d$ |

From this we can conclude that if we want to estimate the gain error $g$ and the phase error $\phi$ based on the DC content of the output signal of the mixer with these signals, we need to know in which range $\phi$ will be, and potentially (depending on the range), we also need to know the duty cycle $d$.

For all relevant possible combinations of the oscillator, RF and filter switches, table 5.2 summarizes the DC contents of the output signals.

If we examine this table, we see that for all equations where the DC content is independent of the duty cycle, the DC content scales with either $4\phi_\mathrm{i}$ or $1 - 4|\phi_\mathrm{i}|$. As $\phi_\mathrm{i}$ is the only parameter we can influence and as all other phase parameters are typically very small, it is best to choose $\phi_\mathrm{i} = 45^0$. This ensures that the resulting output signal is around 0.5 and it maximizes the range of the phase errors which we can estimate. Note that in an actual implementation, the estimator does not need a

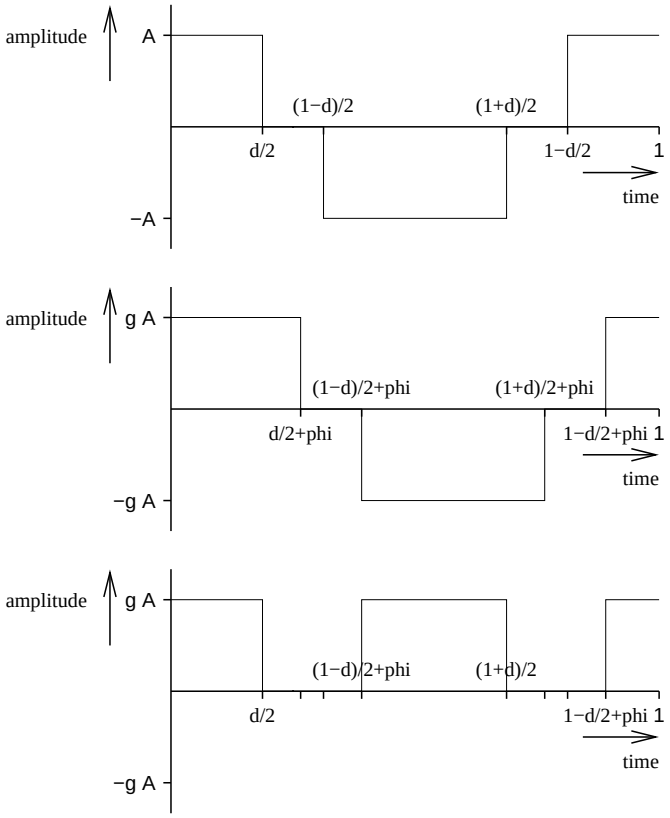


Figure 5.4: Input and output signals for mixer with almost identical signals when $\phi < \frac{1}{2} - d$. Top: input signal at LO port. Middle: input signal at LNA port. Bottom: output signal.

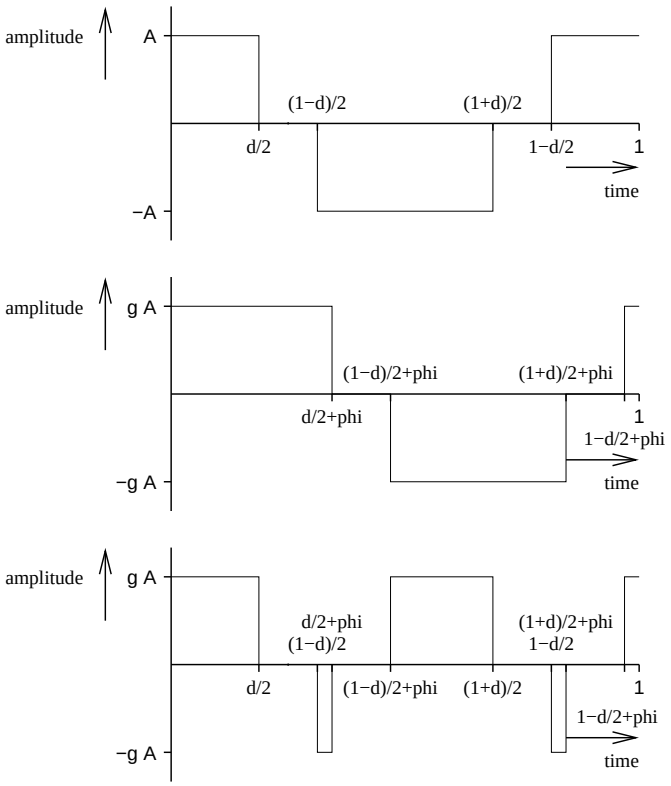


Figure 5.5: Input and output signals for mixer with almost identical signals when $\phi > \frac{1}{2} - d$. Top: input signal at LO port. Middle: input signal at LNA port. Bottom: output signal.

Table 5.2: DC content of the output signals of the sign/multiplier mixer for all relevant switch positions. The codes in the first column indicate the positions of the switches in format ABCD where A indicates the position of the oscillator switch, B the position of the LNA switch, C the position of the filter switch and D indicates whether the Real (inphase) AD convertor or the Imaginary (quadrature) is used.

| Switches | DC content $y$ | Conditions |
|---|---|---|
| CCCR | $2(d-\lvert\phi_{\rm i}\rvert)g_{\rm i}A$ | $\lvert\phi_{\rm i}\rvert < \frac{1}{2}-d$ |
| | $(1-4\lvert\phi_{\rm i}\rvert)g_{\rm i}A$ | $\frac{1}{2}-d \leq \lvert\phi_{\rm i}\rvert \leq d$ |
| SCCR | $2(d-\lvert\phi_{\rm i}\rvert)g_\tau g_{\rm o} g_{\rm i}A$ | $\lvert\phi_{\rm i}\rvert < \frac{1}{2}-d$ |
| | $(1-4\lvert\phi_{\rm i}\rvert)g_\tau g_{\rm o} g_{\rm i}A$ | $\frac{1}{2}-d \leq \lvert\phi_{\rm i}\rvert \leq d$ |
| CSCR | $4(\phi_{\rm i}+\phi_{\rm o})g_{\rm o}g_{\rm i}A$ | $\lvert\phi_{\rm i}+\phi_{\rm o}\rvert < d-\frac{1}{4}$ |
| SSCR | $4(-\phi_{\rm i}+\phi_{\rm o}+\phi_\tau)g_{\rm i}A$ | $\lvert-\phi_{\rm i}+\phi_{\rm o}+\phi_\tau\rvert < d-\frac{1}{4}$ |
| CCSR | $4(-\phi_{\rm i}+\phi_{\rm o}-\phi_{\rm m})g_{\rm i}g_{\rm m}A$ | $\lvert-\phi_{\rm i}+\phi_{\rm o}-\phi_{\rm m}\rvert < d-\frac{1}{4}$ |
| SCSR | $4(\phi_{\rm i}+\phi_{\rm o}+\phi_\tau+\phi_{\rm m})g_\tau g_{\rm o}g_{\rm i}g_{\rm m}A$ | $\lvert\phi_{\rm i}+\phi_{\rm o}+\phi_\tau+\phi_{\rm m}\rvert < d-\frac{1}{4}$ |
| CSSR | $2(d-\lvert\phi_{\rm i}+\phi_{\rm m}\rvert)g_{\rm o}g_{\rm i}g_{\rm m}A$ | $\lvert\phi_{\rm i}+\phi_{\rm m}\rvert < \frac{1}{2}-d$ |
| | $(1-4\lvert\phi_{\rm i}+\phi_{\rm m}\rvert)g_{\rm o}g_{\rm i}g_{\rm m}A$ | $\frac{1}{2}-d \leq \lvert\phi_{\rm i}+\phi_{\rm m}\rvert \leq d$ |
| SSSR | $2(d-\lvert\phi_{\rm i}+\phi_{\rm m}\rvert)g_{\rm i}g_{\rm m}A$ | $\lvert\phi_{\rm i}+\phi_{\rm m}\rvert < \frac{1}{2}-d$ |
| | $(1-4\lvert\phi_{\rm i}+\phi_{\rm m}\rvert)g_{\rm i}g_{\rm m}A$ | $\frac{1}{2}-d \leq \lvert\phi_{\rm i}+\phi_{\rm m}\rvert \leq d$ |
| CCSI | $2(d-\lvert\phi_{\rm i}\rvert)g_{\rm i}g_{\rm f}A$ | $\lvert\phi_{\rm i}\rvert < \frac{1}{2}-d$ |
| | $(1-4\lvert\phi_{\rm i}\rvert)g_{\rm i}g_{\rm f}A$ | $\frac{1}{2}-d \leq \lvert\phi_{\rm i}\rvert \leq d$ |

priori knowledge of the exact value of $\phi_{\mathrm{i}}$, since, as we shall see, the algorithm can estimate $\phi_{\mathrm{i}}$.

Since the set of equations formed by this table is nonlinear, there is no general method to solve them. However, in this specific case, it is possible to solve the equations by sequentially solving the individual parameters.

Observe that we can start solving the equations by estimating the gain mismatch in the filter using

$$\hat{g}_{\mathrm{f}} = \frac{y_{\mathrm{ccsi}}}{y_{\mathrm{cccr}}} \tag{5.3}$$

where $y_{\mathrm{ccsi}}$ indicates the DC content sampled by the quadrature (imaginary) AD convertor when the LO switch was in position "C", the LNA switch was in position "C" and the filter switch was in position "S". Similarly, $y_{\mathrm{cccr}}$ indicates the DC content sampled by the inphase (real) AD convertor when all switches were in position "C".

The gain error caused by the LO can be estimated with

$$\hat{g}_{\mathrm{o}} = \frac{y_{\mathrm{cssr}}}{y_{\mathrm{sssr}}}. \tag{5.4}$$

Once the gain error in the LO is known, the gain error $g_\tau$ can be estimated by

$$\hat{g}_\tau = \frac{y_{\mathrm{sccr}}}{\hat{g}_{\mathrm{o}} y_{\mathrm{cccr}}}. \tag{5.5}$$

With $g_{\mathrm{o}}$ and $g_\tau$ known, the gain error in the mixers can be determined by

$$\hat{g}_{\mathrm{m}} = \frac{\hat{g}_{\mathrm{o}}\hat{g}_\tau y_{\mathrm{ccsr}} + y_{\mathrm{scsr}}}{\hat{g}_\tau y_{\mathrm{cscr}} + \hat{g}_\tau \hat{g}_{\mathrm{o}} y_{\mathrm{sscr}}}. \tag{5.6}$$

Note that estimating $g_{\mathrm{m}}$ in this way, results in a division by 0 in case $\phi_\tau = -2\phi_{\mathrm{o}}$.

Furthermore, if $x$ is defined as

$$x = \frac{y_{\mathrm{scsr}} - \hat{g}_{\mathrm{o}}\hat{g}_\tau\hat{g}_{\mathrm{m}} y_{\mathrm{sscr}}}{\hat{g}_{\mathrm{o}}\hat{g}_\tau\hat{g}_{\mathrm{m}}} \tag{5.7}$$

it is possible to estimate the product of the amplitude $A$ and the attenuation of the injected signal $g_\mathrm{i}$ with

$$\widehat{Ag_\mathrm{i}} = \begin{cases} \frac{1}{2}\left(\frac{y_\mathrm{sssr}}{\hat{g}_\mathrm{m}} - x + y_\mathrm{cccr}\right) & \text{if } -d < \phi_\mathrm{i} + \phi_\mathrm{m} < -(\frac{1}{2} - d) \text{ and} \\ & -d < \phi_\mathrm{i} < -(\frac{1}{2} - d) \\ \frac{1}{4d}\left(\frac{y_\mathrm{sssr}}{\hat{g}_\mathrm{m}} - \frac{x}{2} + y_\mathrm{cccr}\right) & \text{if } -(\frac{1}{2} - d) < \phi_\mathrm{i} + \phi_\mathrm{m} < 0 \text{ and} \\ & -(\frac{1}{2} - d) < \phi_\mathrm{i} < 0 \\ \frac{1}{4d}\left(\frac{y_\mathrm{sssr}}{\hat{g}_\mathrm{m}} + \frac{x}{2} + y_\mathrm{cccr}\right) & \text{if } 0 < \phi_\mathrm{i} + \phi_\mathrm{m} < \frac{1}{2} - d \text{ and } 0 < \phi_\mathrm{i} < \frac{1}{2} - d \\ \frac{1}{2}\left(\frac{y_\mathrm{sssr}}{\hat{g}_\mathrm{m}} + x + y_\mathrm{cccr}\right) & \text{if } \frac{1}{2} - d < \phi_\mathrm{i} + \phi_\mathrm{m} < d \text{ and } \frac{1}{2} - d < \phi_\mathrm{i} < d \end{cases} . \tag{5.8}$$

Once all gain errors are known, it is possible to estimate the phase errors. $\phi_\mathrm{i}$ can be estimated with

$$\hat{\phi}_\mathrm{i} = \begin{cases} \frac{1}{4}\left(\frac{y_\mathrm{cccr}}{\widehat{Ag_\mathrm{i}}} - 1\right) & \text{if } -d < \phi_\mathrm{i} < -(\frac{1}{2} - d) \\ \frac{y_\mathrm{cccr}}{2\widehat{Ag_\mathrm{i}}} - d & \text{if } -(\frac{1}{2} - d) < \phi_\mathrm{i} < 0 \\ -\left(\frac{y_\mathrm{cccr}}{2\widehat{Ag_\mathrm{i}}} - d\right) & \text{if } 0 < \phi_\mathrm{i} < \frac{1}{2} - d \\ -\frac{1}{4}\left(\frac{y_\mathrm{cccr}}{\widehat{Ag_\mathrm{i}}} - 1\right) & \text{if } \frac{1}{2} - d < \phi_\mathrm{i} < d \end{cases} . \tag{5.9}$$

Using this result, $\phi_\mathrm{o}$ can be estimated with

$$\hat{\phi}_\mathrm{o} = \frac{y_\mathrm{cscr}}{4\hat{g}_\mathrm{o}\widehat{Ag_\mathrm{i}}} - \hat{\phi}_\mathrm{i}. \tag{5.10}$$

Finally, with $\phi_\mathrm{o}$ known as well, it is possible to estimate $\phi_\mathrm{m}$ and $\phi_\tau$:

$$\hat{\phi}_\mathrm{m} = -\frac{y_\mathrm{ccsr}}{4\widehat{Ag_\mathrm{i}}\hat{g}_\mathrm{m}} - \hat{\phi}_\mathrm{i} + \hat{\phi}_\mathrm{o} \tag{5.11}$$

and

$$\hat{\phi}_\tau = \frac{y_\mathrm{sscr}}{4\widehat{Ag_\mathrm{i}}} + \hat{\phi}_\mathrm{i} - \hat{\phi}_\mathrm{o}. \tag{5.12}$$

We now have derived equations to estimate all parameters of the IQ imbalance model of figure 5.1 in case the LO produces a square wave form with duty cycle $d$ and infinitely small rise and fall times, and when the mixer is modeled as a sign-multiplier operator. For this estimation, the receiver only needs 8 complex samples. In case DC offset calibration is required, the total number of samples is increased to 16. Note however, that a new sample can only be taken when the IF filters are settled.

**Trapezium wave form**

Figure 5.6 shows a trapezium wave form with rise time $t_{\mathrm{f}}$ and fall time $t_{\mathrm{r}}$. In this case, $t_{\mathrm{f}}$ and $t_{\mathrm{r}}$ are defined as the time it takes for the wave form to go from one extreme to the other.

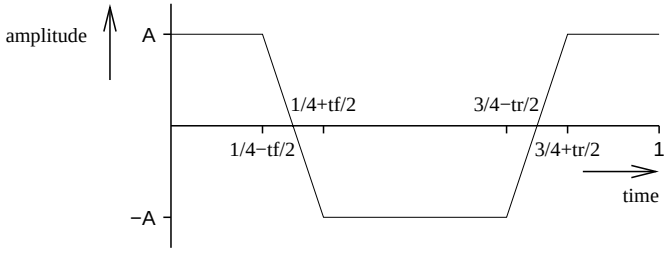


Figure 5.6: Differential LO output signal for a trapezoid wave form.

**Multiplication of two almost orthogonal trapezium wave forms** In case the input signal at the LO port of the sign/multiplier mixer is a trapezium wave form and the input signal at the LNA port is a scaled and almost $90^0$ shifted version of this signal. These signals, as well as the output signal of the mixer, are shown in figure 5.7.

The DC content of the output signal of the mixer is in this case $4\phi gA$, as can be seen by integrating the output signal by one period.

**Multiplication of two almost identical trapezium wave forms** Similar to the situation with a square wave with duty cycle smaller than $50\%$, in case the mixer input signals are trapezium wave forms with rise and fall times larger than 0, we need to distinguish two cases.

The first case is when the phase shift $\phi$ is larger than half of the rise and fall times $t_{\mathrm{r}}$ and $t_{\mathrm{f}}$ of the signals. The input and output signals for this case are shown in figure 5.8. In this case, the DC content of the output signal is $(1 - 4\phi)gA$.

The second case is when the phase shift $\phi$ is smaller than half of the rise and fall times of the signals. Figure 5.9 shows the input and output signals for this case. Integrating the output wave form will show that its DC content is

$$\left(4\left(\frac{1}{t_{\mathrm{r}}} + \frac{1}{t_{\mathrm{f}}}\right)\phi^2 - 2\phi + 1 - \frac{t_{\mathrm{f}}}{2} - \frac{t_{\mathrm{r}}}{2}\right) gA.$$

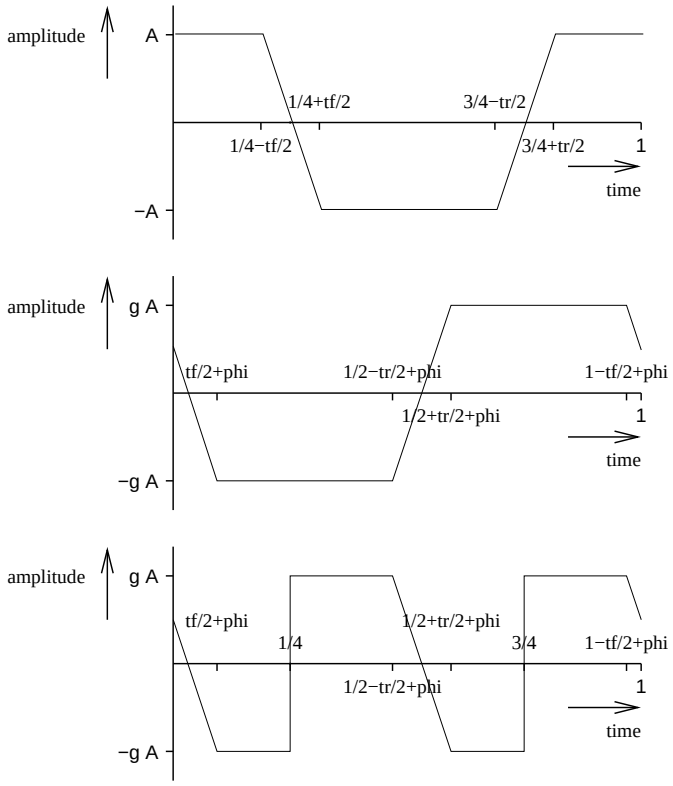


Figure 5.7: Input and output signals for mixer with almost orthogonal signals. Top: input signal at LO port. Middle: input signal at LNA port. Bottom: output signal.

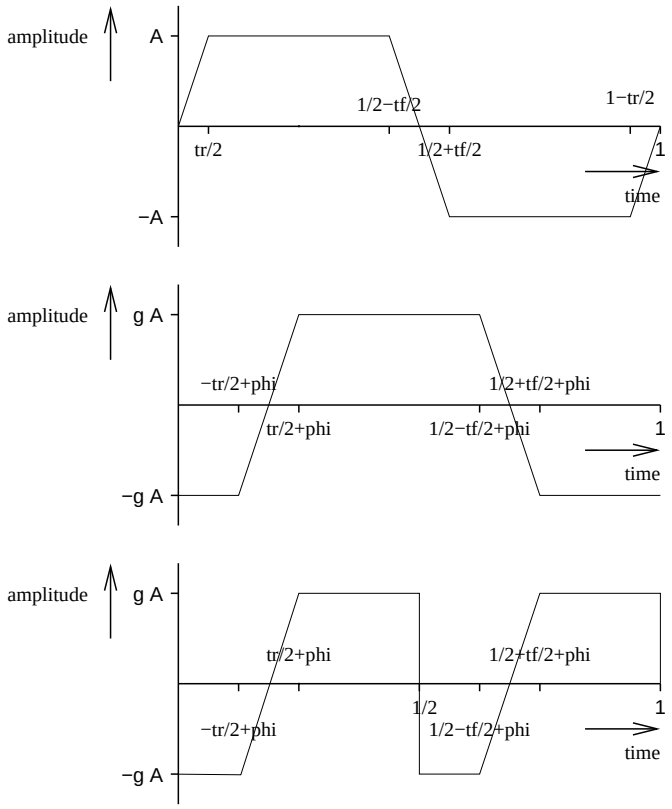


Figure 5.8: Input and output signals for mixer with almost identical signals and $\phi \leq t_{\mathrm{r}}/2$. Top: input signal at LO port. Middle: input signal at LNA port. Bottom: output signal.

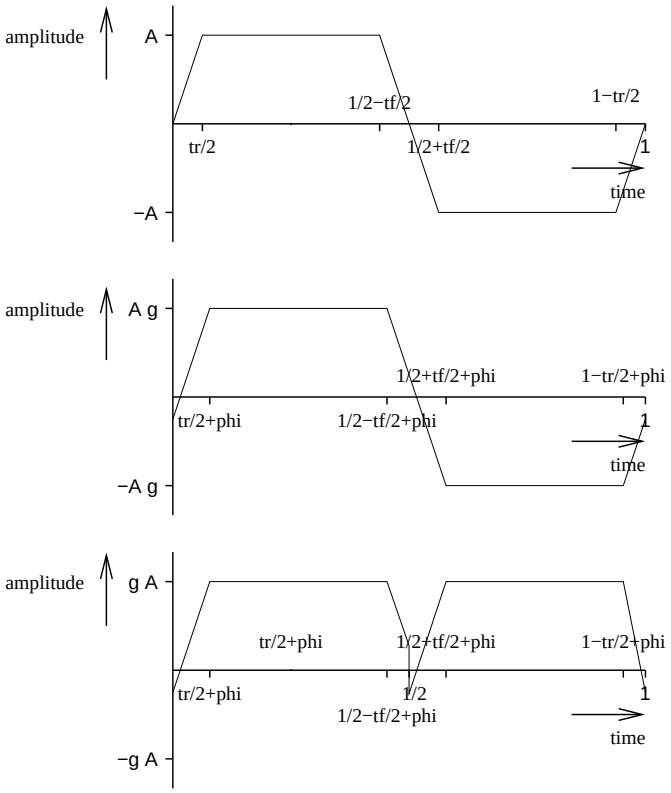


Figure 5.9: 2 Input and output signals for mixer with almost identical signals and $\phi > t_{\mathrm{r}}/2$. Top: input signal at LO port. Middle: input signal at LNA port. Bottom: output signal.

Again, if we also consider negative phase shifts, we can distinguish four possible results, as shown in table 5.3.

Table 5.3: DC content of the output signal of the mixer, depending on phase shift$\phi$ and rise and fall times $t_\mathrm{f}$ and $t_\mathrm{r}$.

| DC content | Conditions |
|---|---|
| $(1+4\phi)gA$ | $-\left(\frac{1}{2}-\{t_\mathrm{f},t_\mathrm{r}\}/2\right) \leq \phi \leq -\{t_\mathrm{f},t_\mathrm{r}\}/2$ |
| $\left(4\left(\frac{1}{t_\mathrm{r}}+\frac{1}{t_\mathrm{f}}\right)\phi^2+2\phi+1-\frac{t_\mathrm{f}}{2}-\frac{t_\mathrm{r}}{2}\right)gA$ | $-\{t_\mathrm{f},t_\mathrm{r}\}/2 < \phi < 0$ |
| $\left(4\left(\frac{1}{t_\mathrm{r}}+\frac{1}{t_\mathrm{f}}\right)\phi^2-2\phi+1-\frac{t_\mathrm{f}}{2}-\frac{t_\mathrm{r}}{2}\right)gA$ | $0 \leq \phi < \{t_\mathrm{f},t_\mathrm{r}\}/2$ |
| $(1-4\phi)gA$ | $\{t_\mathrm{f},t_\mathrm{r}\}/2 \leq \phi \leq \frac{1}{2}-\{t_\mathrm{f},t_\mathrm{r}\}/2$ |

**Comparison of different waveforms**

If we compare the DC contents of the output signals of the mixer when the input signals are square wave forms, we note that this DC content is in both cases $4\phi gA$, independent of duty cycle $d$ and rise and fall times $t_\mathrm{r}$ and $t_\mathrm{f}$, in case the wave forms are almost orthogonal.

In case the wave forms are almost identical, but the phase shift $\phi$ is larger than both $\frac{1}{2}-d$ and $t_\mathrm{r}/2$ and $t_\mathrm{f}/2$, the DC content of the output signal is $(1-4\phi)gA$, again independent of duty cycle $d$ and rise and fall times $t_\mathrm{r}$ and $t_\mathrm{f}$. The DC content of the signal is only dependent on duty cycle or rise and fall times when the phase shift $\phi$ is smaller than the duty cycle or the rise and fall times.

Therefore, if we can guarantee a priori that the conditions as listed in table 5.4 are satisfied, it is possible to estimate all imbalance parameters using the previously derived estimator equations independent of duty cycle and rise and fall times for the case when the mixer behaves as a sign/multiplier operator.

**Implementation costs**

An implementation of the algorithm of equations (5.3) - (5.12) requires 4 real multipliers and 2 real dividers, since almost all estimations need to be done sequentially and there is thus much possibility for hardware reuse. It is recommended though that the dividers are implemented as very fast dividers, since it is reused several

Table 5.4: Estimator conditions for sign/multiplier mixer (assuming that the fall time $t_\mathrm{f}$ equals the rise time $t_\mathrm{r}$)

| | |
|---|---|
| $\frac{t_\mathrm{r}}{2} \leq \phi \leq \frac{1}{2} - \frac{t_\mathrm{r}}{2}$ and $\frac{1}{2} - d \leq \phi \leq d$ | for $\phi = \phi_\mathrm{i}$ and $\phi = \phi_\mathrm{i} + \phi_\mathrm{m}$ |
| $\lvert\phi\rvert \leq \frac{1}{4} - \frac{t_\mathrm{r}}{2}$ and $\lvert\phi\rvert \leq d - \frac{1}{4}$ | for $\phi = \phi_\mathrm{i} + \phi_\mathrm{o}$, $\phi = -\phi_\mathrm{i} + \phi_\mathrm{o} + \phi_\tau$, $\phi = -\phi_\mathrm{i} + \phi_\mathrm{o} - \phi_\mathrm{m}$ and $\phi = \phi_\mathrm{i} + \phi_\mathrm{o} + \phi_\tau + \phi_\mathrm{m}$ |
| $\phi_\tau \neq -2\phi_\mathrm{o}$ | for all $\phi_\tau$ and $\phi_\mathrm{o}$ |

times and prevent that a long calculation time reduces the benefits of requiring a very short sampling time.

### 5.3.2 Mixer modeled as multiplier

Analogue to the previous section, we can make a derivation for the DC content of the output signal of the mixer for different wave forms in case the mixer is modeled as an ideal multiplier.

#### Square wave form

For the case of square wave forms, table 5.5 shows the DC content of the output signals of the mixer.

As we can see, the DC contents for this case are very similar to the case where the sign/multiplier mixer was given square wave forms. However, we have to derive new estimation equations for the ideal multiplier mixer, since the DC contents for this case are not exactly identical to the DC contents of the previous case.

To estimate the gain error in the filter for this case, one can divide the output signals $y_\mathrm{ccsi}$ and $y_\mathrm{cccr}$:

$$\hat{g}_\mathrm{f} = \frac{y_\mathrm{ccsi}}{y_\mathrm{cccr}}. \tag{5.13}$$

The gain error caused by the LO can be estimated with

$$\hat{g}_\mathrm{o} = \sqrt{\frac{y_\mathrm{cssr}}{y_\mathrm{sssr}}}. \tag{5.14}$$

Table 5.5: DC content of the output signals of the ideal multiplier mixer for all relevant switch positions. The codes in the first column indicate the positions of the switches in format ABCD where A indicates the position of the oscillator switch, B the position of the LNA switch, C the position of the filter switch and D indicates whether the Real (inphase) AD convertor or the Imaginary (quadrature) is used.

| Switches | DC content | Conditions |
|---|---|---|
| CCCR | $2(d-\lvert\phi_{\rm i}\rvert)g_{\rm i}A^2$ | $\lvert\phi_{\rm i}\rvert < \frac{1}{2}-d$ |
| | $(1-4\lvert\phi_{\rm i}\rvert)g_{\rm i}A^2$ | $\lvert\phi_{\rm i}\rvert \geq \frac{1}{2}-d$ |
| SCCR | $2(d-\lvert\phi_{\rm i}\rvert)g_\tau^2 g_{\rm o}^2 g_{\rm i}A^2$ | $\lvert\phi_{\rm i}\rvert < \frac{1}{2}-d$ |
| | $(1-4\lvert\phi_{\rm i}\rvert)g_\tau^2 g_{\rm o}^2 g_{\rm i}A^2$ | $\lvert\phi_{\rm i}\rvert \geq \frac{1}{2}-d$ |
| CSCR | $4(\phi_{\rm i}+\phi_{\rm o})g_{\rm o}g_{\rm i}A^2$ | $\lvert\phi_{\rm i}+\phi_{\rm o}\rvert < d-\frac{1}{4}$ |
| SSCR | $4(-\phi_{\rm i}+\phi_{\rm o}+\phi_\tau)g_\tau g_{\rm o}g_{\rm i}A^2$ | $\lvert-\phi_{\rm i}+\phi_{\rm o}+\phi_\tau\rvert < d-\frac{1}{4}$ |
| CCSR | $4(-\phi_{\rm i}+\phi_{\rm o}-\phi_{\rm m})g_{\rm o}g_{\rm i}g_{\rm m}A^2$ | $\lvert-\phi_{\rm i}+\phi_{\rm o}-\phi_{\rm m}\rvert < d-\frac{1}{4}$ |
| SCSR | $4(\phi_{\rm i}+\phi_{\rm o}+\phi_\tau+\phi_{\rm m})g_\tau g_{\rm o}g_{\rm i}g_{\rm m}A^2$ | $\lvert\phi_{\rm i}+\phi_{\rm o}+\phi_\tau+\phi_{\rm m}\rvert < d-\frac{1}{4}$ |
| CSSR | $2(d-\lvert\phi_{\rm i}+\phi_{\rm m}\rvert)g_{\rm o}^2 g_{\rm i}g_{\rm m}A^2$ | $\lvert\phi_{\rm i}+\phi_{\rm m}\rvert < \frac{1}{2}-d$ |
| | $(1-4\lvert\phi_{\rm i}+\phi_{\rm m}\rvert)g_{\rm o}^2 g_{\rm i}g_{\rm m}A^2$ | $\lvert\phi_{\rm i}+\phi_{\rm m}\rvert \geq \frac{1}{2}-d$ |
| SSSR | $2(d-\lvert\phi_{\rm i}+\phi_{\rm m}\rvert)g_{\rm i}g_{\rm m}A^2$ | $\lvert\phi_{\rm i}+\phi_{\rm m}\rvert < \frac{1}{2}-d$ |
| | $(1-4\lvert\phi_{\rm i}+\phi_{\rm m}\rvert)g_{\rm i}g_{\rm m}A^2$ | $\lvert\phi_{\rm i}+\phi_{\rm m}\rvert \geq \frac{1}{2}-d$ |
| CCSI | $2(d-\lvert\phi_{\rm i}\rvert)g_{\rm i}g_{\rm f}A^2$ | $\lvert\phi_{\rm i}\rvert < \frac{1}{2}-d$ |
| | $(1-4\lvert\phi_{\rm i}\rvert)g_{\rm i}g_{\rm f}A^2$ | $\lvert\phi_{\rm i}\rvert \geq \frac{1}{2}-d$ |

Once the gain error in the LO is known, the gain error $g_\tau$ can be estimated by

$$\hat{g}_\tau = \sqrt{\frac{y_{\mathrm{sccr}}}{\hat{g}_\mathrm{o}^2 y_{\mathrm{cccr}}}}. \tag{5.15}$$

With $g_\tau$ known, the gain error in the mixers can be determined by

$$\hat{g}_\mathrm{m} = \frac{\hat{g}_\tau y_{\mathrm{ccsr}} + y_{\mathrm{scsr}}}{\hat{g}_\tau y_{\mathrm{cscr}} + y_{\mathrm{sscr}}}. \tag{5.16}$$

Note that to prevent a division by zero, $\phi_\tau \neq -2\phi_\mathrm{o}$ must hold.

To determine $g_\mathrm{i}$ however, we need to have an indication of the range in which $\phi_\mathrm{i}$ and $\phi_\mathrm{m}$ will be.

If $x$ is defined as

$$x = \frac{y_{\mathrm{scsr}} - \hat{g}_\mathrm{m} y_{\mathrm{sscr}}}{\hat{g}_\mathrm{o}\hat{g}_\tau\hat{g}_\mathrm{m}} \tag{5.17}$$

it is possible to estimate the product of $A^2$ and $g_\mathrm{i}$ with

$$\widehat{A^2 g_\mathrm{i}} = \begin{cases} \frac{1}{2}\left(\frac{y_{\mathrm{sssr}}}{\hat{g}_\mathrm{m}} - x + y_{\mathrm{cccr}}\right) & \text{if } \phi_\mathrm{i} + \phi_\mathrm{m} < -(\frac{1}{2} - d) \text{ and } \phi_\mathrm{i} < -(\frac{1}{2} - d) \\ \frac{1}{4d}\left(\frac{y_{\mathrm{sssr}}}{\hat{g}_\mathrm{m}} - \frac{x}{2} + y_{\mathrm{cccr}}\right) & \text{if } -(\frac{1}{2} - d) < \phi_\mathrm{i} + \phi_\mathrm{m} < 0 \text{ and } -(\frac{1}{2} - d) < \phi_\mathrm{i} < 0 \\ \frac{1}{4d}\left(\frac{y_{\mathrm{sssr}}}{\hat{g}_\mathrm{m}} + \frac{x}{2} + y_{\mathrm{cccr}}\right) & \text{if } 0 < \phi_\mathrm{i} + \phi_\mathrm{m} < \frac{1}{2} - d \text{ and } 0 < \phi_\mathrm{i} < \frac{1}{2} - d \\ \frac{1}{2}\left(\frac{y_{\mathrm{sssr}}}{\hat{g}_\mathrm{m}} + x + y_{\mathrm{cccr}}\right) & \text{if } \phi_\mathrm{i} + \phi_\mathrm{m} > \frac{1}{2} - d \text{ and } \phi_\mathrm{i} > \frac{1}{2} - d \end{cases}. \tag{5.18}$$

With all gain errors known, it is possible to estimate the phase errors. $\phi_\mathrm{i}$ can be estimated with

$$\hat{\phi}_\mathrm{i} = \begin{cases} \frac{1}{4}\left(\frac{y_{\mathrm{cccr}}}{\widehat{A^2 g_\mathrm{i}}} - 1\right) & \text{if } \phi_\mathrm{i} < -(\frac{1}{2} - d) \\ \frac{y_{\mathrm{cccr}}}{2\widehat{A^2 g_\mathrm{i}}} - d & \text{if } -(\frac{1}{2} - d) < \phi_\mathrm{i} < 0 \\ -\left(\frac{y_{\mathrm{cccr}}}{2\widehat{A^2 g_\mathrm{i}}} - d\right) & \text{if } 0 < \phi_\mathrm{i} < \frac{1}{2} - d \\ -\frac{1}{4}\left(\frac{y_{\mathrm{cccr}}}{\widehat{A^2 g_\mathrm{i}}} - 1\right) & \text{if } \phi_\mathrm{i} > \frac{1}{2} - d \end{cases}. \tag{5.19}$$

Using this result, $\phi_\mathrm{o}$ can be estimated with

$$\hat{\phi}_\mathrm{o} = \frac{y_{\mathrm{cscr}}}{4\hat{g}_\mathrm{o}\widehat{A^2 g_\mathrm{i}}} - \hat{\phi}_\mathrm{i}. \tag{5.20}$$

Finally, with $\phi_{\rm o}$ known as well, it is possible to estimate $\phi_{\rm m}$ and $\phi_\tau$:

$$\hat{\phi}_{\rm m} = -\frac{y_{\rm ccsr}}{4\hat{g}_{\rm o}\widehat{A^2 g_{\rm i}}\hat{g}_{\rm m}} - \hat{\phi}_{\rm i} + \hat{\phi}_{\rm o} \tag{5.21}$$

and

$$\hat{\phi}_\tau = \frac{y_{\rm sscr}}{4\hat{g}_{\rm o}\widehat{A^2 g_{\rm i}}\hat{g}_\tau} + \hat{\phi}_{\rm i} - \hat{\phi}_{\rm o}. \tag{5.22}$$

**Trapezium wave form**

Similar to the case of the sign/multiplier mixer, in case input signals of the ideal multiplier have a trapezium shape, the DC content of the output signals are the same as for square wave form input signals, within certain ranges for phase shift $\phi$. Thus, again, we can use the estimation equations derived above for square wave forms. The conditions for which this hold are given in table 5.6.

Table 5.6: Estimator conditions (assuming that fall time $t_{\rm f}$ equals the rise time $t_{\rm r}$)

| | |
|---|---|
| $t_{\rm r} \leq \phi \leq \frac{1}{2} - t_{\rm r}$ and $\frac{1}{2} - d \leq \phi \leq d$ | for $\phi = \phi_{\rm i}$ and $\phi = \phi_{\rm i} + \phi_{\rm m}$ |
| $\lvert\phi\rvert \leq \frac{1}{4} - t_{\rm r}$ and $\lvert\phi\rvert \leq d - \frac{1}{4}$ | for $\phi = \phi_{\rm i} + \phi_{\rm o}$, $\phi = -\phi_{\rm i} + \phi_{\rm o} + \phi_\tau$, $\phi = -\phi_{\rm i} + \phi_{\rm o} - \phi_{\rm m}$ and $\phi = \phi_{\rm i} + \phi_{\rm o} + \phi_\tau + \phi_{\rm m}$ |
| $\phi_\tau \neq -2\phi_{\rm o}$ | for all $\phi_\tau$ and $\phi_{\rm o}$ |

**Implementation costs**

The implementation costs of this algorithm are slightly higher than the previous algorithm, since this algorithm requires a fast square root function. Besides a square root function, 2 fast dividers and 3 multipliers are needed.

## 5.4 Simulation results

The algorithms presented in the previous chapter have been simulated in a time domain system level model in Simulink for different waveforms of the LO signal:

a square wave with 46% duty cycle, a trapezium waveform, a filtered square wave and two real world signals type 1 and type 2 as shown in [25] by Leong which are captured from simulation results of a 2.4 GHz low power LO and a 12 frequency GHz LO for satellite reception. All signals are single ended signals; after the phase shifters, which add the IQ imbalance of the LO, the signals are converted to differential signals.

The trapezium waveform in this simulation has a 50% duty cycle, is 10% of the time rising and 10% of the time falling. The single ended waveform can be seen in figure 5.10. The single ended signals type 1 and type 2 can be seen in figures 5.11 and 5.12 respectively.

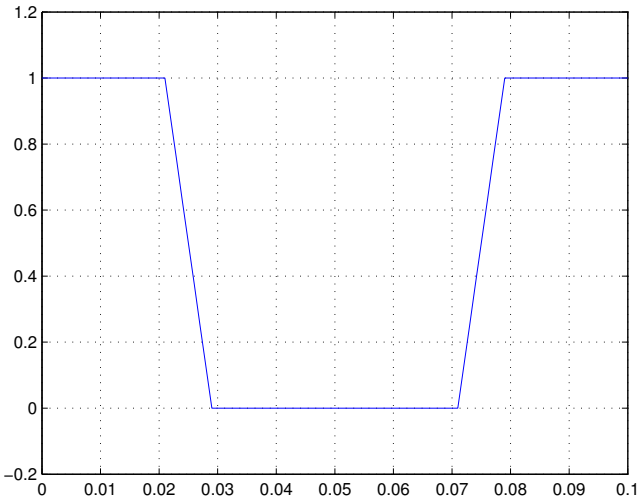


Figure 5.10: Trapezium shaped artificial output signal of LO

In all cases, the imbalance parameters were as shown in table 5.7, resulting in a total image rejection ratio of $30.1\mathrm{dB}$. The peak-to-peak voltage of the single ended LO signal was 1.2V (thus the amplitude of the differential signal was 1.2V and $A = 1.2$).

The next sections discuss the simulation results for two individual cases: the first is when the mixer is modeled as an ideal multiplier, and the second when the mixer is modeled as a concatenation of a sign operator and an ideal multiplier.

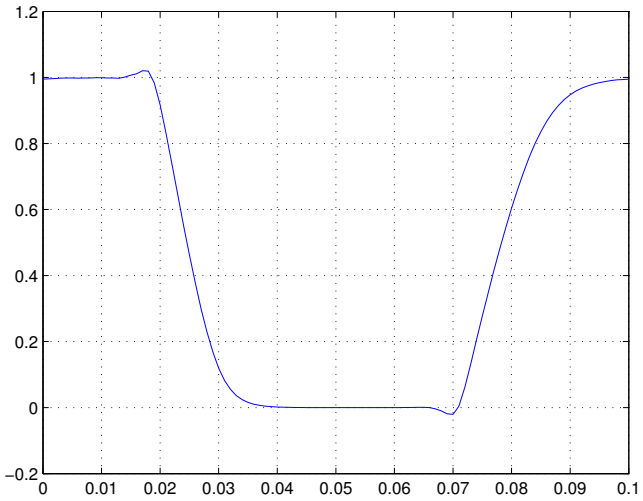


Figure 5.11: Signal type 1: output signal of a 2.4 GHz LO for low power applications

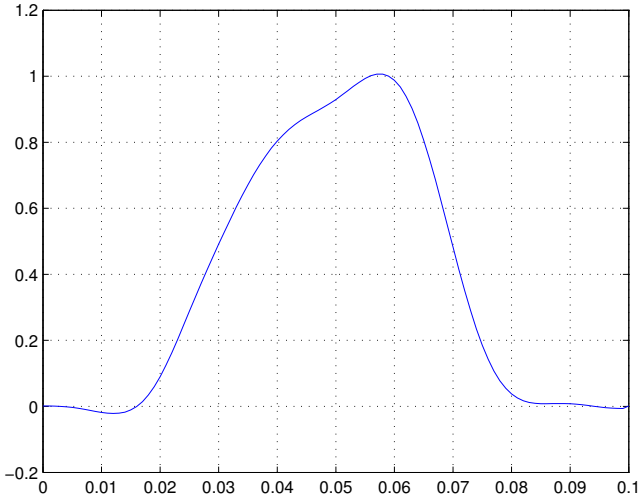


Figure 5.12: Signal type 2: output signal of a 12 frequency GHz LO for satellite reception

Table 5.7: Imbalance parameters for simulation.

| Parameter | Value |
|---|---|
| $g_{\mathrm{o}}$ | $0.97$ |
| $\phi_{\mathrm{o}}$ | $-1.8^0$ |
| $g_{\tau}$ | $1.02$ |
| $\phi_{\tau}$ | $1.8^0$ |
| $g_{\mathrm{i}}$ | $0.001$ |
| $\phi_{\mathrm{i}}$ | $45^0$ |
| $g_{\mathrm{m}}$ | $0.99$ |
| $\phi_{\mathrm{m}}$ | $1.8^0$ |
| $g_{\mathrm{f}}$ | $1.04$ |
| IRR | $30.1\mathrm{dB}$ |

### 5.4.1 Mixer modeled as ideal multiplier

Table 5.8 shows the result for the case when the mixer is modeled as an ideal multiplier.

Table 5.8: Simulation results for mixer modeled as ideal multiplier.

| Waveform | IRR (dB) for different estimators | |
|---|---|---|
| | Square wave multiplier | Square wave sign/multiplier |
| Square wave, 46% duty cycle | $\infty$ | 1.5 |
| Trapezium wave | $\infty$ | 1.9 |
| Filtered square wave, 46% duty cycle, $\omega_{\mathrm{b}} = 50\,\omega_{\mathrm{c}}$ | 57.5 | 2.0 |
| Filtered square wave, 46% duty cycle, $\omega_{\mathrm{b}} = 20\,\omega_{\mathrm{c}}$ | 38.9 | 7.7 |
| Signal type 1 | 37.3 | 8.1 |
| Signal type 2 | 32.1 | 12 |

As we can see in this table, the IRR after estimation and compensation when the output signals of the LO are ideal square wave signals or trapezium signals is infinite. This confirms the conclusion of the algorithms in the previous chapter, that if the signals satisfy the conditions listed in table 5.6, the estimator will give the exact values of the mismatch parameters.

If, however, the square waveform is filtered by a first order low pass filter, the conditions are no longer satisfied, and estimator performance drops; if the relative cutoff frequency $\omega_\mathrm{b}$ is 50 times the LO frequency, the image rejection ratio after compensation is 57.5 dB. If the relative cutoff frequency is even lower, the IRR is reduced further; for example, if the cutoff frequency is 20 times the LO frequency, the IRR is reduced to 38.9 dB.

For the real world signals type 1 and type 2 we observe image rejection ratios of 37.3 and 44.8 dB respectively. This is caused by the relatively small bandwidth of these signals, and thus not satisfying the conditions listed in table 5.6.

### 5.4.2 Mixer modeled as sign/multiplier

Table 5.9 shows the simulation results for the case when the mixer is modeled as a concatenation of a sign operator and an ideal multiplier.

Table 5.9: Simulation results for mixer modeled as sign/multiplier.

| Waveform | IRR (dB) for different estimators | |
|---|---|---|
| | Square wave multiplier | Square wave sign/multiplier |
| Square wave, 46% duty cycle | 31.5 | $\infty$ |
| Trapezium wave | 31.4 | $\infty$ |
| Filtered square wave, 46% duty cycle, $\omega_\mathrm{b} = 50\,\omega_\mathrm{c}$ | 31.5 | 65.0 |
| Filtered square wave, 46% duty cycle, $\omega_\mathrm{b} = 20\,\omega_\mathrm{c}$ | 34.0 | 40.5 |
| Signal type 1 | 34.3 | 39.5 |
| Signal type 2 | 38.2 | 33.4 |

This table shows very similar results as the previous table with simulation results: for wave forms that satisfy the conditions in table 5.4, performance is very good, but when those conditions are not met, performance degrades significantly.

We can thus conclude that the estimators derived in the previous section perform well when the assumptions about the behaviour of the mixer and the shape of the waveform are valid. When these assumptions are not valid, performance can degrade significantly.

## 5.5 Prototype implementation

To test the behaviour of these methods in a more real-world setting, a prototype implementation was made. Since no RF chip was available which had the necessary switches at the right places, and since designing and creating one would take far too much time, we reverted to a prototype at a very low frequency, using multiple standard components. An additional benefit was that using this approach, it would be easy to experiment with different gain and phase errors at several points in the prototype.

Figure 5.13 shows a block diagram of the prototype system. As we can see, the prototype consists of several different blocks:

- Frequency divider
- I/Q swap
- I/Q select and I/Q inject
- Mixers
- Transimpedance amplifiers (TIAs)
- Analog to digital convertors (ADCs)
- Delay blocks $\tau_{\mathrm{o}}$ and $\tau_{\mathrm{i}}$
- DC bias and variable gain buffers

These blocks will be discussed in more detail below.

Note that this block diagram does not show the post-processing of the measurement data. After digitizing the measurement data in the ADCs, the data is transferred via a logic analyzer to LabView. From LabView, this data is saved in text files on a PC, after which Matlab is used to post-process this data and use this data to estimate and compensate for the IQ imbalance parameters.

### 5.5.1 Frequency divider

Figure 5.14 shows a schematic for the frequency divider. The frequency divider consists of three D-type flip-flops, provided by two 74HC74 chips. If at the left side, a 4 MHz square wave 3 Vpp input signal is applied, output 1Q of the first flip-flop will be a 2 MHz 6 Vpp square waveform, and output 1!Q will be the inverse

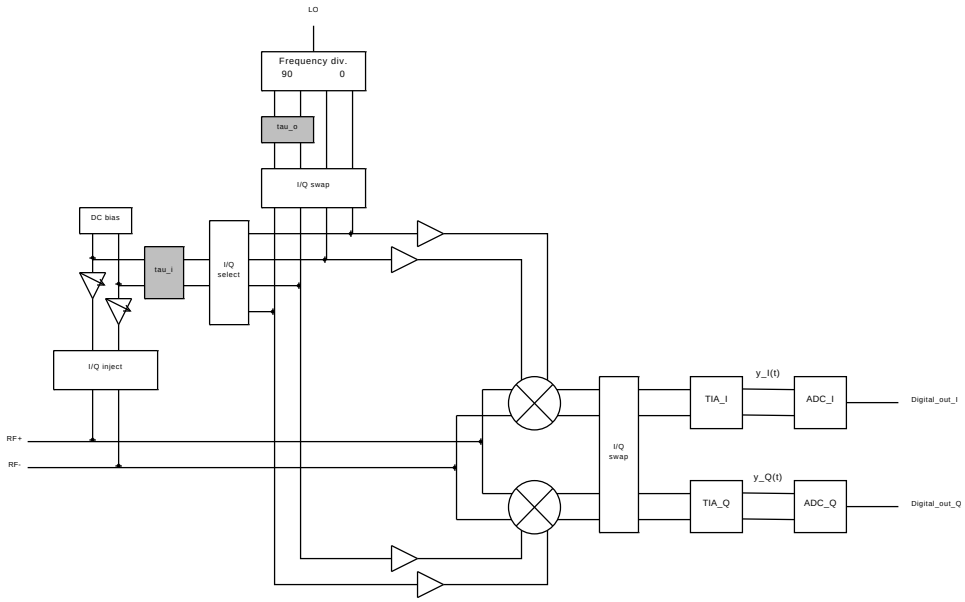


Figure 5.13: Block diagram of the prototype system.

of this waveform. These two signals are passed to the other two flip-flops which will divide the frequency again by 2, resulting in signals $\mathrm{LO}_{\mathrm{I}+}$, $\mathrm{LO}_{\mathrm{I}-}$, $\mathrm{LO}_{\mathrm{Q}+}$ and $\mathrm{LO}_{\mathrm{Q}-}$.

The low pass filter at the input of 2CP will provide a phase offset for signals $\mathrm{LO}_{\mathrm{Q}+}$ and $\mathrm{LO}_{\mathrm{Q}-}$. By varying the capacitor in this filter, we can change the phase offset for the LO signals.

Note that in the previous sections we derived the estimation algorithms assuming that signals $\mathrm{LO}_{\mathrm{I}-}$ and $\mathrm{LO}_{\mathrm{Q}-}$ were $180^0$ shifted versions of $\mathrm{LO}_{\mathrm{I}+}$ and $\mathrm{LO}_{\mathrm{Q}+}$. However, in this implementation, $\mathrm{LO}_{\mathrm{I}-}$ and $\mathrm{LO}_{\mathrm{Q}-}$ are not shifted but inverted versions of $\mathrm{LO}_{\mathrm{I}+}$ and $\mathrm{LO}_{\mathrm{Q}+}$. In case the duty cycle $d$ is not 50%, the resulting differential waveform will then be different from what we assumed in our derivations. However, a quick calculation shows that for inverted versions of the waveforms, the algorithms will give the same results as for shifted versions, since the resulting signals at the output of the mixer do not depend on the duty cycle.

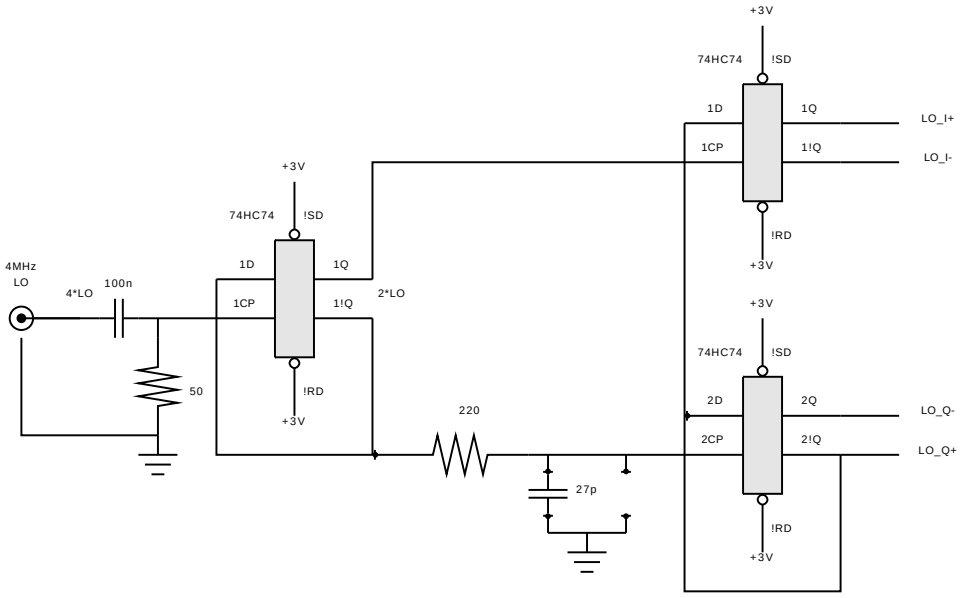


Figure 5.14: Schematic of the frequency divider.

### 5.5.2 I/Q swap

In figure 5.15, a schematic is shown to swap I and Q signals. This circuit is implemented using a 74HC4066 chip which acts as a pass-gate. For differential signals, this circuit should be implemented twice, once for $+$ signals and once for $-$ signals.

### 5.5.3 I/Q select and I/Q inject

Figure 5.16 shows the schematic to select either I or Q signal. This circuit is implemented using a 70HC4066 chip. Note that in the prototype the same circuit was used to inject the attenuated LO signal at the RF input of the mixer. In that case, $\mathrm{IN_{Q+}}$, $\mathrm{IN_{Q-}}$ and $\mathrm{Select_Q}$ were not connected, and $\mathrm{OUT_+}$ and $\mathrm{OUT_-}$ were directly connected to $\mathrm{RF_+}$ and $\mathrm{RF_-}$.

### 5.5.4 Mixer

In figure 5.17, a schematic is shown for the mixer circuit. A 70HC4066 chip performs the actual mixing operation. The two 270 $\Omega$ resistors at the input convert the

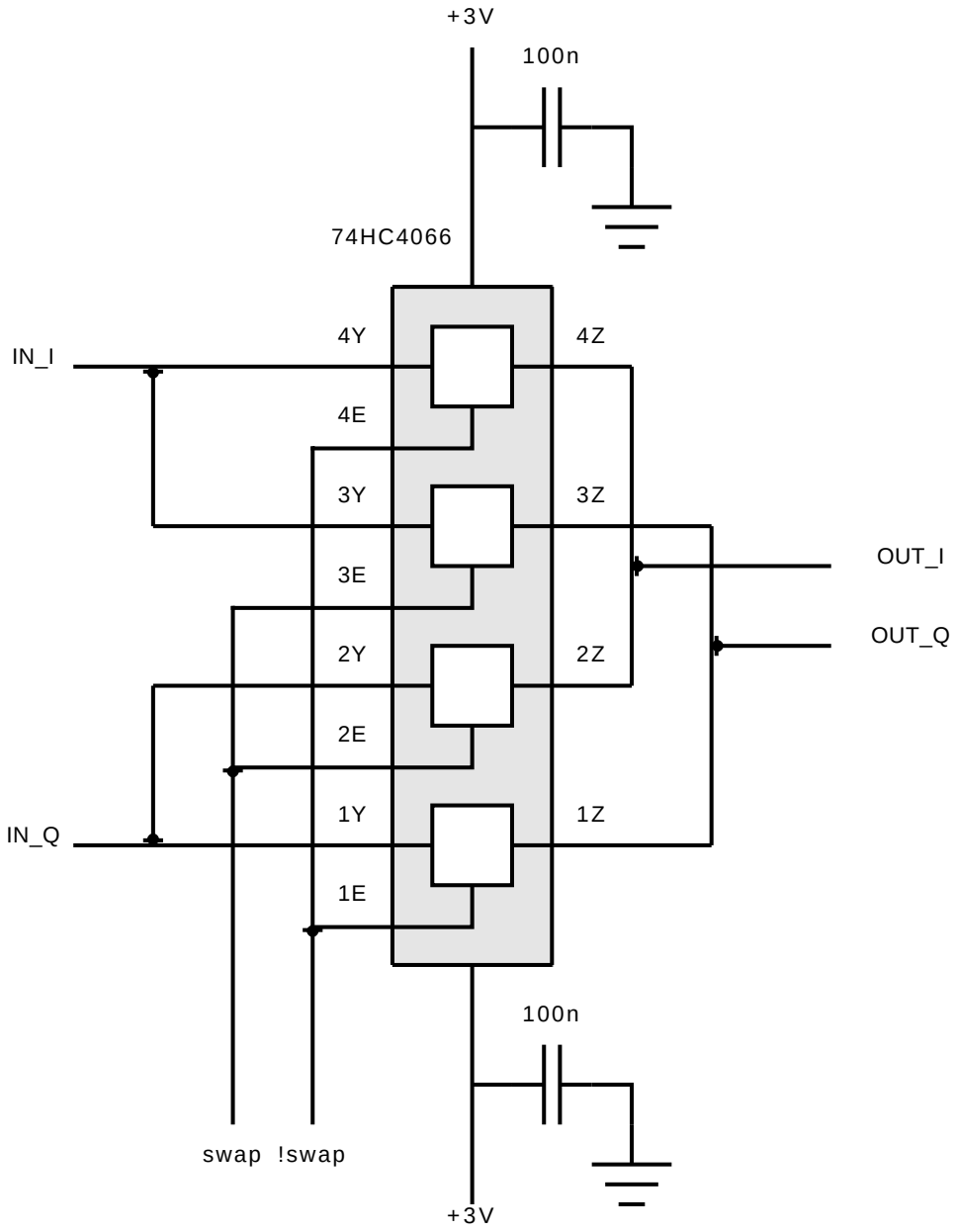


Figure 5.15: Schematic of IQ swap.

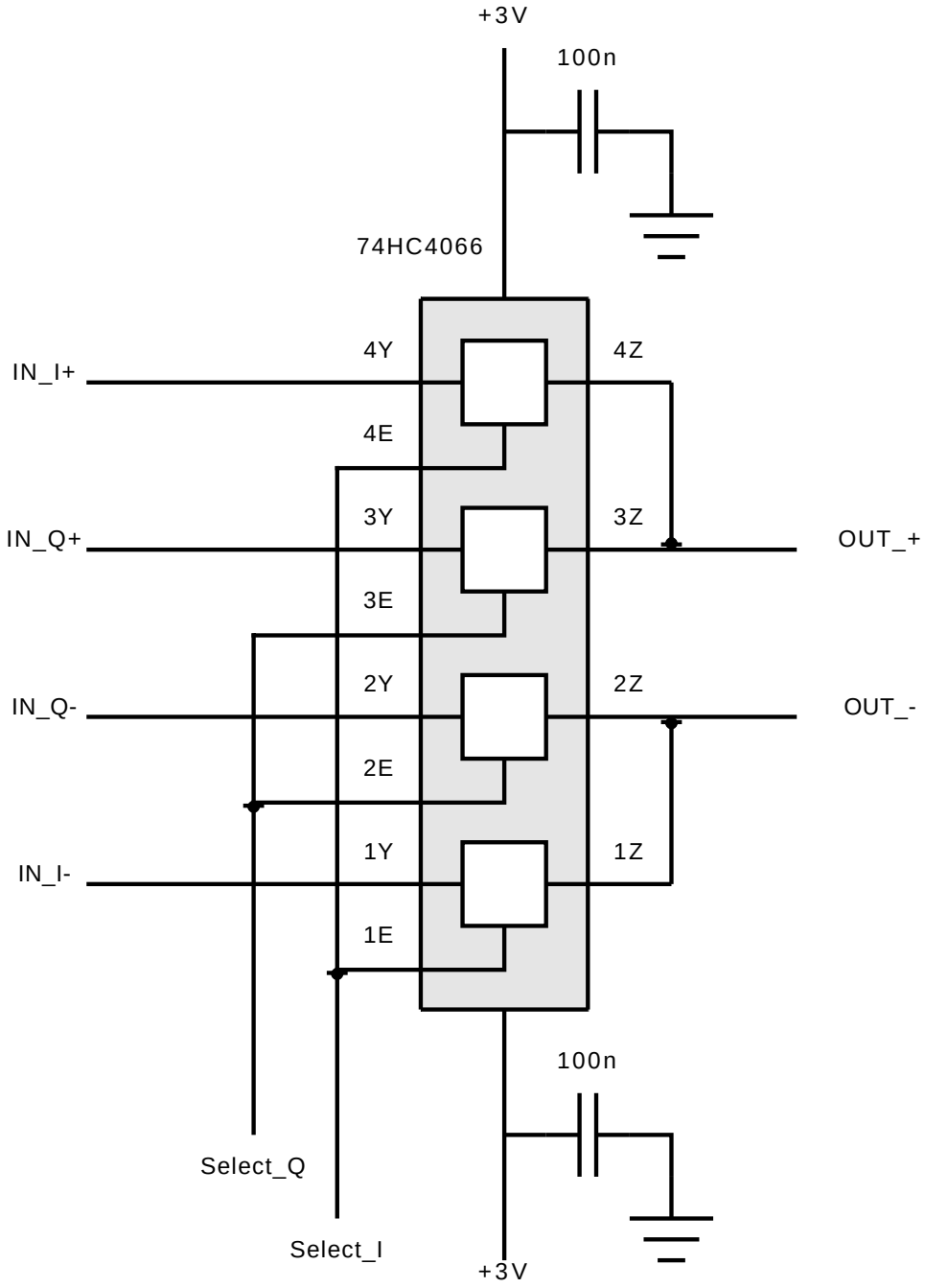


Figure 5.16: Schematic of IQ select.

voltage signals to current signals, which are later on converted back to voltage signals by the TIAs. The 100 nF capacitors block DC components in the input signals of the mixer. The 10 nF capacitors at the output of the mixer are actually part of the input of the TIA, but the separation of the boards is done exactly at this point: the mixers and the 10 nF capacitors are on the first board, while the I/Q swap and TIAs are one the second board.

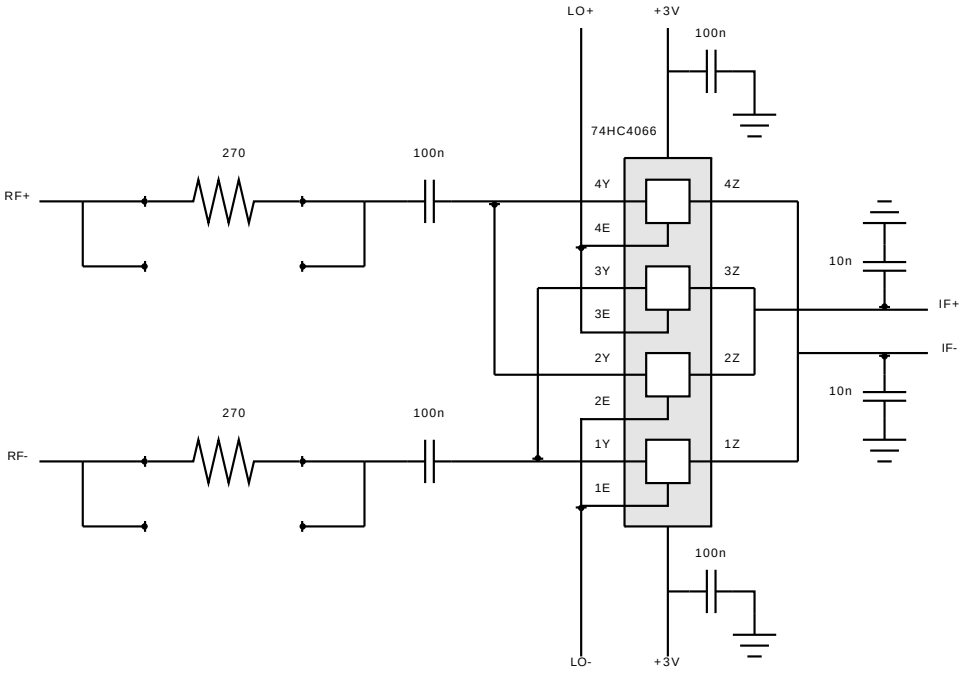


Figure 5.17: Schematic of mixer.

### 5.5.5 Transimpedance amplifiers

Figure 5.18 shows the schematic for a TIA. This amplifier has an active first order low pass filter with a cutoff frequency of 50 kHz. The output signals are biased at $0.75V$ so that the TIAs can directly drive the ADCs. Note that for the prototype, the circuit is implemented twice, once for the inphase signal and once for the quadrature signal.

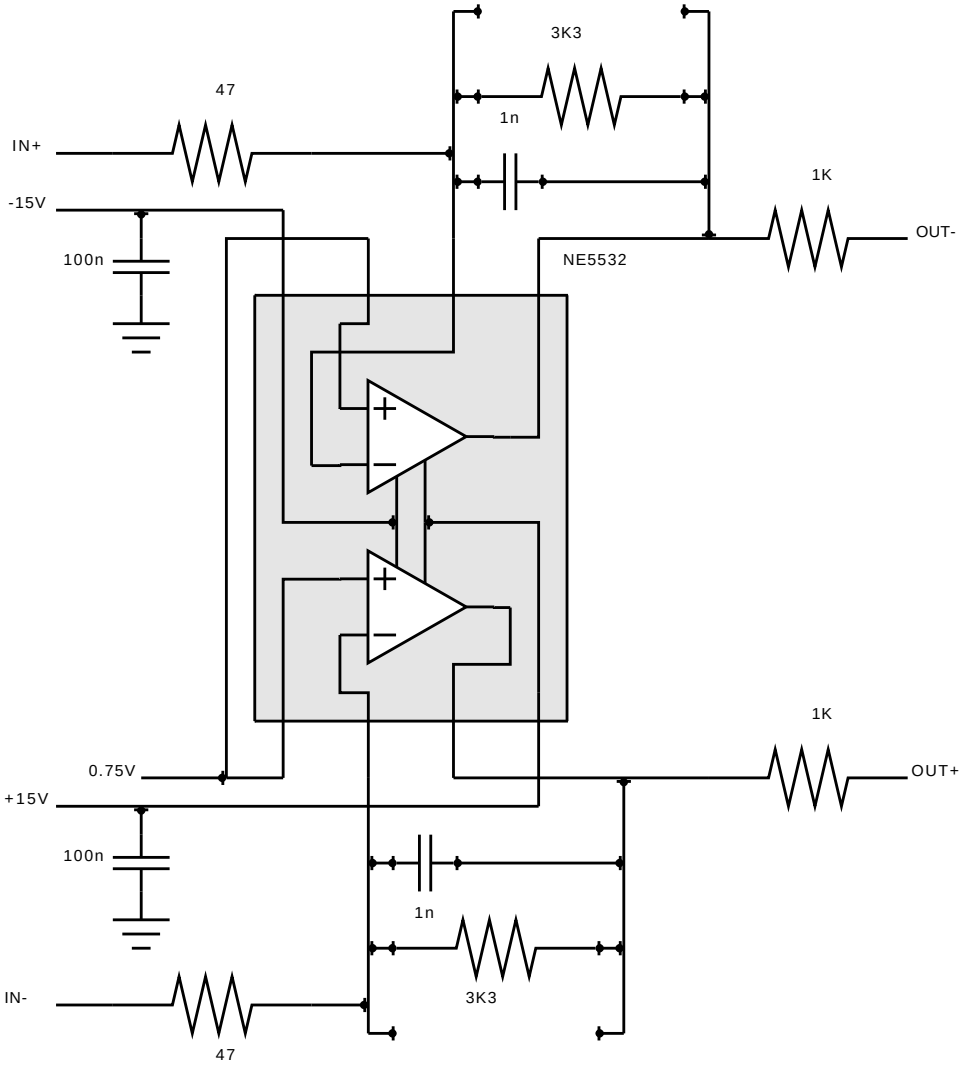


Figure 5.18: Schematic of TIA.

### 5.5.6 Analog to digital convertors

For ADC we used a sigma-delta ADC with 26 MHz sampling frequency which was already available including PCB. Detailed information on this ADC can be found in [26] by Van Veldhoven. A logic analyzer was used to transfer the digitized signal to a computer with LabView.

### 5.5.7 Digital postprocessing

Digital postprocessing was implemented in two programs. LabView was used to transfer the digitized signal from the ADC to the computer and to store this signal in text files. Those text files were then imported in Matlab and filtered with a decimation filter as shown in figures 5.19 and 5.20.

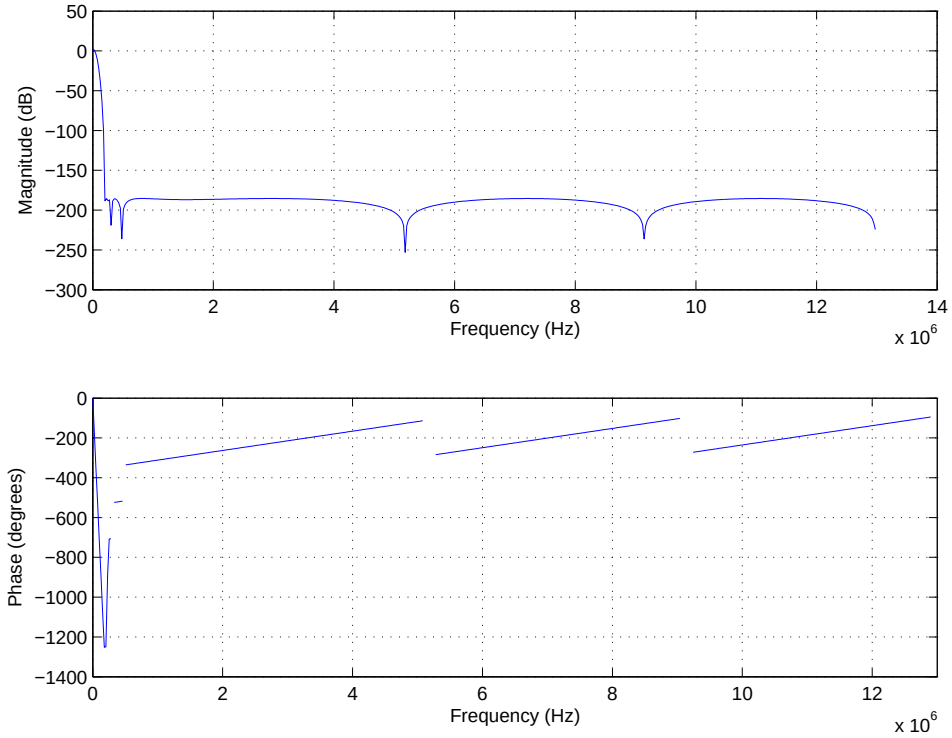


Figure 5.19: Decimation filter: full frequency response from 0 to 13 MHz.

As we can see from these figures, the filter has a 3 dB cutoff frequency of 50 kHz

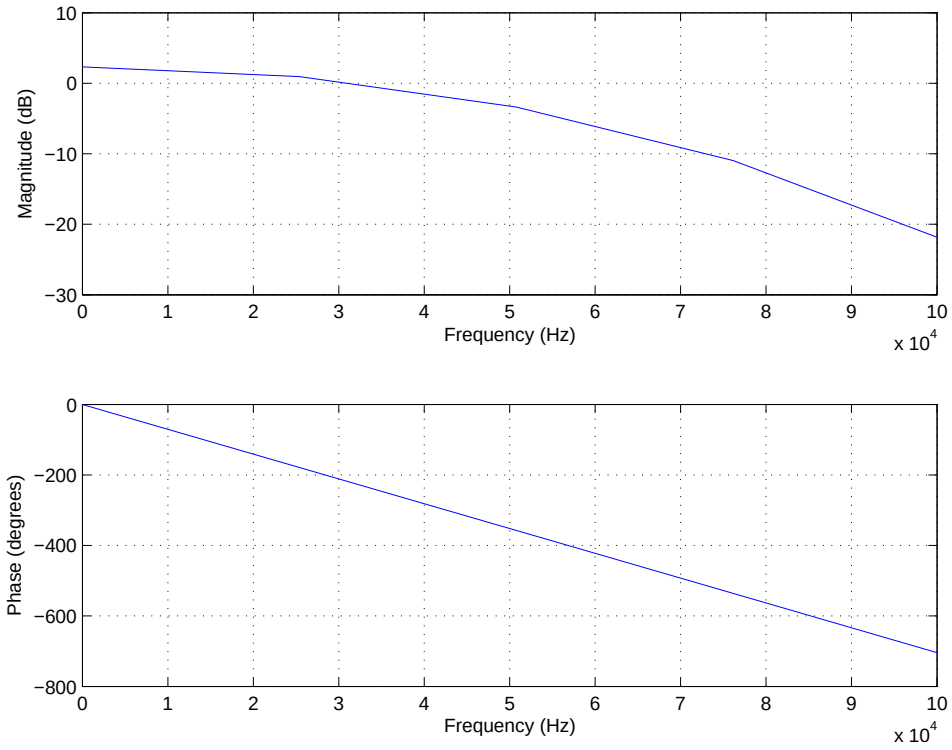


Figure 5.20: Decimation filter: magnified frequency response from 0 to 100 kHz.

and has a very steep transition between 50 and 200 kHz. At 200 kHz, the signal is attenuated by almost 200 dB.

Since the information of the IQ imbalance parameters is in the DC levels, the Matlab program calculated the sample means of the filtered signals. After DC offset calibration, the program used equations (5.3)-(5.12) from the sign-multiplier mixer algorithm to estimate the IQ imbalance parameters.

### 5.5.8 Delay blocks and variable gain buffers with DC bias

In the block diagram of figure 5.13 there are two delay blocks, labeled $\tau_{\mathrm{i}}$ and $\tau_{\mathrm{o}}$. The block labeled $\tau_{\mathrm{o}}$ influences the phase error of the LO and the circuit for that is included in the schematic for the frequency divider in figure 5.14.

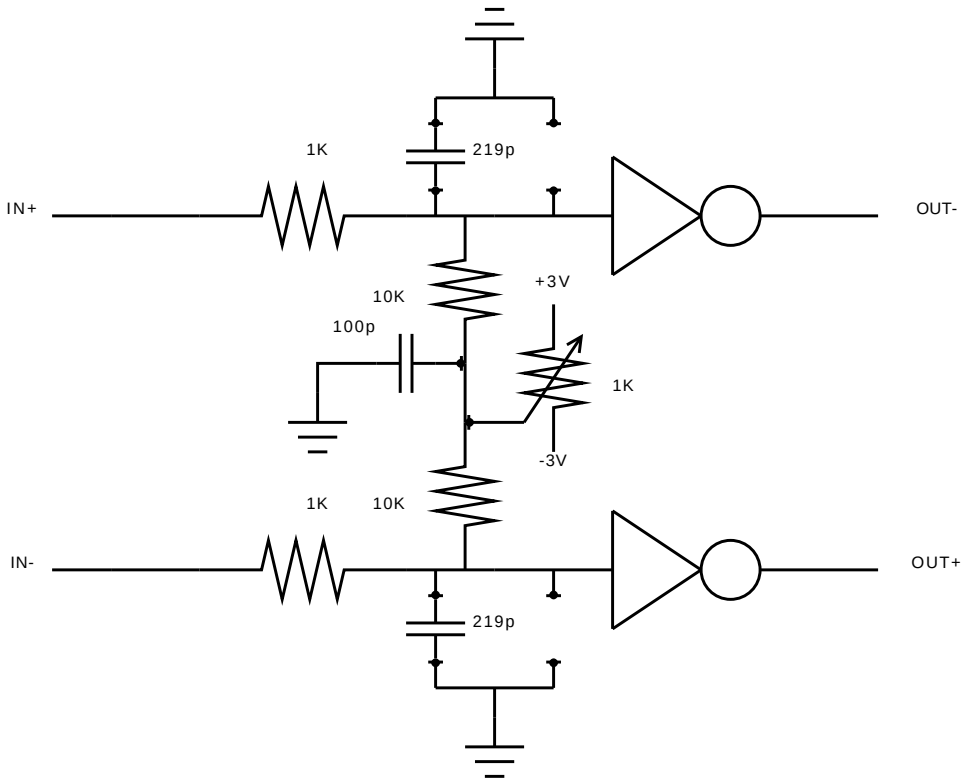


Figure 5.21: Schematic of delay block.

The block labeled $\tau_{\mathrm{i}}$ influences the phase delay $\phi_{\mathrm{i}}$ of the signal that is injected at

the RF input of the mixer. An optimal value for this phase shift is $45^0$, but the algorithm is insensitive to the actual phase shift, since it will estimate $\phi_{\mathrm{i}}$. The phase shift is realized by a low pass filter followed by a buffer to restore the square waveform. This buffer is implemented using a 74HC04 inverter as can be seen in the schematic in figure 5.21.

To remove any change in duty cycle caused by a non-zero switching level of the inverters, a DC bias is added which can be controlled with a potentiometer.

This circuit uses only two of the 6 inverters provided by the 74HC04. The other 4 inverters were used to buffer the I and Q signals before driving the LO inputs of the mixers.

### 5.5.9 Hardware realization

Figures 5.22 - 5.26 show the realization of the prototype. Since the complete circuit did not fit on one board, two boards were used. Figure 5.22 shows the two boards stacked on top of each other. Figures 5.23 and 5.24 show the top and bottom of the upper board which contains the frequency divider, the IQ swap, IQ select and IQ injection blocks, the delay and buffer block and the mixers. Figures 5.25 and 5.26 show the top and bottom of the lower board, which contains an IQ swap block and the TIAs.

In the top view figures some of the blocks from the block diagram are highlighted.

## 5.6 Measurement results

For the measurement setup, we used two triple power supply units, three signal generators, one clock generator, one logic analyzer, one 4 channel oscilloscope and two multimeters. The exact type and function of these instruments is listed in table 5.10.

### 5.6.1 Single tone measurement

In this test, no additional capacitors or resistors were used to alter the gain or phase mismatch in the prototype. One sinusoidal tone at 1.005 MHz was applied at the balun input. The power of this signal was adjusted such that the output signal of the TIAs was almost full swing of the ADC input (0 - 1.4 V). The resulting received spectrum is shown in figure 5.27.

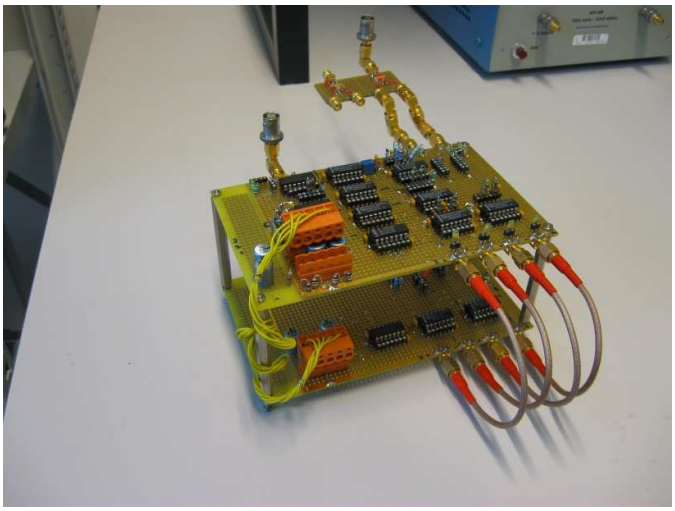

Figure 5.22: Realization of prototype: stacking of both boards.

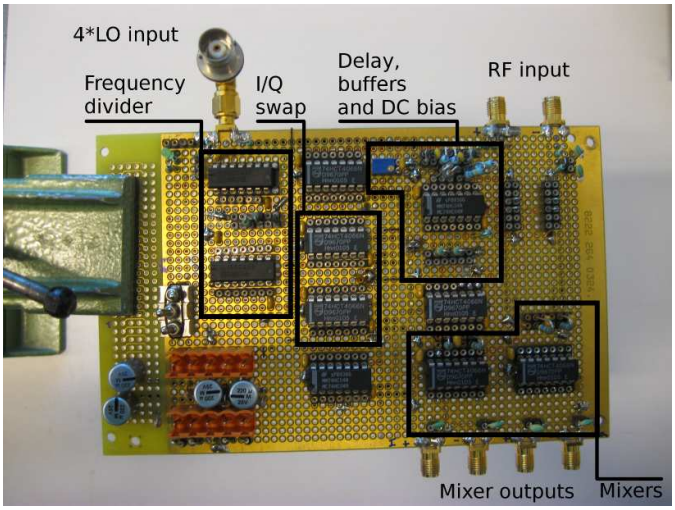


Figure 5.23: Realization of prototype: board 1, top view

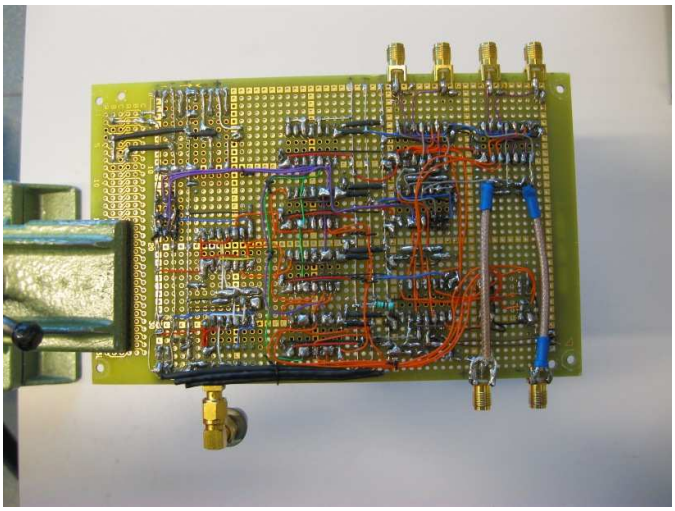

Figure 5.24: Realization of prototype: board 1, bottom view

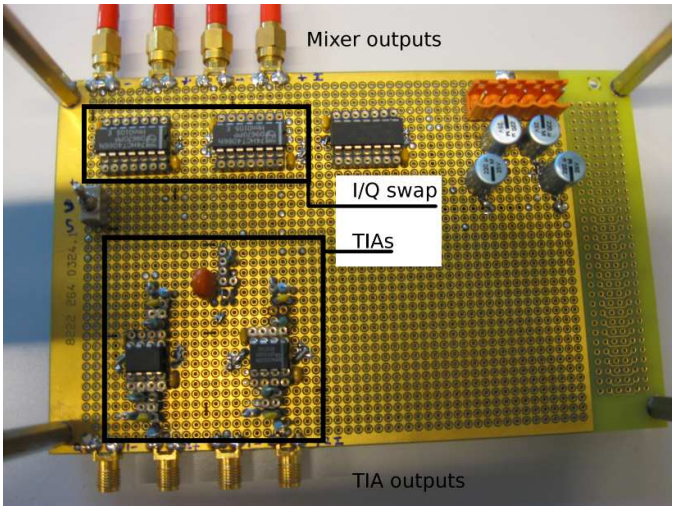


Figure 5.25: Realization of prototype: board 2, top view

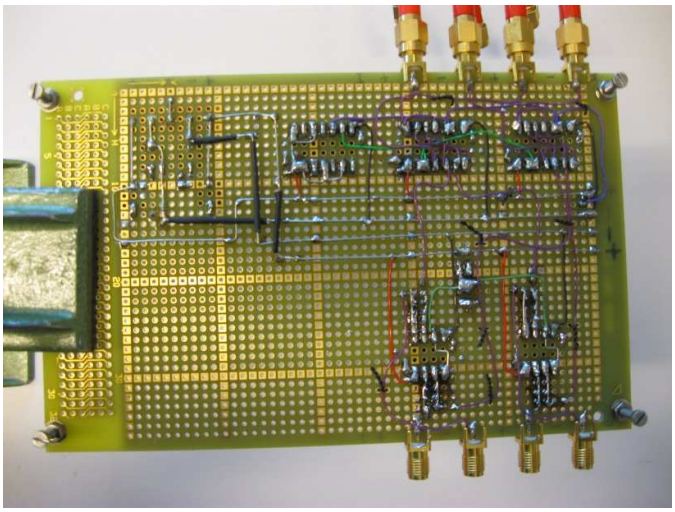

Figure 5.26: Realization of prototype: board 2, bottom view

Table 5.10: Measurement instruments

| # | Function | Brand and model | Notes |
|---|---|---|---|
| 2 | Power supply | Agilent E3631A | +3, -3, +5, +15 and -15 V |
| 3 | Signal generator | Agilent 33220A, 20 MHz | 4 MHz square wave (LO signal), 1 MHz sine wave |
| 1 | Clock generator | HP 8131A, 500 MHz | 52 MHz reference clock for ADC |
| 1 | Logic analyzer | Agilent 1682 AD | Transfers ADC digital outputs to Matlab |
| 1 | Balun | ADT1-1WT, 0.4 - 800 MHz | Converts single ended inputs to differential |
| 1 | Oscilloscope | Philips PM 3394, 200 MHz | |
| 2 | Multimeter | Keithley 2001 | |

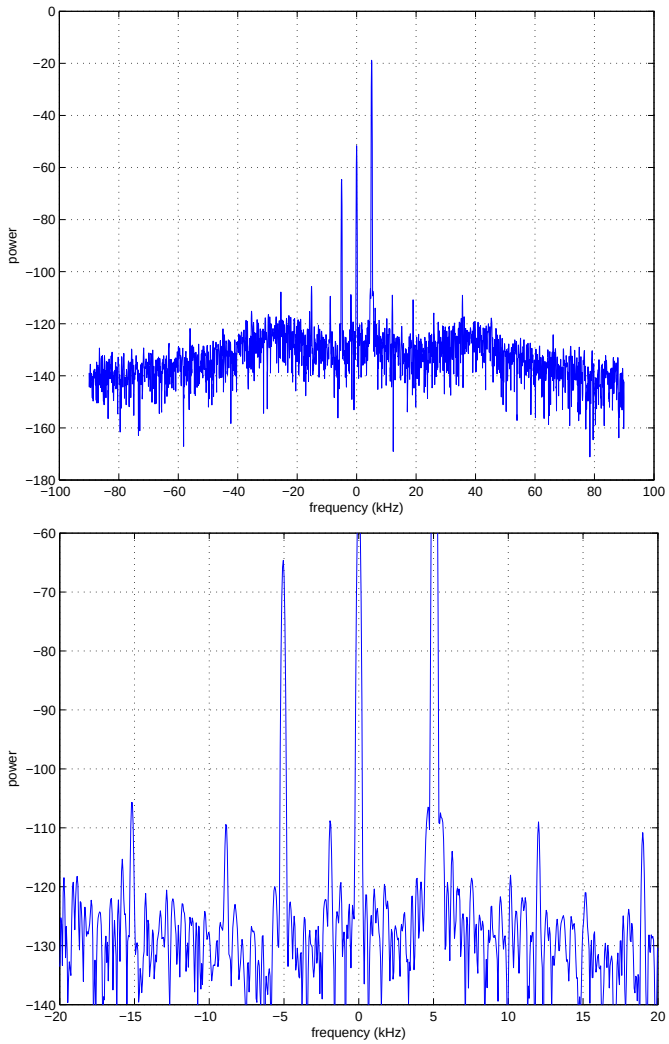


Figure 5.27: Single tone measurement result. Top: full spectrum. Bottom: magnified. Resolution bandwidth is 52 Hz.

In this figure, a clear -19 dB signal can be seen at 5 kHz. As we can see, there is also a strong DC component present of -49 dB, and an image of -65 at -5 kHz. Furthermore, calculating the noise power between -50 and 50 kHz and the signal power between 4.6 and 5.4 kHz results in 76 dB SNR.

The 2 ADCs combined have an SNR of 99 dB when given a -3 dB input signal. Therefore, if the signal at 5 kHz would be increased by 16 dB, the resulting SNR of the total system would be 92 dB, which is well within the expected range.

Second order nonlinearities would produce signal components at 0, 10 and -10 kHz. The output power at -10 kHz is -128 dB and at 10 kHz it is -118 dB, but both are almost indistinguishable from noise. The output intercept point of the second order harmonic is therefore according to Leenaerts in [27] $OIP2 = 2P_{\mathrm{o},1} - P_{\mathrm{o},2} = 2 \cdot -19 - -118 = 80\ \mathrm{dB}$.

Third order nonlinearities would produce signal components at 15 and - 15 kHz. At -15 kHz we observe a signal component of -106 dB, but at 15 kHz, the signal component is indistinguishable from noise. The output intercept point of the third order harmonic is thus $OIP3 = 1.5P_{\mathrm{o},1} - 0.5P_{\mathrm{o},3} = 1.5 \cdot -19 - 0.5 \cdot -106 = 24.5\ \mathrm{dB}$ according to Leenaerts in [27].

These results are summarized in table 5.11.

Table 5.11: Measurement results from single tone test

| Property | Value |
|---|---|
| SNR | 76 dB (between -50 and 50 kHz) |
| IRR | 46 dB (at 5 kHz) |
| OIP2 | 80 dB |
| OIP3 | 24.5 dB |

### 5.6.2 Two tone measurement

For the two tone test, no additional capacitors or resistors were used to alter the IQ imbalance of the prototype. The first test tone was placed at 1.013 MHz and the second at 1.017 MHz. Both tones were equal in strength and their power was adjusted such that the output signal of the TIAs was almost full swing of the ADC input. The resulting received spectrum is shown in figure 5.28.

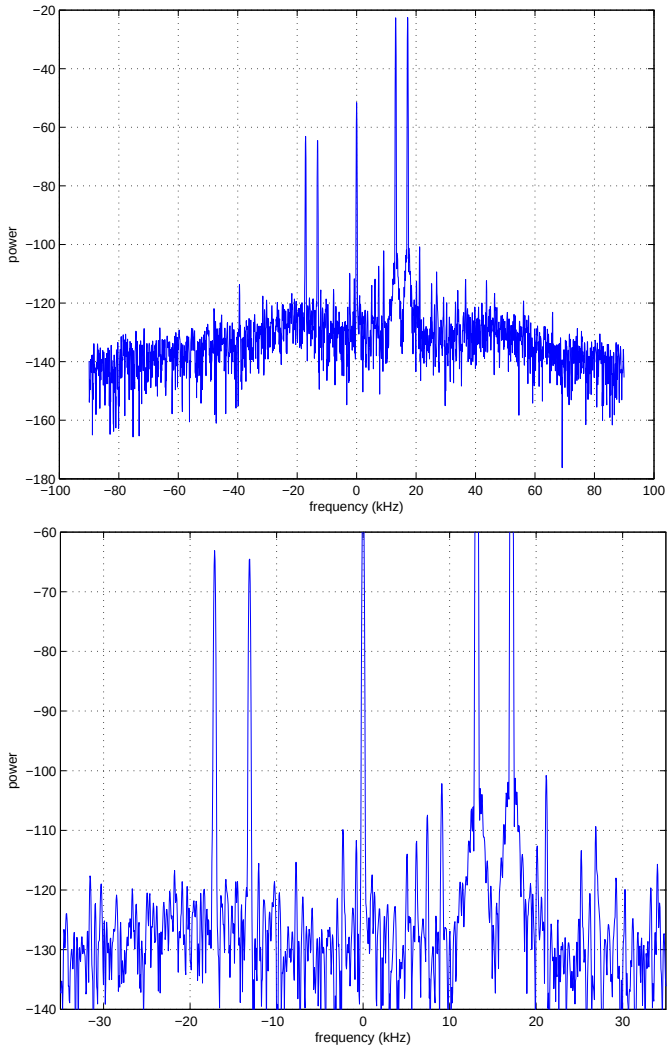


Figure 5.28: Two tone measurement result. Top: full spectrum. Bottom: magnified. Resolution bandwidth is 52 Hz.

In this figure, the signals at 13 and 17 kHz are -22 dB. Clear image signals can be seen at -13 and -17 kHz, resulting in an IRR of 43 respectively 41 dB. Integrating the noise power between -50 and 50 kHz results in 75 dB SNR.

Second order nonlinearities would produce signal components at 4 and 30 kHz, and at -30 kHz we measure the largest signal component of -125 dB. The output intercept point of the second harmonic distortion ($OIP2$) of 87 dB.

Third order nonlinearities would produce signal components at 9 and 21 kHz. At 21 kHz, we observe a peak of -101 dB. This results in an output intercept point of the third order harmonic distortion ($OIP3$) of 22 dB.

These results are summarized in table 5.12.

Table 5.12: Measurement results from two tone test

| Property | Value |
|---|---|
| SNR | 75 dB (between -50 and 50 kHz) |
| IRR | 43 dB (at 13 kHz)<br>41 dB (at 17 kHz) |
| OIP2 | 87 dB |
| OIP3 | 22 dB |

If we compare these results with the results from the single tone measurement, we see a 7 dB difference in OIP2 and 2.5 dB difference in OIP3. The 7 dB difference can be explained by the fact that the measured levels of second order output power are so small that they are almost indistinguishable from noise.

Furthermore, we notice that the image rejection ratio is frequency dependent: closer to the edge of the IF bandwidth, the IRR is lower than at the center.

From the single tone and two tone measurements we can conclude that the even order distortion is so small that it will not affect the IQ imbalance measurements.

### 5.6.3 IQ imbalance measurement

For the IQ imbalance measurement, we deliberately lowered the IRR of the prototype by placing a 27pF capacitor in the quadrature branch of the frequency divider. We did this for two reasons:

- to bring the IRR of the prototype closer to the IRR of an actual chip,

- to ensure that $\phi_\tau \neq -2\phi_\mathrm{o}$ holds.

We performed the measurements by sampling the output signal of the prototype for all possible combinations of the switches. During this measurement, no input signal was applied at the RF inputs and the balun was disconnected.

The 8 measurements where switch S_LNA was in position "n" (on the prototype: switch 3 was in position "C") are DC level estimations, the other 8 measurements are the measurements needed as input for the algorithm.

After performing these measurements, we connected the balun and applied a test signal. We swept this test signal from 1.055 MHz to 945 kHz in 5 kHz steps and skipped the frequency of 1.000 MHz. At every step, we sampled the output signals of the TIAs.

Figure 5.29 shows the output spectrum of this sweep, the image rejection ratios and the gain and phase errors before we applied IQ imbalance compensation.

As we can see in this image, the IRR is 32.1 dB and varies approximately 0.8 dB over the whole band. The gain error is approximately -0.39% around DC, but changes to -0.8% at the edge of the band. The phase error is $2.82^0$ at DC, but this changes to $3.10^0$ at -55 kHz and $2.55^0$ at 55 kHz.

Note that the gain error is symmetric around DC and the phase error is point symmetric, with an offset of $2.82^0$. This behaviour indicates that the most dominant frequency selective behaviour occurs in the IF stage, and that the phase offset of $2.82^0$ occurs at RF. Furthermore, the frequency selective gain and phase error match well with the gain and phase errors caused by a mismatch in cutoff frequencies in the IF filters, as shown in figure 2.3.

Figure 5.30 shows the output spectrum of the sweep, the image rejection ratios and the gain and phase errors after we applied the IQ imbalance compensation.

As we can see, the IRR at DC is increased with approximately 17.1 dB to 49.2 dB. We see furthermore that the IRR has become much more frequency dependent, changing from 44.2 dB at 55 kHz to 53.8 dB at -55 kHz and showing a peak of 56.6 dB at -35 kHz. This indicates that while before the frequency independent IQ imbalance in the RF stage was dominant, now the frequency selective IQ imbalance in the IF stage is becoming dominant.

However, a small amount of frequency independent IQ imbalance remains, as can be seen by the gain and phase errors at DC. As we can see, the gain error at DC is reduced from -0.39 to 0.10% and the phase error at DC is reduced from 2.82 to $-0.40^0$.

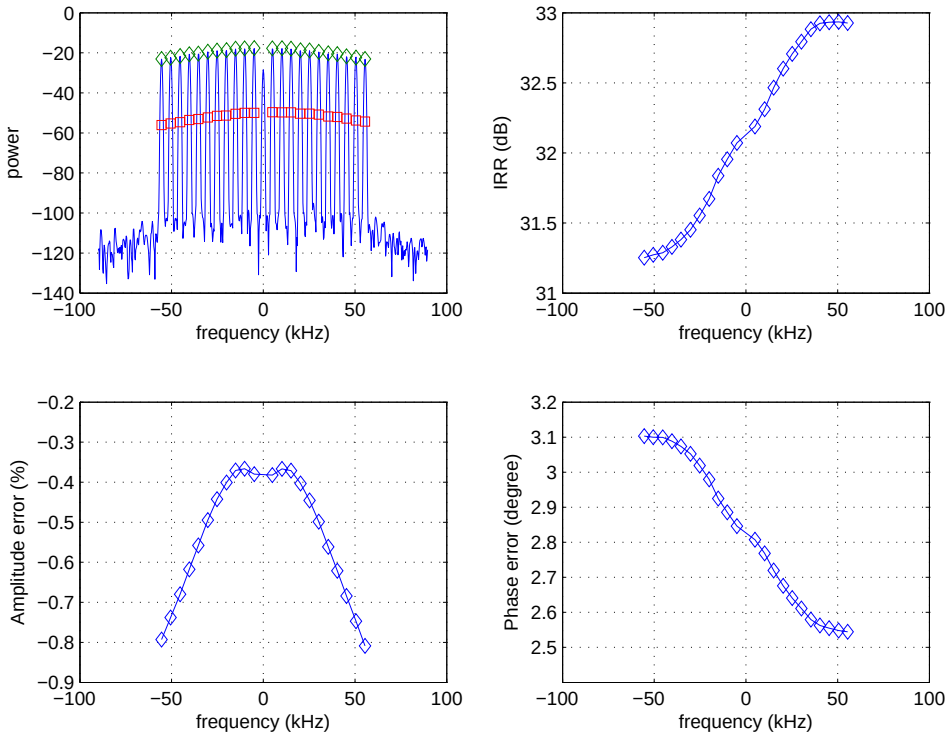


Figure 5.29: Frequency spectrum, IRR and gain and phase errors before IQ imbalance compensation. Resolution bandwidth is 260 Hz.

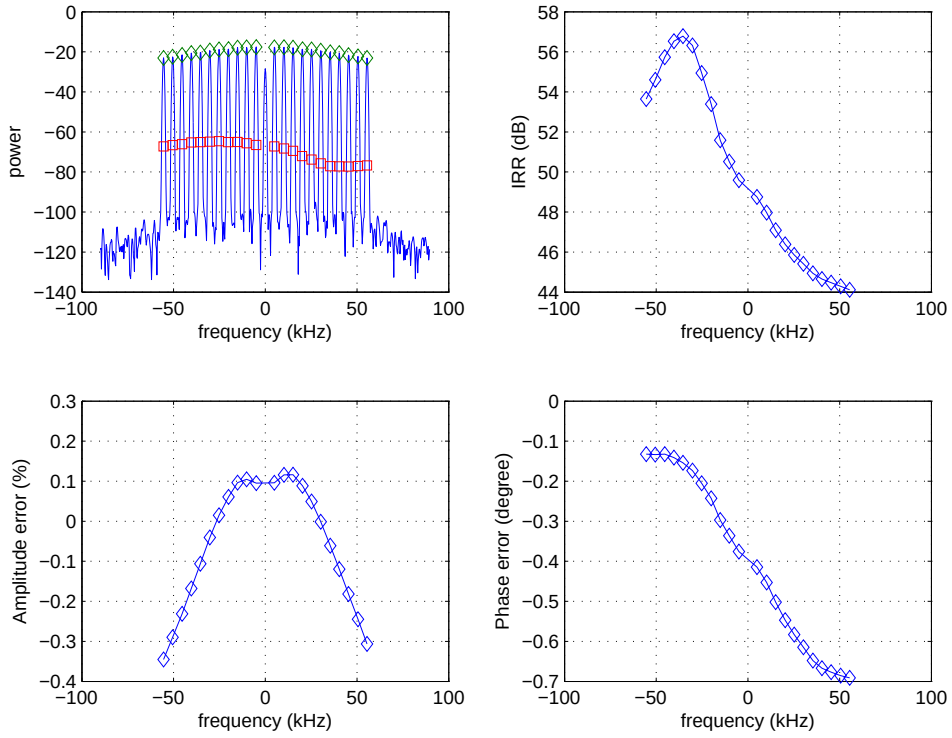


Figure 5.30: Frequency spectrum after IQ imbalance compensation. Resolution bandwidth is 260 Hz.

The frequency selective gain error is uncompensated, and thus, after frequency independent compensation, the gain error again decreases with approximately 0.42% to -0.33% at the edge of the band. The frequency selective phase error is also uncompensated and changes with $0.28^0$ to -0.13 and $-0.69^0$ at the edges of the band.

The IRR after compensation is limited to 49.2 dB. The most likely causes of this limitation are:

- PCB parasitics and IC bandwidth limitations give high frequency roll-off of the square wave signal. As we have seen in simulations, the algorithm is very sensitive to the higher order frequency components of the injected signal.
- To reduce implementation complexity and board space, the buffers for the LO signals to drive the mixers were implemented in the same 74HC04 chip as the buffers for the injected signal. However, this does increase the risk of interference from the LO signals at the injected signals, especially at the transition moments of the LO signals. Inspection with an oscilloscope showed some significant switching noise. Although the peaks caused by the switching were very narrow (in time), their amplitude was as high as 200 mV. This could have some very small influence on the DC content of the waveform.

We conclude now that the method can indeed estimate gain and phase errors and can successfully compensate for these errors. However, the accuracy of the estimates is limited by the quality of the injected waveform.

## 5.7 Summary

In this chapter we have derived a method to estimate IQ imbalance errors by injecting the signal from the local oscillator at the RF input of the mixer. The main advantages of this method are that it is standard independent and that it only requires 16 samples. In addition to IQ imbalance estimation, also DC offset calibration is performed.

We have derived two estimation algorithms: one for the case assuming that the mixer in the receiver behaves as an ideal multiplier, multiplying the injected signal with the LO signal, and one for the case assuming that the mixer behaves as a sign/multiplier, multiplying the injected signal with the sign of the LO signal.

The algorithms were derived for LO signals that were modeled as square waveform signals with a duty cycle less than 50% and as trapezium waveform signals. It was

observed that under certain conditions (as listed in tables 5.4 and 5.6), the estimator algorithms are relatively simple and optimal for both waveforms.

The implementation costs of both algorithms were quite modest: the algorithm for the sign-multiplier mixer requires 4 real multipliers and 2 fast dividers and the algorithm for the multiplier mixer requires one fast square root function, 2 fast dividers and 3 real multipliers.

Simulations indicated that performance of the estimator strongly depends on the output signal of the LO and the behaviour of the mixer. In case the signal that is to be injected is an ideal square waveform and there is no noise in the system, the estimators correctly estimate the IQ imbalance parameters, and image rejection ratios in excess of 200 dB are possible.

However, when this signal is more limited in bandwidth, the performance of the estimator is reduced. If the first order cutoff frequency is approximately 50 times the fundamental frequency, the IRR is reduced to 60 dB. If the bandwidth of the signal is even more limited, the IRR is reduced even further.

Moreover, although not shown in simulations, it is to be expected that the estimator is sensitive to even order distortion, since even order distortions will cause a change in the DC level of the IF signal.

The prototype system proved that it is possible to use this method to estimate the IQ imbalance parameters. It successfully increased the IQ imbalance from 32.1 to 49.2 dB. However, it also showed that even at such a low frequency, the method is sensitive to imperfections in the signal that is injected.

# Chapter 6

# Conclusions

In the final chapter of this report, a short summary of the previous chapters will be given. Furthermore the most important conclusions will be highlighted and indications for future research will be given.

## 6.1 Summary and conclusions

Chapter A.1 gave the background for this work, showed why standard independent estimators are relevant for multi-standard receivers and discussed the outline of this document.

Chapter 2 discussed several models for IQ imbalance, which showed the effect of gain and phase errors in the analog front-end on the received signal. It gave an overview of methods to mitigate this problem, where emphasize was given to methods which used digital estimation and compensation. For methods which use digital compensation, an equation to calculate the image rejection ratio when the estimated errors have limited accuracy was derived. The chapter ended with a list of requirements that the methods for this project should satisfy. The main requirements were that the methods should achieve at least 50 dB IRR, should have a rate of convergence 100 times faster than the well known statistical methods, should be possible to integrate on chip, should not use a dedicated test tone generator and should be completely standard independent.

Chapter 3 showed why the intuitive method of source neglecting to estimate the IQ imbalance parameters can be devastating to the received signal.

Chapter 4 derived two methods to estimate the IQ imbalance parameters by exploiting statistical properties of the received signals. One method operated on a time

domain description of the received signals while the other method operated on the frequency domain description. The advantages of these methods is that they do not require any additional analog hardware, that they are relatively easy to implement in digital baseband, and that they can operate not only on an actual received signal but also on only noise originating from the antenna and LNA. However, the major drawback of this method is its slow convergence: depending on the power levels of the input signal, this method needs $10^1$ to $10^5$ samples to achieve 50 dB IRR, assuming that the input signals are sampled at the Nyquist rate.

It was shown both in simulations and by theoretical analysis that the rate of convergence for the statistical methods depends on the ratio of the powers of the wanted and interfering signals. This property can be exploited to increase the rate of convergence in a novel way by adding a tunable notch filter at the RF input of the mixer: for every 3 dB suppression, the system needs 4 times less samples in case there is a strong difference in power levels of the input signals. In actual implementations however, we can expect only 1.5 to 3 dB suppression of the notch filter, which corresponds with a factor of 2 to 4 in speed improvement. This directly translates into 2 to 4 times less samples that cannot be decoded correctly by the digital baseband processor and a shorter startup delay.

Furthermore, a novel estimator was derived to estimate the frequency dependent gain and phase errors of a system impaired with frequency selective IQ imbalance in the IF stages. If this frequency selective behaviour was caused by a mismatch in cutoff frequency of the IF filters, a novel nonlinear fitting function function was derived which can be used to estimate the cutoff frequencies based on the phase estimates. These estimated cutoff frequencies can then be used to improve the frequency selective gain and phase error estimates. Finally, it was shown by simulations that it is possible to concatenate the frequency domain statistical method which estimates frequency independent IQ imbalance errors occurring in the RF stages and the statistical method and the nonlinear fitting function which estimate frequency selective IQ imbalance errors occurring in the IF stages. This concatenation can successfully estimate both type of IQ imbalance parameters.

It was also shown that the frequency independent estimation algorithms are rather modest in implementation requirements. However, the frequency selective estimation algorithms are more expensive to implement. While the basic frequency selective algorithm is comparable in implementation costs to the frequency independent algorithms per pair of frequency bins, the total costs scale linearly with the number of frequency bins that are needed to compensate for the frequency selective IQ imbalance. The nonlinear fitting function, which can be used to improve the estimates form the frequency selective estimator, has an even higher implementation cost, requiring several nonlinear functions and a matrix pseudo inverse. If

implementation costs for this algorithm cannot be greatly reduced, this algorithm is only suitable for implementation in base stations, where the focus is more on performance and less on size and computational limitations.

Chapter 5 finally, showed a derivation for a novel method to estimate the IQ imbalance parameters using only 16 samples. This method works by injecting the LO signal into the RF input of the mixers. The resulting output signal contains a DC signal whose value depends on the gain and phase errors. By adding 4 switches to the system, the system can collect 16 independent samples. These samples can be used to perform an accurate DC calibration and to estimate the IQ imbalance parameters. The sample rate of this method is limited by the settling time of the IF stages.

The implementation costs for this method is rather modest, requiring only multipliers and dividers. However, to benefit from the short sampling time needed by this method, it is recommended to implement the dividers as two parallel and fast dividers.

Simulations indicated that this method works very well if the system can inject very accurate square waveforms. However, if the bandwidth of this waveform is limited, performance is reduced greatly.

This method is demonstrated in a low frequency prototype system. In this system, the IQ imbalance could be manually adjusted by changing capacitor values in critical points of the system. The system could successfully increase the IQ imbalance from 32.1 to 49.2 dB. At this level of image rejection ratio, a strong frequency selective IQ imbalance behaviour became visible.

Which of those standard independent method a designer should choose depends ironically mostly on the system that is to be implemented. If the system operates on relatively low RF frequencies and if a very short estimation time is of critical importance, the deliberate LO self mixing method is preferable.

If however, the system works at very high RF frequencies but a short estimation time is less important, the statistical methods are preferred, especially when one can expect frequency selective IQ imbalance. The estimation time of these methods can optionally be decreased somewhat by including a tunable notch filter at RF.

## 6.2 Future work

Future work in the area of standard independent IQ imbalance estimators which should satisfy the requirements as listed in section 2.4 can be divided in work aimed

at improving the statistical methods and work aimed at improving the deliberate LO self mixing method.

Future work on statistical methods can include:

- To increase accuracy of the nonlinear fitting function of the frequency selective IQ imbalance estimator, a low pass filter might be applied just before applying the nonlinear fitting function, to reduces the noise on the phase error estimates.
- The nonlinear fitting function of the frequency selective IQ imbalance estimator assumes a first order low pass filter. For other types of filters, different fitting functions must be derived.
- A better concatenation or closer integration of the frequency independent and the frequency selective IQ imbalance estimator might make the resulting estimation system less sensitive to estimation errors in the frequency independent error estimate.
- The statistical methods are very attractive to adjust to time varying IQ imbalance estimators. An interesting topic for research for this application is for example the type of filters that can be used in such estimators. These methods can optionally be assisted by a temperature measurement circuit on chip to track fast changing IQ errors.

Future work on the deliberate LO self mixing method can include:

- Implement this method in an actual IC design.
- Since the performance of this method depends strongly on the shape of the signal that is injected, it might be relevant to investigate methods to estimate some parameters of this signal, such as the bandwidth, and on estimation methods which use this information.
- This method might be used to initialize one of the statistical methods, to give it an initial speed boost. Therefore, the system needs to have an indication on the accuracy of the estimate of the deliberate LO self mixing method, so that it can determine how big this speed boost is and how many more samples it needs for the statistical method to reach the target image rejection ratio. However, currently no method is known for the system to have an indication on the accuracy of the estimate of the deliberate LO self mixing method.

- For very high RF frequency systems, the bandwidth of the LO signal might be so limited that even the third order harmonic is almost absent. For such a system, one could assume that the signal that is injected is a pure sine wave. In that case, a different estimator is needed, and future work in this area is warranted. An interesting approach in this area is for example to develop first order Taylor approximations around $\phi_{\mathrm{i}} = 45^0$.

# Appendix A

# Project control document

## Revision history

The revision history of this document is summarized in table A.1.

Table A.1: Revision history

| Version | Date | Changes |
|---|---|---|
| 0.1 | 10 April 2008 | Initial version |
| 0.2 | 6 November 2008 | Major update |
| 0.2.1 | 9 November 2008 | Minor update |

## A.1 Introduction and background

Since the introduction of the mobile phone near the end of last century, the mobile phone has evolved from a device which can be used to make phone calls, to something which not only can make phone calls, but which can also be used to play music and videos, to synchronize your agenda, to play games, to exchange files with other phones, to access the Internet and even to tell your exact location and give you directions when you are on the road. The addition of all those services has increased the number of wireless connections in a phone from one to four or often even more.

In current mobile phones, most of these connections are created with dedicated RF hardware front-ends, which takes up precious space in the mobile phone and

besides that, the application engineers should be very careful to minimize any interference between these front-ends. Therefore, the current trend in RF transceivers is towards more flexible hardware which can be reprogrammed on the fly for different wireless standards. With such a flexible RF front-end, only one front-end is needed to allow the phone to access different wireless standards, thereby decreasing the occupied space in the phone and making it easier for mobile phone designers to integrate various wireless standards in the device.

Designing such flexible RF front-ends however, is more difficult than designing traditional RF front-ends, especially if the front-end has to operate in a mobile phone, where cost, power and space are very limited. The trend in current research is therefore to investigate if digital baseband processors can be used to assist analog front-ends, in order to meet the specifications of the wireless standards, as well as the specifications for cost, power and space. Special interest in research is for DC offsets, gain and phase (IQ) mismatches, small nonlinearities and noise reduction.

The aim of this project is to investigate the impact of IQ mismatches and small nonlinearities in analog front-ends for a multi-standard radio, and to investigate compensation techniques. The standards of interest are GSM, GPRS, UMTS and LTE.

Update: since the problem of IQ mismatches required more time than initially estimated and since the required prototype is more complex and will require more development time than initially expected, it was decided to skip the nonlinearities and to focus completely on IQ mismatches.

The supervisors of this project are Jan van Sinderen and Robert van Veldhoven from NXP Research Eindhoven and Peter Baltus from Eindhoven University of Technology.

## A.2 Project result

### A.2.1 Background

The background of this project is described in chapter A.1. The project is of special interest to NXP since NXP is a leading digital baseband and RF chip supplier for GSM in mobile phones.

Update: During the project, a reorganization inside NXP has taken place, and the focus of NXP has shifted towards multi-standard receivers for car applications, such as car radio. Examples of such standards are FM radio and Sirius/XM Radio.

### A.2.2 Problem definition

The problem can be divided in two sub-problems: the problem of IQ mismatch and the problem of nonlinearities. This document is the baseline document for IQ mismatch. For nonlinearities, a similar document will be made once the IQ mismatch problem is finished.

Update: as explained in the previous chapter, the IQ imbalance topic will be extended and nonlinearities will not be covered in this project.

It can be assumed that both problems are present in a multi-mode GSM / GPRS / UMTS / LTE receiver, using a very high speed sigma delta ADC. The receiver is in principal a near zero IF receiver.

For both problems, the impact on the received signal quality should be analyzed, and solutions should be investigated. Since the RF front-end should support such a wide range of standards, the solutions should be standard independent.

#### IQ mismatch

The error in the phase of the local oscillator can be expected to be in the order of 2 or 3 degrees, and the error in the gain of the quadrature branch can be expected to be in the order of 2 or 3 percent, resulting in a image rejection ratio of 30 dB.

However, according to the GSM specification, the adjacent channel rejection ratio should be 50 dB. Therefore, when using a near zero IF down convertor, the adjacent channel is down converted to the image channel of the desired signal, and at least 50 dB image rejection ratio is required.

### A.2.3 Deliverables

The result of this project will be tested algorithms (both in computer simulations and using an experimental setup), a report and a presentation.

The report will include:

- a detailed problem description
- a summary of the requirements that the solutions should satisfy
- derivation and analysis of the algorithms
- simulation results

- implementation details
- a description of the hardware prototype
- test results of the implemented algorithms
- recommendations for applications and future study.

### A.2.4 Delimiters

The project will not necessarily include:

- solutions for other sources of errors, such as DC offsets, phase noise or thermal noise
- testing the algorithms in real world scenarios
- truly optimized and production quality ready implementations of the investigated algorithms
- since the project results should be delivered by a certain date, no hard guarantees can be given for the quality of the final result.

## A.3 Results achieved

10 April. The present status of the project is in the middle of the design phase for the IQ mismatch problem. However, the initiation phase and especially the definition phase should still be formally closed. While this does not seem very logical, it was possible since the project members were already very familiar with the problem of IQ mismatch. The current work is therefore an exploration of different algorithms, which can be used to select a final algorithm once the initiation and definition phases are completed.

6 November. After selecting the most promising algorithm to estimate the IQ mismatch parameters, several iterations were required to come to a good system level model, and for every system level model, an algorithm was derived. Therefore, the definition phase and design phase required much more time than initially expected. Therefore we decided to change the goal of the project to only cover IQ mismatch.

10 November. Implementation of prototype started.

22 December. Working prototype; tuning, debugging and measurements can start.

9 February. Tuning and debugging are finished. Most measurements are finished as well. Found interesting ideas for different methods to estimated IQ imbalance parameters. These ideas will be theoretically analyzed and simulated in unpayed extra time.

## A.4 Phasing plan

The complete project lasts 41 weeks and is divided into 19.5 weeks for IQ mismatch, 19.5 for nonlinearities and 2 weeks to finalize the report and presentation. Starting at 3 March 2008, this means that the complete project is finished at 12 December 2008.

We have accounted for 1600 man hours. While 41 weeks amounts to 1640 man hours, 40 hours are reserved for holidays.

Update November 9: Since the project is refocused, the phasing plan has to be adjusted as well. The main tasks that have to be done are creating an experimental setup, performing measurements and writing a report.

There are 6 weeks left until December 25, which means 3 weeks for the experimental setup and measurements and 3 weeks for writing the report.

Any extra time needed by the main project contributor will not include payment of this project contributors salary.

### A.4.1 Initiation phase

**End date:** 9 May 2008

In this phase, the specifications of the hardware platform and the target specifications of the result will be investigated.

**Outcome:**

- project assignment

### A.4.2 Definition phase

**End date:** September 2008

In this phase, definition of IQ mismatch and nonlinearities from a signal processing perspective will be made clear, and the impact of those imperfections will be investigated.

**Outcome:**

- signal model of imperfections
- report with a study of the impact of the imperfections.

### A.4.3 Design phase

**End date:** November 2008

In the design phase, algorithms to estimate and compensate the imperfections will be investigated.

**Outcome:**
The outcome of the design phase will be a report consisting of:

- derivation of the investigated algorithms
- analysis of the investigated algorithms
- simulation results of the algorithms

The analysis of the algorithms will include:

- bias analysis of the algorithm (ideally, the bias is 0)
- number of samples that the algorithm needs to achieve the design goal
- type and number of operations needed for the algorithm

### A.4.4 Preparation phase

**End date: 14 November 2008**

In the preparation phase, preparations for creating the experimental setup will be made.

**Outcome:**

- All required components are delivered.

### A.4.5 Realization phase

**End date: 30 November 2008**

In the realization phase, the experimental setup will be created and measurements will be taken.

**Outcome:**

- measurement report

### A.4.6 Follow up phase

For this project, no follow up phase is foreseen.

## A.5 Control plan

### A.5.1 Time/Capacity

Table A.2 summarizes the time table of the project plan.

There will be weekly meetings with both supervisors from NXP and with the supervisor from TU/e.

### A.5.2 Money

#### Salaries

The salaries of Jan van Sinderen and Robert van Veldhoven will be payed by NXP, the salary of Peter Baltus will be payed by TU/e. The salary of Admar Schoonen will be payed by TU/e until 31 December 2008.

#### Software and hardware costs

All major equipment and software for the project is standard material available at NXP. We therefore do not foresee any large additional costs.

Table A.2: Time and capacity summary

| | **Final date** | **Margin** |
|---|---|---|
| Start of the project | 3 March 2008 | - |
| End of the project | 25 December 2008 | - |
| Duration of the project | 41 weeks | 12 days |
| | **Man hours** | **Margin** |
| Capacity | 1600 | 96 hours |
| **Duration of the phases for IQ mismatch** | **# Weeks** | **Margin** |
| Initiation phase[1] | 10 | - |
| Definition phase[1] | 17 | - |
| Design phase[1] | 3 | - |
| Preparation phase | 1 | - |
| Realization phase | 2 | - |

[1] Initiation phase, definition phase and part of the design phase for IQ mismatch are done in parallel.

For the implementation of the prototype however, some materials, such as PCBs, passive and active components, connectors etc, will have to be bought. These materials are available at MiPlaza; the cost of these materials will directly be billed on the MiPlaza account of the RFIC group at NXP.

Since these components are not priced in the MiPlaza shop, an actual estimate of the cost of the prototype cannot be given. However, looking up the bill of material in the Conrad store [28], an estimate can be made of the cost of the prototype. Table A.3 shows the estimate of the cost of the prototype based on prices in the Conrad online store.

Note that, in contrast to the standard materials that are already available, these materials cannot be reused in other components.

### A.5.3 Quality

The outputs after each phase are a phase report and (optional) a presentation; these outputs are objects of evaluation for quality control.

Table A.3: Prototype component cost estimate

| Type | # | €/ piece | € |
|---|---|---|---|
| ICs | 20 | 1.00 | 20.00 |
| Passive components | - | - | 20.00 |
| PCBs | 2 | 5.00 | 10.00 |
| Power supply connectors | 2 | 2.00 | 4.00 |
| SMA connectors | 16 | 5.00 | 80.00 |
| IC sockets | 20 | 0.50 | 10.00 |
| Other | - | - | 20.00 |
| Total | | | 164.00 |

Since the project is limited in time, the quality of the output depends on the amount of time.

### A.5.4 Organization

Since Admar Schoonen is full time employee of TU/e and therefore TU/e is responsible for the standard employee insurances etc. All responsibilities and authorities belonging specifically to this project are in NXP and TU/e only has an advisory role.

In principal, every Monday there will be a meeting with Peter Baltus at TU/e and every Tuesday a meeting with Jan van Sinderen and Robert van Veldhoven at NXP to discuss the progress of the project. When necessary, Jan van Sinderen and Robert van Veldhoven can be contacted throughout the rest of the week.

There are no third parties involved in this project.

## A.6 Risk analysis

### A.6.1 Risk list

A list of the risks of this project and their expected impact and probability is shown in table A.4. From this table, three risks are selected and precautions are taken to reduce these risks and their impacts.

Table A.4: Risk list

| Risks | Impact[1] | Probability[2] | Total | Select |
|---|---|---|---|---|
| Delay due to unexpected event | 1 | 2 | 2 | * |
| Delay due to lack of technical knowledge[a] | 2 | 3 | 6 | * |
| Request to change the objectives | 2 | 2 | 4 | * |
| Absence of supervisors | 1 | 1 | 1 | |

[1] Impact (severity): 1: small, 2: middle, 3: great
[2] Probability: 1: rare, 2: possible, 3: likely
[a] Since the main project team member (Admar Schoonen) doesn't have any experience with programming FPGAs, it is likely that this could cause a delay in the project.

### A.6.2 Risk management

#### Delay due to unexpected event

If some unexpected event occurs, and the scheduled margin is not enough, it might be necessary to reduce the amount of work. Since the project consists of two sub-projects, it is possible to compromise on the second project. One of the compromises could be to not implement the algorithms for nonlinearities on the FPGA, but to only perform measurements and process the measurements offline in Matlab.

Update 9 November: it is decided to only perform measurements and process the measurements offline in Matlab.

#### Delay due to lack of technical knowledge

In case there are many problems with implementing the algorithms on the FPGA, it might be possible to only perform measurements and to process these measurements offline in Matlab.

#### Request to change the objectives

Weekly meetings with all supervisors will help to have a continuous direction and activity in the project and therefore to reduce the impact of any changes in the objectives.

# Bibliography


[1] N. Golmie, Chevrollier, and O. N. Rebala, "Bluetooth and WLAN coexistence: Challenges and solutions," *IEEE Wireless Communications*, vol. 10, pp. 22–29, Dec. 2003.

[2] R. Punnoose, R. Tseng, and D. Stancil, "Experimental results for interference between bluetooth and IEEE 802.11b DSSS systems," in *Vehicular Technology Conference*, vol. 1, 2001, pp. 67–71.

[3] B. Razavi, "Design considerations for direct-conversion receivers," in *IEEE Transactions on Circuits and Systems II: Analog and Digital Signal Processing*, June 1997, pp. 428–435.

[4] M. Windisch and G. Fettweis, "Standard-independent I/Q imbalance compensation in OFDM direct-conversion receivers," in *Proc. of 9th Intl. OFDM Workshop*, 2004.

[5] J. Finol and M. Buchholz, "Design of an inphase and quadrature phase and amplitude imbalance compensation in quadrature receivers," in *Proc. of ICCDCS 2004*, Nov. 2004, pp. 254–258.

[6] M. Valkama, M. Renfors, and V. Koivunen, "Advanced methods for I/Q imbalance compensation in communication receivers," *IEEE Trans. on Signal Proc.*, vol. 49, no. 10, pp. 2335–2344, Oct. 2001.

[7] A. Schoonen, "IQ imbalance in OFDM wireless LAN systems," Master's thesis, Eindhoven University of Technology, Jan. 2006.

[8] K. Maeda, W. Hioe, Y. Kimura, and S. Tanaka, "Wideband image-rejection circuit for low-IF receivers," in *Proc. of ISSCC 2006*, Feb. 2006, pp. 1912–1221.

[9] J. Liu, A. Bourdoux, J. Craninckx, P. Wambacq, B. Côme, S. Donnay, and A. Barel, "OFDM-MIMO WLAN AP front-end gain and phase mismatch calibration," in *IEEE Radio and Wireless Conference*, Sept. 2004.

[10] T. Schenk, *RF Imperfections in High-rate Wireless Systems*. Springer, 2008.

[11] J. Tubbax, "A digital approach to low-cost low-power broadband radios," Ph.D. dissertation, K. U. Leuven, 2004.

[12] A. Tarighat, R. Bagheri, and A. Sayed, "Compensation schemes and performance analysis of IQ imbalances in OFDM receivers," *IEEE Transactions on Signal Processing*, vol. 53, pp. 3257–3268, aug. 2005.

[13] A.-J. Van der Veen, *Signal processing for communications (lecture notes for course ET4147)*. Delft: Delft University of Technology, 2004.

[14] G. Wetzker, "IQ-mismatch estimation and correction - a study for car radio FM systems," *Nat.Lab. Technical Note 2002/030*, 2002.

[15] I. Elahi, K. Muhammad, and P. Balsara, "I/Q mismatch compensation using adaptive decorrelation in a low-IF receiver in 90-nm cmos process," *IEEE Journal of Solid-State Circuits*, vol. 41, pp. 395–404, Feb. 2006.

[16] N. Moseley and C. Slump, "A low-complexity feed-forward I/Q imbalance compensation algorithm," in *17th Annual Workshop on Circuits*, Nov. 2006, pp. 158–164.

[17] L. Yu and W. Snelgrove, "A novel adaptive mismatch cancellation system for quadrature IF radio receivers," in *IEEE Trans. on Circuits and Systems-II: Analog and Digital Signal Processing*, vol. 46, Jun. 1999, pp. 789–801.

[18] M. Valkama, M. Renfors, and V. Koivunen, "Compensation of frequency-selective I/Q imbalances in widebandreceivers: Models and algorithms," in *IEEE Third Workshop on Signal Processing Advances in Wireless Communications (SPAWC 2001)*, Mar. 2001, pp. 42–45.

[19] R. Goldschmidt, "Applications of division by convergence," Ph.D. dissertation, Massachusetts Institute of Technology, 1964.

[20] A. Kaw, *Numerical Methods with Applications*, 1st ed. Autar Kaw, 2008.

[21] J. Proakis, *Digital Communications*, 4th ed. McGraw-Hill, 2001.

[22] D. Montgomery and G. Runger, *Applied Statistics and Probability for Engineers*, 3rd ed. John Wiley & Sons, Inc., 2003.

[23] E. Weisstein, "Central limit theorem," http://mathworld.wolfram.com/CentralLimitTheorem, MathWorld – A Wolfram Web Resource (retrieved on 2009-04-03).

[24] M. Windisch and G. Fettweis, "Performance analysis for blind I/Q imbalance compensation in low-if receivers," in *First Intl. Symposium on Control, Communications and Signal Processing*, 2004, pp. 323–326.

[25] F. Leong, "Design of an oscillator for satellite reception," Master's thesis, University of Twente, 2007.

[26] R. van Veldhoven, "A triple-mode continuous-time $\sigma\delta$ modulator with switched-capacitor feedback dac for a gsm-edge/cdma2000/umts receiver," *IEEE Journal of Solid-State Circuits*, vol. 38, pp. 2069–2076, Dec. 2003.

[27] D. Leenaerts, J. van der Tang, and C. Vaucher, *Circuit Design for RF Transceivers*. Dordrecht, The Netherlands: Kluwer Academic Publishers, 2001.

[28] "Conrad Electronic," http://www.conrad.nl, Conrad Electronic Benelux BV (retrieved on 2009-04-16).